Escola d'Enginyeria de Telecomunicació i Aeroespacial de Castelldefels

UNIVERSITAT POLITÈCNICA DE CATALUNYA

TREBALL DE FI DE CARRERA

TÍTOL DEL TFC: Production of low cost Cu-based metallic glasses from recycled Cu

TITULACIÓ: Enginyeria Tècnica Aeronàutica, especialitat Aeronavegació

AUTOR: Marta García Vera

DIRECTOR: Pere Bruna Escuer

DATA: 15 de juny de 2012

Títol: Production of low cost Cu-based metallic glasses from recycled Cu

Autor: Marta García Vera

Director: Pere Bruna Escuer

Data: 15 de juny de 2012

Resum

Els vidres metàl·lics tenen un gran interès científic i industrial. Des de la producció de les primeres cintes metàl·liques amorfes mitjançant subrefredament ràpid, un gran nombre de aliatges metàl·lics amorfs s'han produït mitjançant diversos mètodes. Els vidres metàl·lics massius (BMG) es defineixen com aliatges metàl·lics amorfs que es poden obtenir amb dimensions característiques del mil·límetre o, fins i tot, majors. Des de finals de la dècada de 1980, una gran quantitat d'aliatges en forma de BMGs s'han reportat, basats en quasi tots els metalls amb interès tecnològic. Les propietats mecàniques no convencionals dels BMGs, com ara l'alt quocient entre la resistència i la densitat i els coeficients de restitució molt elevats durant la deformació elàstica, combinat amb la possibilitat de produir peces relativament grans amb característiques complexes mitjançant la tècnica de refredament amb motlle, fa que els BMGs siguin uns materials molt prometedors per a ús industrial.

Els vidres metàl·lics basats en Cu són de gran interès, ja que mostren millors propietats mecàniques que els aliatges cristal·lins amb composicions similars. El grup d'investigació de l'estudiant ha establert una col·laboració amb una de les empreses espanyoles més importants en la producció de coure: el grup La Farga. La Farga és el líder en el reciclatge de coure i, en l'actualitat, està subministrant productes de Cu d'alt valor, majoritàriament per a aplicacions de potència.

L'objectiu d'aquest projecte és explorar la possibilitat de produir vidres metàl·lics en el sistema binari Cu-Zr amb Cu residual subministrat per La Farga, el qual té diversos graus d'impuresa (fins a un 13%). L'èxit del projecte implica, d'una banda, la possibilitat de produir vidres metàl·lics sense utilitzar elements d'alta puresa, reduint així el seu cost i, d'altra banda, la possibilitat per la Farga d'obtenir guanys pel Cu amb residus que actualment no té cap utilitat.

Title: Production of low cost Cu-based metallic glasses from recycled Cu

Author: Marta García Vera

Director: Pere Bruna Escuer

Date: June, 15th 2012

Overview

Metallic glasses have a large scientific and industrial interest. Since the production of the first metallic amorphous ribbons by fast undercooling a large number of amorphous metallic alloys have been produced by using several methods. Bulk metallic glasses (BMG) are defined as amorphous metallic alloys that can be obtained with characteristic dimensions of millimetre or larger. Since the late 1980's a large amount of BMG alloys have been reported, based in almost all metals with technological interest. The non-conventional mechanical properties of BMG, such as high strength to density ratios and very high restitution coefficients during elastic deformation combined with the possibility of producing relatively large parts and complex characteristics by mould casting make BMG highly promising materials for industrial use.

Cu-based metallic glasses are of high interest, as they show better mechanical properties than crystalline alloys with similar compositions. The research group of the student has already established collaboration with one of the most important Spanish companies of Cu production, La Farga Group. La Farga is leader in Cu recycling, and is at present supplying high value Cu products, mostly for power applications.

The aim of this project is to explore the possibility of producing binary Cu-Zr metallic glasses using residual Cu supplied by La Farga that has several degrees of impurity (up to 13%). The exit of the project will imply, on the one hand, the possibility of producing metallic glasses without using high purity elements, thus reducing their cost and, on the other hand, the possibility for La Farga to obtain profit from residual Cu that nowadays has no use.

ACKNOWLEDGMENTS

I would like to express my gratitude to my thesis tutor, Pere Bruna, for giving me support and the opportunity to do this project, with which I have learnt a lot.
I would also like to thank my parents, María and Pedro for the support they have provided me through my entire life and in particular, I must acknowledge my boyfriend Jonatan, for giving a breath of fresh air to my life every day and to make me see the light at times of maximum darkness.

“Put your heart, mind, intellect and soul
even to your smallest acts.
This is the secret of success”.
(Swami Sivananda)

INDEX

FIGURE INDEX

TABLE INDEX

INTRODUCTION

Metallic glasses are a new class of materials discovered in 1960 and, from the beginning they attracted the interest of the scientific community.
The research performed in these 50 years has uncovered more than a thousand compositions of amorphous metallic alloys, which some hundreds of them have interesting properties for technological applications and most of them can be produced in dimensions suitable for its industrial use.

In addition, Cu-based metallic glasses are of high interest as they show better mechanical properties than crystalline alloys with similar compositions. In this context, the present thesis reports the study of the production of Cu-based metallic glasses with the melt-spinning technique, its analysis and the characterization of its mechanical and thermal properties.

The composition chosen for this project is $Cu_{64,5+x}Zr_{35,5-x}$ with x = -1, 0, 1 at.% because it can be produced as a bulk metallic glass (BMG) due to its high glass forming ability (GFA).
We produce the alloys with the desired compositions using, on the one hand, copper and zirconium with 99,99% purity and, on the other hand, using three different types of copper with an unknown amount of impurities; all of them supplied by LaFarga Company. The use of non-pure Cu may diminish the glass forming ability of this composition. Therefore, the aim of this project is to study the effect of several degrees of impurities in the easiness of glass formation of this binary system.
The ribbons were analysed by X-ray diffraction (XRD) to assure if they are or not completely amorphous and by the scanning electron microscopy (SEM) to determine its real composition.
The hardness of the $Cu_{64,5+x}Zr_{35,5-x}$ ribbons was analysed with the microhardness testing method and the characterization of its thermal properties was extracted after the analysis of the ribbons in the differential scanning calorimeter (DSC).

This thesis is divided in several parts. At the beginning, it is presented an introduction to metallic glasses and a brief explanation of the Cu-Zr binary alloy, from its basic properties to the analysis of its phase diagram in order to determine the best composition to produce amorphous alloys.
Following, the techniques used to produce and characterize the alloys are described, in particular, the arc melting and the melt spinner techniques.
Next, the characterization techniques used in this work (x-ray diffraction, scanning electron microscopy, microhardness testing and differential scanning calorimetry) are detailed with all the results obtained in for the ribbons.
After the production methods, it is found an explanation of how rods with 1 mm of diameter and the $Cu_{64,5}Zr_{35,5}$ composition can be produced, and finally, the work finishes with the conclusions and an outlook of the further work that can be done.

CHAPTER 1. METALLIC GLASSES

1.1. Definition

An amorphous metal is a metallic material with a disordered atomic-scale structure.
Unlike most metals, which are crystalline and have a highly ordered arrangement of atoms, amorphous alloys are non-crystalline.
Materials in which such a disordered structure is produced directly from the liquid state during cooling are called "glasses", so amorphous metals are commonly referred as metallic glasses.
So, the term metallic glass makes reference to a metallic material with a disordered internal structure. That is, while a traditional metallic metal has an ordered structure of atoms called crystalline structure, metallic glasses have an atomic disorder typical of liquids (Fig. 1.1). [1]

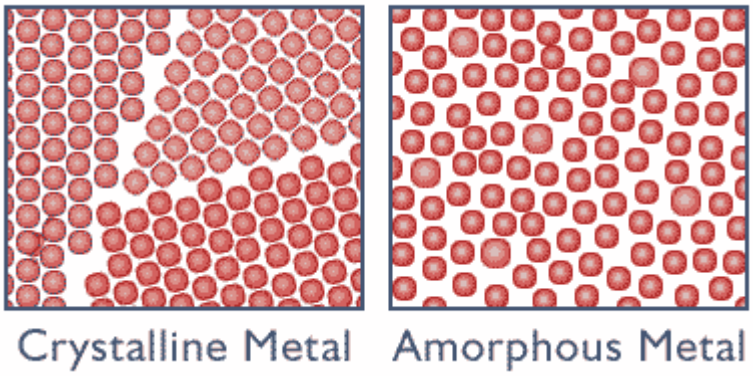

Fig.1.1 The difference between crystalline and amorphous metal internal structures [2].

1.2. History

The first reported amorphous metal was an alloy of Au and Si ($Au_{75}Si_{25}$). Its discovery was published in 1960 by the Belgian scientist P. Duwez and its colleagues W. Klement and R.H. Willens.
This discovery showed that the process of nucleation and growth of the crystalline phase might be avoided in some alloys to finally obtain a super cooled liquid configuration. This fact was possible due to the development of super-fast cooling techniques for the molten metals, allowing the metal to cool at speeds of 10^5-10^6 K/s.
The problem with these techniques was that, due to the high cooling speeds required, the manufacture of metallic glasses was limited to ribbons, foils or wires [3]. This problem only allowed using these materials for applications which use their electrical, magnetic or chemical properties, which means that their good mechanical and structural applications could not be seized.

Years later, D.Turnbull realized that, for each material, the glass transition occurred at a definite temperature. With the glass transition temperature (T_g) and melting temperature of the material (T_m), he defined a reduced temperature of glass transition ($T_{rg}= T_g / T_m$) that was used as a criterion to define the ability of a material or an alloy to form an amorphous solid: the Glass-Forming Ability (GFA). It is considered that a material has a good GFA when the T_{rg} ratio is around or higher than 0,6 [4].
Producing alloys with a higher GFA, the minimization of the cooling rate was achieved, which made possible to use other methods of amorphous metals production to create pieces of some millimetres or centimetres. These pieces were called BMG (Bulk Metallic Glasses). A pioneer in the creation of BMGs is A. Inoue, from whose investigations emerged the three rules of thumb to create amorphous metals with relatively low cooling temperatures that will be described in the next section [5].

1.3. Glass forming ability (GFA)

One of the most important factors to take into account to obtain an amorphous material is the GFA [6].
If we can increase the GFA, the easier the materials become amorphous when cooled, which means the materials will need a lower cooling rate and simpler techniques to create it.
This increase in GFA will be achieved by increasing the ratio T_g/T_m. In order to do this, the three rules of Inoue are the following ones: [7]

1. The alloy has to be made of, at least, three elements.
This point is related to the ease of the material to crystallize. The more elements the material contains, the more complex the unit cell of the crystal structure will be. Thus, the atoms will find more difficult reaching a position of maximum stability.

2. There must be at least 12% of difference between the atomic radiuses of the elements of the alloy.
This difference is because, this way, there will be a higher packing in the liquid phase, since the smaller atoms fit into the gaps left by bigger ones. This higher packing makes the liquid phase more viscous, which favours the GFA because there is less interatomic space to perform the necessary movements for the crystallization.

3. The enthalpy of the alloy must be negative between the principal elements of the sample.
The enthalpy of the principal elements in the material must be negative. Thus the elements will be easily dissolved in a homogeneous mixture when they are melted and the creation of crystallization nuclei around particles of a material that is not well mixed will be avoided.

The use of T_{rg} as a criterion for GFA also explains the well known fact that the glass formation is favoured in an alloy with a deep eutectic. [8]

A deep eutectic reaction means that the liquidus or melting temperature is the lowest one for obtaining a particular crystalline phase, thus increasing the value of T_{rg}. Thus, the GFA is greatly favoured thermodynamically [9].

However, no BMGs have been found at the eutectics in various binary systems studied to date. In many systems, the better glass formers are found at off-eutectic compositions, which remain an unsolved puzzle so far. [10]

1.4. Cu-Zr binary alloy

From the 1980s it is known that metallic glasses can be formed in the Cu-Zr system in a wide range of compositions, from the ones with a dominant percentage in copper ($Cu_{70}Zr_{30}$) to the ones with a dominant percentage in zirconium ($Cu_{25}Zr_{75}$) [11].
These amorphous alloys are produced in a ribbon-shaped form, typically of 1 mm wide and 20 μm of thickness with the melt spinner technique.
Previously all the elements have been alloyed in its corresponding proportions in an arc furnace.
An important point of this process is the need to use high purity elements, at least of a 99,99% pureness.
Binary alloys capable of forming bulk metallic glasses in the Cu-Zr system have been discovered recently. Since binary alloys are easier to model than alloys with more elements, this makes Cu-Zr an attractive bulk metallic glass to study. [12]
In particular, Cu-Zr alloy was studied and reported as BMG by A. Inoue, X.M. Wang and W. Zhang, better known as Sendai Group in 2001 (it is considered this year since it was the year of publication of the first paper about this binary system in the BMG form) [13].
Moreover, the fact that this alloy is one of the best known transition metal-metal binary system which may be obtained in a glassy state by conventional melt-spinning technique over a wide range of composition [14], is an additional driving force for all the researchers around the world and for our project.

First of all, to start our study, we must decide which composition is the most suitable in order to produce Cu-Zr amorphous ribbons using non purity elements. The composition is decided from the study of the corresponding phase diagram.

1.4.1. Cu-Zr phase diagram

The solid state materials can consist of several phases. The combination of these phases defines many of the properties that the material under analysis has. [15]
The tool that allows us to describe these material phases is, precisely, the phase diagram.
Specifically, the phase diagram for the Cu-Zr alloy is the following one (Fig. 1.2):

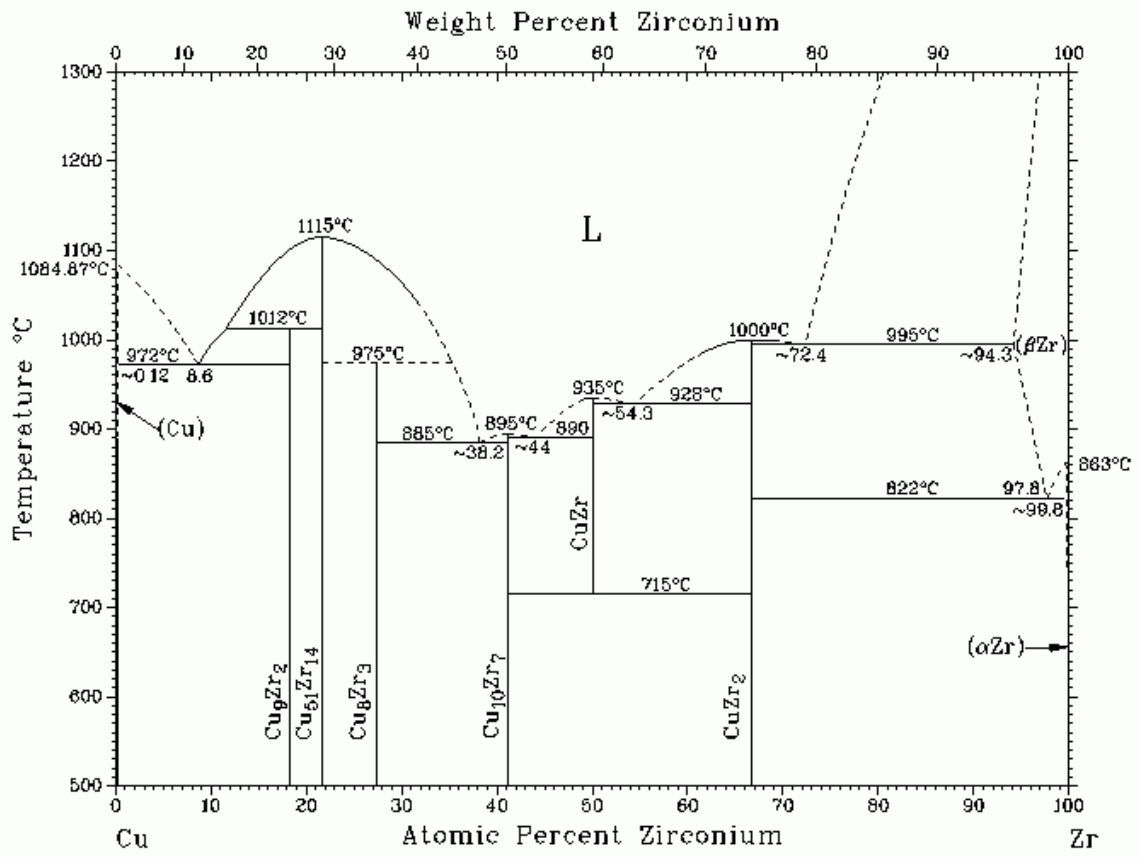

Fig 1.2 Cu-Zr alloy phase diagram [16]

The binary Cu-Zr system contains 12 phases: HCP_A3 (low temperature Zr), BCC_A2 (high temperature Zr), FCC_A1 (Cu), intermetallic compounds Cu_9Zr_2, $Cu_{51}Zr_{14}$, Cu_8Zr_3, Cu_2Zr, $Cu_{10}Zr_7$, CuZr, Cu_5Zr_7, $CuZr_2$ and liquid [17].
Besides, in the diagram, we notice that there are five eutectic points in the binary Cu-Zr system. At these points, the liquid begins its phase transformation to a solid. This solid is called eutectic solid. In turn, the eutectic solid is always formed at the same temperature, which it is called eutectic temperature.

Fig. 1.3 shows that the eutectic reaction of Cu_8Zr_3-$Cu_{10}Zr_7$ with X_{eu}= 38,2 at. % Zr has the lowest eutectic temperature of 885ºC but the $Cu_{61,8}Zr_{38,2}$ is not fully amorphous as crystalline phases are present when researchers were trying to produce the alloy as a BMG [18].

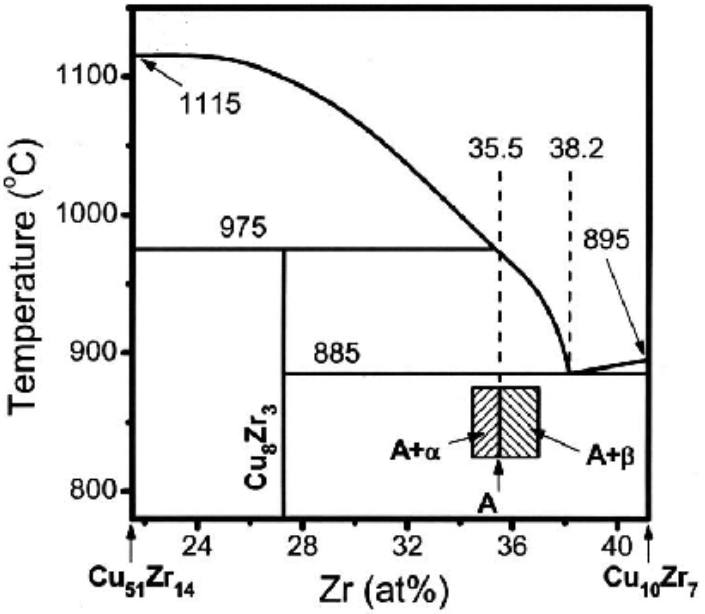

Fig 1.3 Part of the Cu-Zr phase diagram with the area of interest in our project [19]

Only a completely BMG has been found around the $Cu_{61,8}Zr_{38,2}$ eutectic: it comes from an alloy with 64,5 at.% Cu and 35,5 at.% Zr.[20]

The aim of this project is to produce metallic glasses in the Cu-Zr system using recycled copper from the waste supplied by LaFarga company, instead of pure copper. So, in our project, using the Cu-Zr binary system, we will show that amorphous ribbons can be obtained using the melt spinner technique and then, we are going to see if we can produce amorphous rods, which is a BMG, by copper mold casting even if we do not use pure elements.
Not using pure copper in the preparation of the alloys does not give us any guarantee about that the chosen composition will be amorphous.
Thus, we proceed to study three compositions around the composition with the optimum GFA ($Cu_{64,5+x}Zr_{35,5-x}$) with x = -1,0,1. We also have three types of recycled copper supplied by LaFarga which we have labelled in our project as recycled copper type 1, 2 and 3 and we only know that each one has an increased percentage of impurities. In addition, we have also produced the three alloys using pure copper (99,99%) as a reference [21]. Moreover, the zirconium used is of high purity and all the alloys have a mass between 3,5 and 5 g.

CHAPTER 2. SAMPLES PRODUCTION

For this project we will produce a total of 12 samples. The composition is based around the one with optimum GFA: $Cu_{64,5+x}Zr_{35,5-x}$ with x = -1, 0, 1 and, in turn, all the compositions are prepared for each type of copper.

Before explaining how we have produced the samples, it is necessary to define a set of concepts which will be useful in order to understand the calculations to produce them.

2.1. Definitions

Atomic weight: The average mass of atoms of an element, calculated using the relative abundance of isotopes in a naturally-occurring element. It is the weighted average of the masses of naturally-occurring isotopes. Sometimes it is also known as atomic mass and it is expressed in [g/mol] [22].
Atomic per cent: Atomic percent is one way of representing the concentration of an element in a compound or a component in a mixture. Atomic per cent can range from 0% to 100% [23].
Molecular weight: is the result of multiplying the atomic weight by the atomic per cent [24].
Mass percentage: mass percentage is one way of representing the concentration of an element in a compound or a component in a mixture. Mass percentage is calculated as the mass of a component divided by the total mass of the mixture, multiplied by 100 [25].

2.2. Calculations

The calculations are divided into two parts: first, we have to do the calculations to find the mass percentage and, once we have it, we have to use it to calculate the mass of zirconium corresponding to the piece of copper that we have.
We proceed to work this way because, as copper is an element which is difficult to work with, we take a piece of an unknown mass and we calculate the needed zirconium in order to have the desired composition. Thus we lose control over the total mass of the alloy but this is not important as long as we are into the mass range we have set for our project

2.2.1. Calculation of the mass percentage

This process is divided in three steps:
1- We have to determine the molecular weight of the compound.
2- For each element in the compound, we have to multiply the atomic weight of that element by the number of times it occurs in the compound. We have to do this for each element if we want to know which is the weight per cent for each one.

3- For each element, we take the answer in step 2, we divide it by the number we got in step 1 and then we multiply the result by 100. In other words, we take the weight of each element in the compound, we divide it by the total weight, and then we multiply it by 100 to make it a per cent, instead of a fraction, and we will have the per cent by mass.

2.2.2. Calculation of the required mass of zirconium

First of all, we have to define the restrictions for our sampling method, which are the following ones:
- Samples should weigh between 3,5 g and 5 g.
- The relative error between the ideal and the actual sample cannot be greater than 1% in absolute value.

To make our samples we have copper pieces with predetermined mass, therefore, what we have to do in order to get the desired composition is to calculate the mass of zirconium corresponding to the set copper mass.

First of all, we must weigh the piece of copper on a precision scale (see Fig. 2.1) to determine its mass.

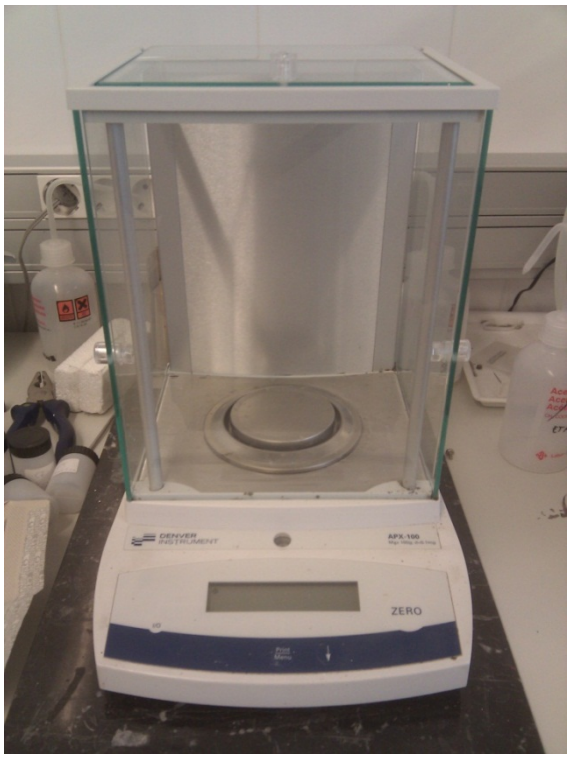

Fig. 2.1 Scale used for the sampling method

The precision scale has a resolution of 0,0005 g, so in this project, all the results which come from balance measurements, will have this resolution.

Second, we calculate the total mass dividing the actual mass of copper by the molecular weight of the copper.
And finally, we calculate the corresponding mass of zirconium as the total mass multiplied by the molecular weight of zirconium and dividing by 100.

Once we have the ideal zirconium mass that corresponds to the particular piece of copper, we proceed to weight the zirconium on the scale until the measurement obtained will give us a relative error less than 1%.
The relative error is calculated as the absolute value between the actual mass minus the ideal mass, all divided by the ideal mass and that result multiplied by 100 in order to express it in terms of percentage.

To see how we have performed all these calculations, we show below an example used in this project.

2.2.3. Example

For this example we will take the pure copper (99,9%) sample of a $Cu_{64,5}Zr_{35,5}$ alloy.

What is the mass percentage of this alloy?
First, we must find the molecular weight of the compound. To do that, we must find how many atoms of the element are in 100 molecules, multiply that number by the atomic weight of each atom and add these products together:

$$(64{,}5 * 63{,}546) + (35{,}5 * 91{,}224) = 7337{,}169\ g/mol \quad \textbf{(2.1)}$$

Now, let us look at copper. According to the formula, in each 100 molecules, there are 64,5 copper atoms. Multiplying them as in step 2, we have:

$$64{,}5 * 63{,}546 = 4098{,}717\ g/mol \quad \textbf{(2.2)}$$

Finally, we take the result above and we divide it by the total weight:

$$4098{,}717 \div 7337{,}169 = 0{,}5586237689 \quad \textbf{(2.3)}$$

Then, we multiply this by 100, in order to obtain a percentage:

$$0{,}5586237689 * 100 = 55{,}86237689\ wt\%\ Cu\ \ in\ Cu_{64,5}Zr_{35,5} \quad \textbf{(2.4)}$$

Now, we do the same for the zirconium. To find the mass percentage of Zr, it would be enough to perform the following operation:

$$wt\%\ Zr = 100 - wt\%\ Cu \quad \textbf{(2.5)}$$

This would be correct since the alloy is binary but we do all the calculations below to check that the procedure we are following is correct.

$$35{,}5 * 91{,}224 = 3238{,}452\ g/mol \quad \textbf{(2.6)}$$

$$3238{,}452 \div 7337{,}169 = 0{,}441376231 \quad \textbf{(2.7)}$$

$$0{,}441376231 * 100 = 44{,}1376231\ wt\%\ Zr\ \ in\ Cu_{64{,}5}Zr_{35{,}5} \quad \textbf{(2.8)}$$

Following this example, we have a piece of copper of 2,2319 grams. The total mass of the alloy is calculated as follows:

$$(2{,}2319 * 100) \div 55{,}862377 = 3{,}99535452\ g \quad \textbf{(2.9)}$$

Taking the total mass, we proceed to calculate the corresponding mass of zirconium to obtain the desired alloy:

$$(3{,}99535452 *\ 100) \div 44{,}1376231 = 1{,}76345452\ g \quad \textbf{(2.10)}$$

Based on this mass, for this example, we have weighed the zirconium, obtaining a mass of 1,7648 grams.

And, finally, we have to check that the ideal mass and actual mass of the alloy does not exceed the relative error of 1%:

$$\left|\left((3{,}9967 - 3{,}99535452) \div 3{,}99535452\right) * 100\right| = 0{,}0337\% \quad \textbf{(2.11)}$$

As we can see, the results are correct according to the restrictions marked.

The rest of the calculations to obtain the desired samples can be found in annex 3.

After all the calculations, we use two devices: the arc melter, to produce the alloys and the melt spinner, to produce the ribbons (see Fig. 2.2).

Fig. 2.2 Arc melter (left) and melt spinner (right)

2.3. Arc melter

An arc melter offers the ability to melt and rapidly solidify metal alloys of nominal 10-20 gram mass using a clean Cu cold crucible [26].
The elements are placed in a base called a crucible, enclosed in a container where a pure Argon atmosphere environment is created. There is a purge consisting in three cycles of vacuum (-1 bar relative vacuum pressure) and argon filling. In the last cycle the container is filled with Ar until the desired working pressure is achieved (800 mbar in our case).

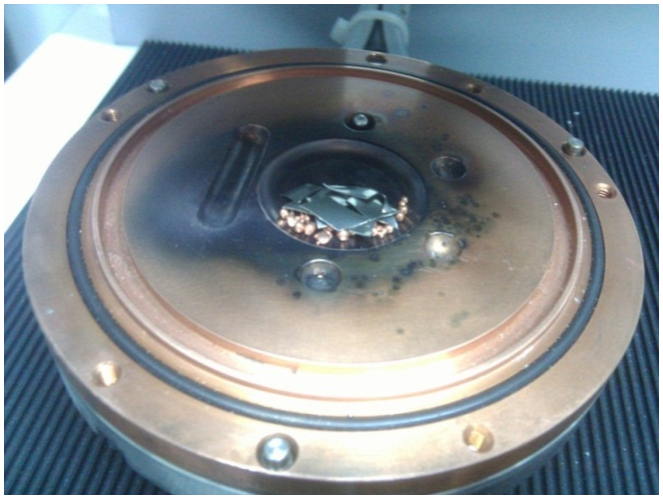

Fig. 2.3 Samples on the crucible of the arc melter.

This technique uses two electrodes with an electric potential difference between them to generate an electric arc which enables to obtain temperatures up to 3773,15 K [27], a temperature at which many metals melt easily.
Before starting the melting process, we have to check the quality of the Argon atmosphere, for that, a ball of titanium is put down on the base to be melted before the metals because titanium is a good absorber of oxygen when heated. Once we have the titanium heated, with the help of a command rod, the arc can be moved at wish.
The metals, which are placed on the copper crucible plate, are melted by a short contact with a charged electrode that has a tungsten pin (tungsten is used due to its high melting point (3695,15 K)) [28]. In turn, these metals are cooled by water, which circulates inside the crucible, at a controlled rate.
When the melting is done, the first thing to do is to extract the Argon atmosphere to eliminate possible gasses formed during the melting. Then, when the sample is already cold, we have to remove it and we proceed to clean the chamber with ethanol or acetone.

The arc melter has also two safety functions:
- Eye protection is mandatory, due to the fact that high-energy ultraviolet radiation can seriously damage the retina.
- The arc is switched off automatically if the temperature of the copper crucible plate exceeds a given limit, or if the eye protection cover is opened.

Fig. 2.4 Arc Melter

Copper and zirconium samples were melted together at the arc melter. Once the material is melted and cooled it is ovoid-shaped due to the superficial tension of the melt.

Fig. 2.5 A sample of Cu-Zr alloy after the arc melting

The melted samples were also weighted in order to check the goodness of the composition, i.e., that no mass losses took place during the melt. The results can be seen in tables 2.1, 2.2, 2.3 and 2.4.

Table 2.1. Results for pure copper samples after the arc melting process.

Type of copper	Sample	% Cu	% Zr	Cu sample [g]	Zr sample [g]	Mass before arc melter [g]	Mass after arc melter [g]	Relative error
Pure copper 99,9%	1	63,5	36,5	2,1911	1,8085	3,9996	3,998	0,04
	2	64,5	35,5	2,2319	1,7648	3,9967	3,9945	0,055
	3	65,5	34,5	2,2786	1,7228	4,0014	3,9999	0,0375

Table 2.2. Results for type 1 of recycled copper samples after the arc melting process.

Type of copper	Sample	% Cu	% Zr	Cu sample [g]	Zr sample [g]	Mass before arc melter [g]	Mass after arc melter [g]	Relative error
Recycled Cu Type 1	1	63,5	36,5	2,6529	2,1915	4,8444	4,8402	0,0867
	2	64,5	35,5	2,3341	1,8414	4,1755	4,1692	0,1509
	3	65,5	34,5	2,4936	1,8879	4,3815	4,3807	0,0183

Table 2.3. Results for type 2 of recycled copper samples after the arc melting process.

Type of copper	Sample	% Cu	% Zr	Cu sample [g]	Zr sample [g]	Mass before arc melter [g]	Mass after arc melter [g]	Relative error
Recycled Cu Type 2	1	63,5	36,5	2,3407	1,9329	4,2736	4,258	0,365
	2	64,5	35,5	2,7227	2,1518	4,8745	4,8561	0,3775
	3	65,5	34,5	2,6135	1,9774	4,5909	4,5731	0,3877

Table 2.4. Results for type 3 of recycled copper samples after the arc melting process.

Type of copper	Sample	% Cu	% Zr	Cu sample [g]	Zr sample [g]	Mass before arc melter [g]	Mass after arc melter [g]	Relative error
Recycled Cu Type 3	1	63,5	36,5	2,3946	1,9757	4,3703	4,3524	0,4096
	2	64,5	35,5	2,4019	1,8963	4,2982	4,2805	0,4118
	3	65,5	34,5	2,8232	2,1344	4,9576	4,9329	0,4982

As we have seen in the tables above, the relative error of Cu-Zr samples increases as we use a different type of recycled copper (the relative error is lower for pure copper samples and higher for the third type of recycled copper samples). From this fact, we can conclude that the samples with greater relative error are those which have copper with more impurities because these impurities could have been made the easy melting of the sample difficult (the more impurities, the more relative error before the arc melting).
As we have mentioned in the introduction part, the composition of recycled copper samples is unknown for the time being, until we proceed to perform its analysis and see if these conclusions extracted from experimental results match with reality.

2.4. Melt Spinner

The melt spinner is a device which allows the production of amorphous metallic ribbons from a molten alloy.

Fig. 2.6 Melt spinner

The alloy is placed in a quartz crucible with a small hole at the end in order to allow evacuation of the material once the injection has occurred. This crucible is placed in an induction coil through which flows a steady current, creating a magnetic field that induces the creation of eddy currents. The Joule effect produced by these eddy currents increases the temperature enough to melt the sample inside the crucible. Therefore, the technique of melt spinner can only be used with alloys which contain metallic materials. Thus, the sample can be heated above the melting point and then by the application of an overpressure inside the crucible, the molten alloy can be injected through the hole of the crucible impacting against the copper wheel while it is rotating.
Due to the high thermal conductivity of copper and high linear velocity of the wheel (up to 60 m/s) [29], the liquid can be cooled in a very fast rate (about 10^6 Kelvin per second [K/s]) [30]. Therefore, the atoms cannot be rearranged in the equilibrium position and then we can obtain an amorphous material without any crystalline order.
This process takes place into a chamber with an argon atmosphere of 400 mbar after purging the chamber several times.

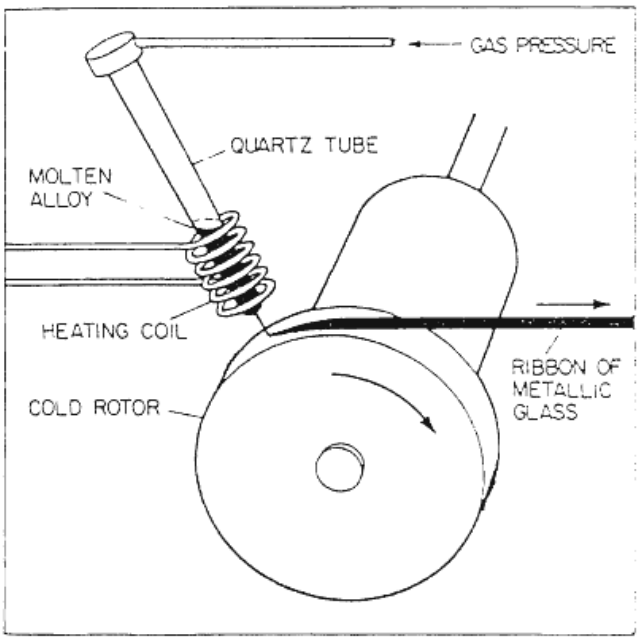

Fig. 2.7 Scheme of the melt spinning of a metallic glass [31].

2.4.1. Melt Spinner results

The parameters we have used to produce the ribbons are the following:

Table 2.5. Parameters set for the ribbons production.

Crucible hole diameter [mm]	0,5
Distance between the wheel and the crucible [mm]	1
Velocity of the wheel [m/s]	40
Chamber pressure [mbar]	400
Injection pressure [mbar]	800

After the production of the alloy in the arc melter, we place the sample into the crucible which is located inside the chamber of the melt spinner. To do this, on top of the crucible we roll up a little bit of Teflon to keep the crucible in a piece of copper which is in the top of the chamber. Once we have done this, we screw the crucible, which is subject as we can see in Fig. 2.8.

Fig. 2.8 Crucible subjected in the melt spinner

After this, we lower the copper support with the crucible until the distance of the crucible and the wheel is 1 mm. Once this condition is fulfilled, we can close the door of the chamber to make the vacuum inside.
The first vacuum is obtained with the rotary pump, followed by high vacuum pump that can be used to obtain a pressure of 10^{-3} mbar. The removal of oxygen from the chamber is necessary to prevent oxidation of the metals during the melting process.
When we have achieved the desired pressure, we fill the chamber with an Ar atmosphere of 400 mbar. We also have to fill the tanks with Ar at a pressure of 800 mbar for the injection.
After that, we choose the desired speed of the wheel, in our case 40 m/s and we proceed to switch on the cooling circuit in order to avoid the damage of the pump and the induction coil.
At that time, we can switch on the induction furnace and proceed to melt the sample and inject it into the spinning wheel and, in that moment, we obtain the ribbons (see Fig. 2.9).
With the initial parameters, we obtain ribbons with a width between 1 and 2 mm and a thickness between 20 and 60 μm.

Fig. 2.9 Ribbon obtained with the melt spinner

The results obtained in the melt spinner can be seen in tables 2.6, 2.7, 2.8 and 2.9.

Table 2.6. Results for pure copper samples after the melt spinning process.

PURE COPPER				
Ribbon	% Cu	%Zr	Temperature of injection[ºC]	Comments
1	63,5	36,5	1610	It has not injected in the first attempt. We have raised the crucible and reaching 1610ºC it has injected (in the second attempt) but not immediately, we have waited for, approximately, 3 seconds. Quality of the ribbon: Very short and very thin. There is quite a lot of mass stuck inside the crucible.
2	64,5	35,5	1580	It has not injected in the first attempt. We have raised the crucible and reaching 1510ºC it has injected (in the second attempt). Quality of the ribbon: Very short and very thin. There is quite a lot of mass stuck inside the crucible.
3	65,5	34,5	1210	We have injected without problems. Quality of the ribbon: good and of a considerable width. No mass without injecting.

Table 2.7. Results for the type 1 of recycled copper samples after the melt spinning process.

RECYCLED COPPER. TYPE 1				
Ribbon	% Cu	%Zr	Temperature of injection[ºC]	Comments
1	63,5	36,5	1260	We have injected without problems. Quality of the ribbon: very good and of a considerable width. No mass without injecting
2	64,5	35,5	1571	We have injected without problems. Quality of the ribbon: good and of a considerable width. No mass without injecting.
3	65,5	34,5	1502	We haven't injected until the third attempt. Quality of the ribbon: good although we have obtained a very few pieces. There is quite a lot of mass stuck inside the crucible.

Table 2.8. Results for the type 2 of recycled copper samples after the melt spinning process.

RECYCLED COPPER. TYPE 2				
Ribbon	% Cu	%Zr	Temperature of injection[ºC]	Comments
1	63,5	36,5	1300	We have injected without problems. Quality of the ribbon: good but some pieces of the ribbon are very thin. No mass without injecting.
2	64,5	35,5	1350	We have injected without problems. Quality of the ribbon: very good and of a considerable width. There is quite a lot of mass stuck inside the crucible.
3	65,5	34,5	1280	We have injected without problems. Quality of the ribbon: good and of a considerable width. No mass without injecting.

Table 2.9. Results for the type 3 of recycled copper samples after the melt spinning process.

RECYCLED COPPER. TYPE 3				
Ribbon	% Cu	%Zr	Temperature of injection[ºC]	Comments
1	63,5	36,5	1300	We have injected without problems. Quality of the ribbon: good, of a considerable width and in a huge quantity. No mass without injecting. Note: the pyrometer has stopped working for a few seconds.
2	64,5	35,5	1280	We have injected without problems. Quality of the ribbon: very good and of a considerable width. There is quite a lot of mass stuck inside the crucible.
3	65,5	34,5	1270	We have injected without problems. Quality of the ribbon: good, but some pieces are very thin. No mass without injecting.

After making the ribbons, we proceed to weigh them in order to determine the amount of mass that they have lost in the melt spinning process. These results are summarized in the following tables:

Table 2.10. Relative error between the samples after the arc melting and after the melt spinning for the pure copper samples.

PURE COPPER						
Ribbon	%Cu	%Zr	Mass before melt spinner [g]	Mass after melt spinner [g]	Relative error	Mass of Cu-Zr remains (if any) [g]
1	63,5	36,5	3,998	0,8623	78,4317	-
2	64,5	35,5	3,9945	2,098	47,4778	-
3	65,5	34,5	3,9999	2,8972	27,5682	0,1213

Table 2.11. Relative error between the samples after the arc melting and after the melt spinning for the type 1 of the recycled copper samples.

RECYCLED COPPER. TYPE 1						
Ribbon	%Cu	%Zr	Mass before melt spinner [g]	Mass after melt spinner [g]	Relative error	Mass of Cu-Zr remains (if any) [g]
1	63,5	36,5	4,8402	3,379	30,18887	-
2	64,5	35,5	4,1692	3,5941	13,794	-
3	65,5	34,5	4,3807	0,2202	94,97340	4,4191

Table 2.12. Relative error between the samples after the arc melting and after the melt spinning for the type 2 of the recycled copper samples.

RECYCLED COPPER. TYPE 2						
Ribbon	%Cu	%Zr	Mass before melt spinner [g]	Mass after melt spinner [g]	Relative error	Mass of Cu-Zr remains (if any) [g]
1	63,5	36,5	4,258	2,8788	32,3908	-
2	64,5	35,5	4,8561	3,7103	23,5951	-
3	65,5	34,5	4,5731	3,1487	31,1474	-

Table 2.13. Relative error between the samples after the arc melting and after the melt spinning for the type 3 of the recycled copper samples.

RECYCLED COPPER. TYPE 3						
Ribbon	%Cu	%Zr	Mass before melt spinner [g]	Mass after melt spinner [g]	Relative error	Mass of Cu-Zr remains (if any) [g]
1	63,5	36,5	4,3524	4,341	0,2619	-
2	64,5	35,5	4,2805	2,8282	33,9283	-
3	65,5	34,5	4,9329	4,0823	17,2434	-

Regardless of the ribbons that have some sort of error in the injection, we calculate the average relative error between before passing the sample through the melt spinner and after doing so, obtaining an average loss of mass of 25,7596 %.

From this data, we determine that, in comparison with the arc melter, this technique is much less efficient, since in the arc melter the samples barely lost mass but when we have made the ribbons, it has remained some useless material in a shape of small cones (attached to the crucible) or wire-shaped particles of a very small thickness.

CHAPTER 3. ANALYSIS OF STRUCTURAL AND CHEMICAL PROPERTIES

3.1. XRD

Max von Laue, in 1912, realized that a crystalline sample would cause the X-ray to diffract as the interatomic distance in a crystalline structure is of the same order as the wavelength of the X-ray. Although the X-ray photons typical energy is between 100eV and 100keV in X-ray diffraction a shorter wavelength is used and the energy of these X-rays is between 1keV and 120keV.

X-ray powder diffraction (XRD) is, then, a rapid analytical technique primarily used for the identification of crystalline compounds by their diffraction pattern. From these patterns it can be determined the crystalline phases present in various materials in solid or powder form.

Other applications of XRD are listed in the table 3.1:

Table 3.1. XRD applications [32]

XRD APPLICATIONS
Characterization of crystalline materials
Identification of fine-grained minerals such as clays and mixed layer clays that are difficult to determine optically
Determination of unit cell dimensions
Measurement of sample purity
Determination of crystal structures using Rietveld refinement
Determination of modal amounts of minerals (quantitative analysis)
Characterization of thin ribbons samples by: - Determining lattice mismatch between film and substrate and to inferring stress and strain - Determining dislocation density and quality of the film by rocking curve measurements - Measuring super lattices in multi-layered epitaxial structures - Determining the thickness, roughness and density of the film using glancing incidence X-ray reflectivity measurements
Making textural measurements, such as the orientation of grains, in a polycrystalline sample

An explanation of the XRD instrumentation and physical basis is placed in annex 5.

3.1.1. Diffraction patterns

As each crystalline material has its characteristic atomic structure, it will scatter the X-ray in a unique way.

Varying the angle of incidence, it is originated a characteristic diffraction spectrum of the sample.
A typical diffraction spectrum for a crystalline sample (see Fig. 3.1) is a graph showing the relationship between reflected intensities and the observed angle (2θ). The small accentuated peaks show that the sample analysed is crystalline.

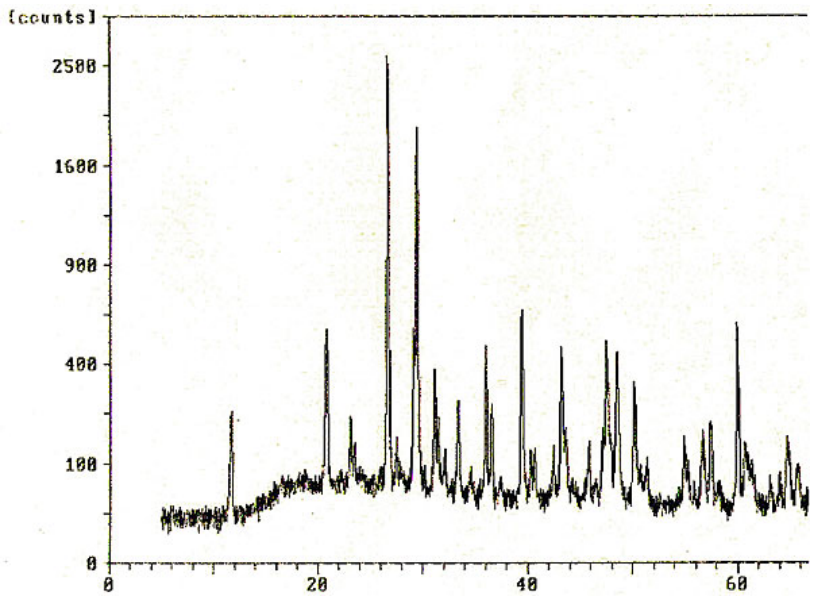

Fig 3.1 A crystalline XRD pattern [33]

On the other hand, if we analyse an amorphous sample, the scatter spectrum would look rather different (see Fig. 3.2).
In an amorphous material, the atoms are randomly distributed and, therefore, the interatomic distances that separate the atoms are extremely variable and well- defined atomic planes do not exist. Given this fact, then the Bragg law is not fulfilled, because the wavelength of the incident ray, which is also monochromatic, must be related to the distance between atoms and the angle of diffraction. Therefore, the constructive interference will not exist in an amorphous sample and, as a result, peaks in the diffraction spectrum are not distinguished.

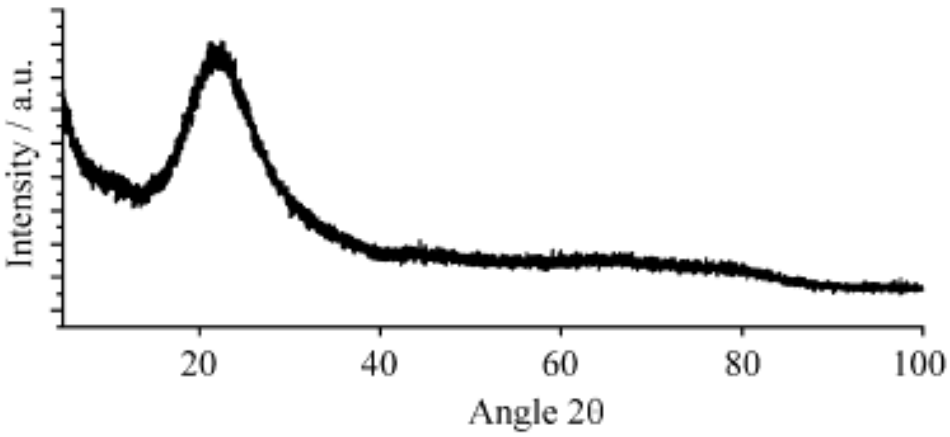

Fig. 3.2 An amorphous XRD pattern [34]

3.1.2. XRD Results

We need to know if the ribbons that we have produced are amorphous or not. In order to know it, we have studied the ribbons with the x-ray diffraction (XRD) technique. The analysis was made in the Centre of Research in NanoEngineering (CRNE) located in Barcelona, Spain.
The diffractometer used for the XRD is the Bruker D8 Advance (see Fig. 3.3).

Fig. 3.3 Diffractometer Bruker D8 Advance [35]

The data generated with the diffractometer have been obtained as a text file so, in order to represent them as a diffraction pattern, we have used MATLAB.
The code used to plot the graphs can be found in annex 10.

From Fig. 3.4. to Fig. 3.7 we can see the diffraction pattern of the twelve ribbons that we have produced, grouping the patterns by the four types of copper used for the project.

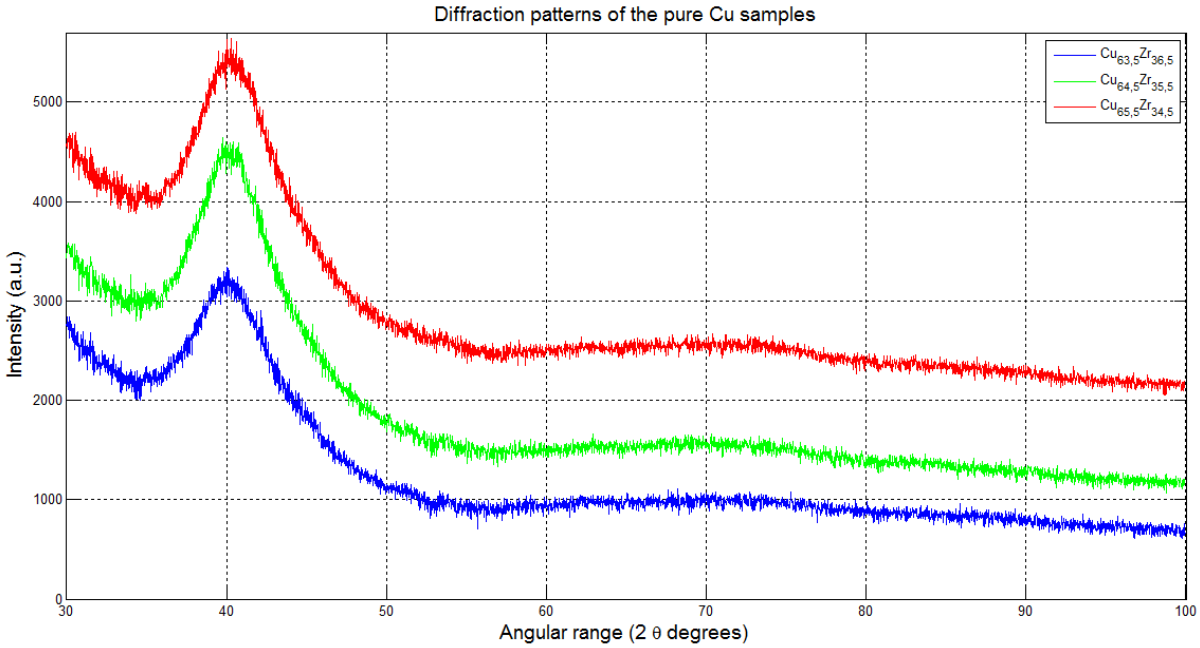

Fig 3.4 Diffraction of the pure Cu samples

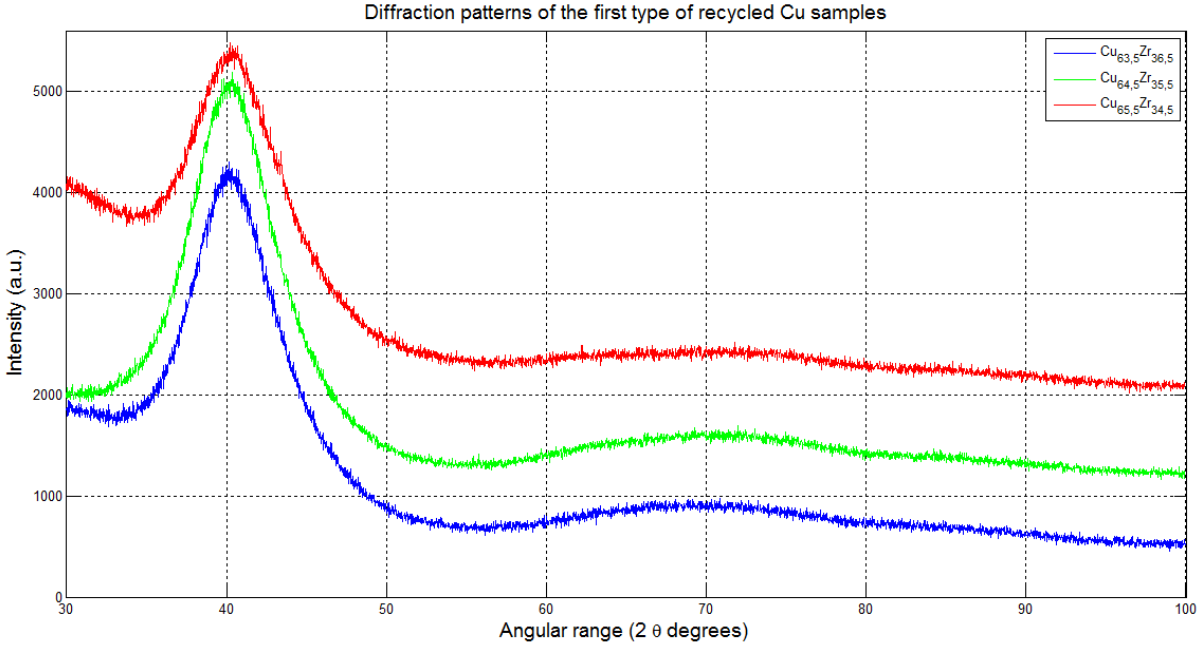

Fig. 3.5 Diffraction of the first type of recycled Cu samples

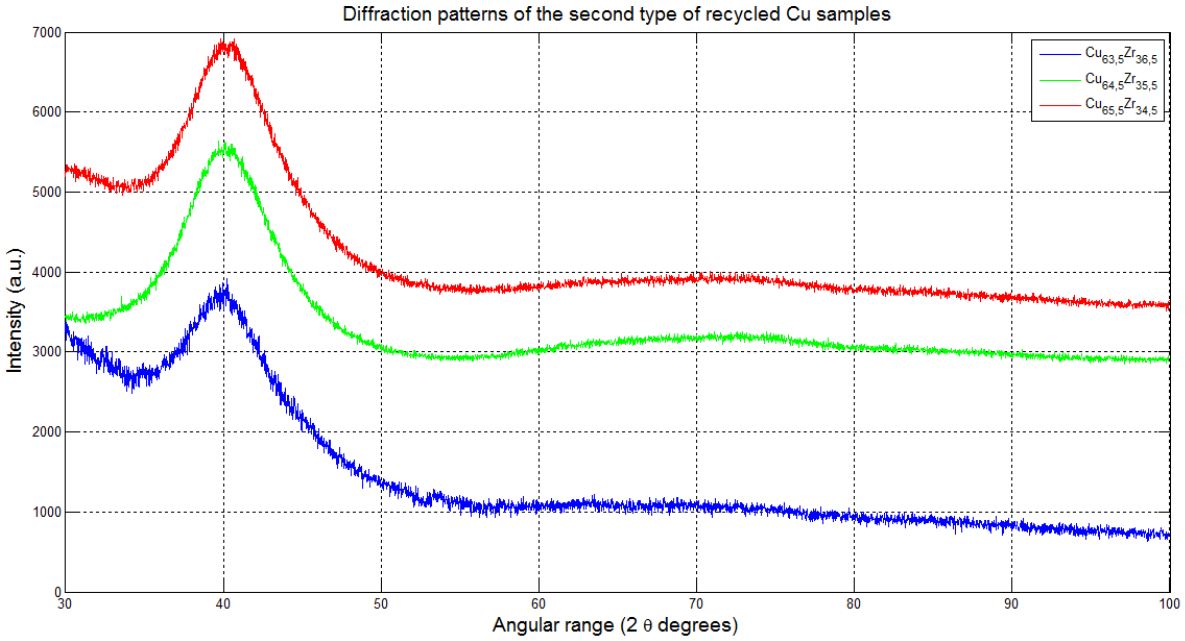

Fig 3.6 Diffraction of the second type of recycled Cu samples

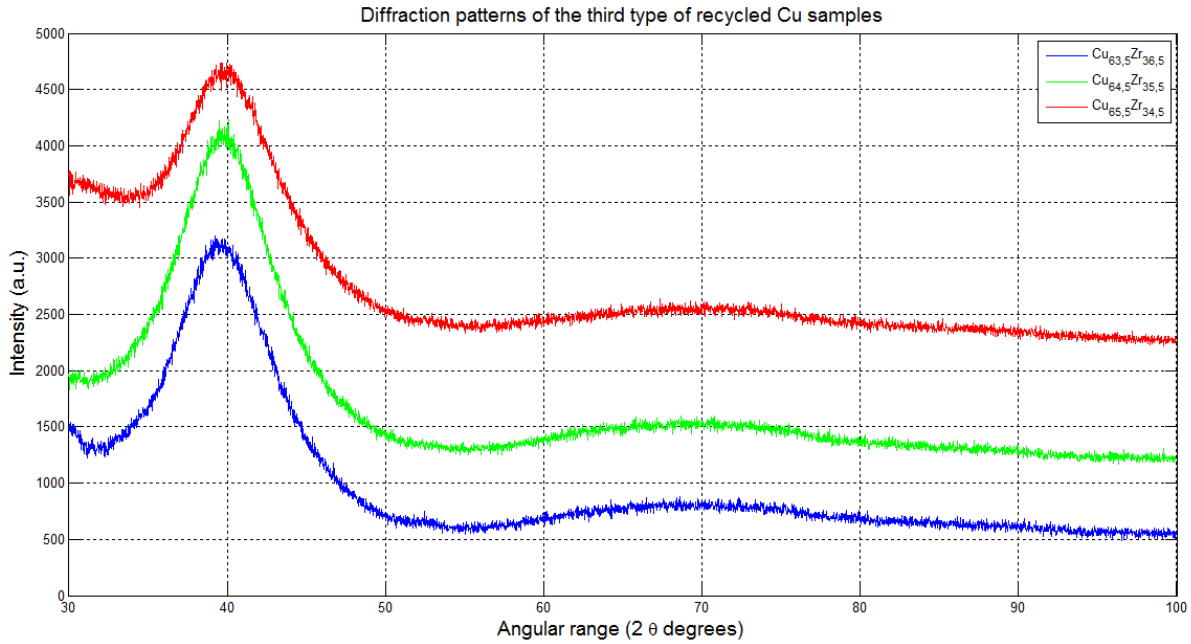

Fig. 3.7 Diffraction of the third type of recycled Cu samples

In the above figures we can observe the radiation pattern for the four types of copper. These graphs show the refracted beam intensity versus the angle of incidence of the beam on the sample.
We can clearly see the absence of well-defined peaks in all graphs which mean that there is no existence of a crystalline phase in any of the samples.

Moreover, all of the patterns have a broad peak which means that all the ribbons that we have produced are amorphous.
From this fact we can conclude that with this technique, at very high cooling rates, we can obtain metallic glasses and, also, that we do not need to use pure materials in order to obtain amorphous materials.

3.2. SEM

The Scanning Electron Microscope (SEM) is an electronic microscope that was developed at the University of Cambridge in 1951. Unlike an optical microscope, which uses photons of the visible spectrum, the image presented by the SEM is generated by the interaction of an electron beam, narrow and well defined, that sweeps horizontally a given area over the surface of the sample.

The main advantages are its high resolution (~100 Å), the large depth of field that gives three-dimensional look to the images captured and simple sample preparation, since they only need to be, or become, electrically conductive [36].

Regarding the applications of the SEM, in the field of materials, we can detail the following:

Table 3.2. SEM applications [37]

SEM APPLICATIONS
Microstructural characterization of materials
Identification, analysis of crystalline phases and phase transitions in various materials such as metals, ceramics, composites, semiconductors polymers and minerals.
Surface composition and grain size.
Assessment of deterioration of materials.
Determining the degree of crystallinity and defects presence.
Identification of the type of degradation, fatigue, corrosion, embrittlement, etc.

An explanation of the SEM instrumentation and physical basis can be found in annex 6.

3.2.1. Chemical analysis of the recycled copper

As we have said in the introduction part, the composition of the different recycled copper samples was unknown to us until the ribbons have been analysed in the SEM, thus we can get an idea of what is the composition of the recycled copper used in the production of our samples.
The only thing we knew is that each type of copper had more impurities than the previous one, so we have labelled them in our project as type 1, 2 and 3

Before analysing all the ribbons in the SEM, we have sent a sample of each type of recycled copper to the Max-Planck-Institut für Eisenforschung GmbH (MPIE), situated in Düsseldorf, Germany in order to perform a chemical analysis to discover which are the elements for each type of recycled copper, obtaining the following results:

Table 3.3. Composition of the three types of recycled copper in percent by weight.

Cu Type	C	Cu	Fe	N	Ni	O	P	Pb	S	Sn	Zn
1	0,0057	Bal.	0,053	0,0013	0,081	0,015	<0,01	0,33	0,042	0,41	0,12
2	<0,001	Bal.	<0,005	0,0014	0,43	0,0032	1,20	1,39	0,031	1,89	0,03
3	<0,001	Bal.	0,0057	0,0019	0,38	0,025	<0,01	4,84	0,016	5,69	0,68

3.2.2. SEM results

In our case, the method used for the determination of the chemical composition of the sample is the EDS (Energy Dispersive Spectroscopy) which is a chemical microanalysis technique that detects the emitted X-ray when the sample is excited by an electron beam. Thus, we can characterize the elemental composition of the sample analysed.

This analysis was made in the Centre of Research in NanoEngineering (CRNE) located in Barcelona, Spain. The microscope used for the SEM is the Zeiss Neon 40 (see Fig. 3.8).

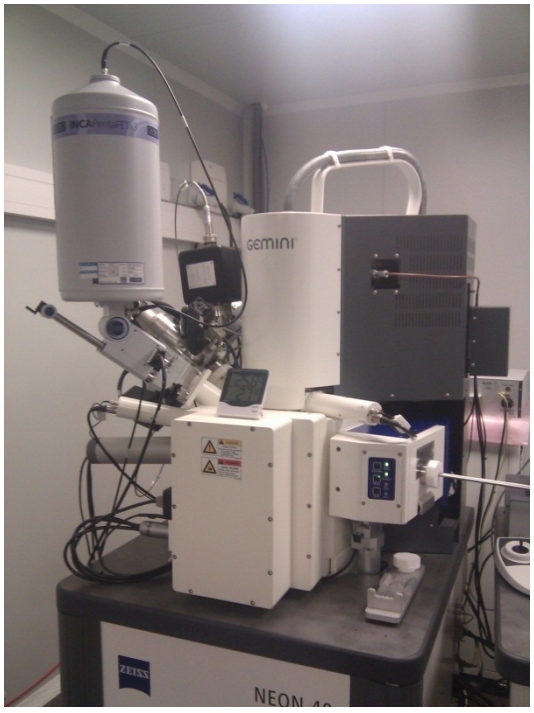

Fig. 3.8 Scanning Electron Microscope

As mentioned above, when a sample is bombarded by an electron beam, some electrons leave the atoms in the sample. This vacancy is occupied by an electron from the upper layer and the energy difference between one layer and the other is released by the emission of an X-ray.
The EDS X-ray detector measures the number of X-ray of a particular energy, which is characteristic of the element which has emitted the beam.
Finally, the energy spectrum is obtained on the relative values of all the detected X-ray (see Fig. 3.9) and it can be evaluated for qualitative and quantitative determination of the elements in the sample analysed.

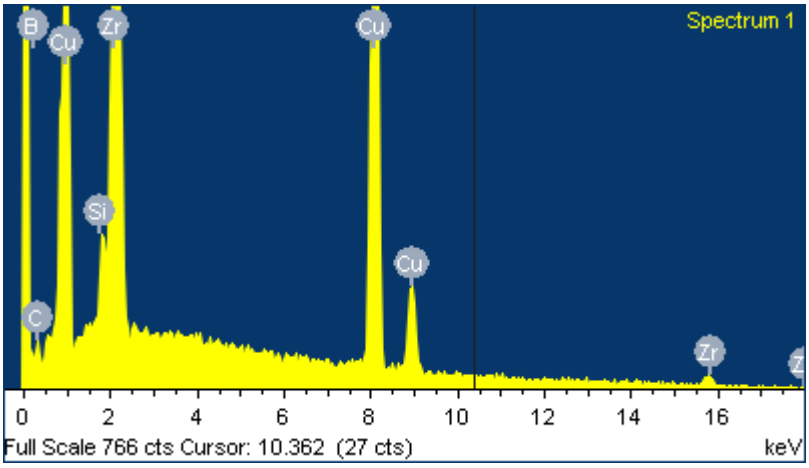

Fig. 3.9 EDS spectrum

We have analysed the twelve ribbons and we have obtained the weight percentage and the atomic percentage.
The next tables report the average of the weight and the atomic percentage. From the tables we can notice that, in the pure copper ribbons, the analyses show other elements apart from Cu and Zr, but the existence of these elements in these measures is not reliable because we know that the ribbons are only made by Cu and Zr.

Basically, it is necessary to subtract from the total weight the sum of the unreliable elements, and then to calculate the percentage that it represents relative to the total. The applied formula to calculate the total percentage composed only by the detected elements is the following one:

$$\%\ useful\ sample = \frac{Total - \sum(\%\ unreliable\ elements)}{Total} \cdot 100 \qquad \textbf{(3.1)}$$

The next step is to normalize the other components dividing the weight percentage of every useful element on the sample. The sum of the percentages has to be the same as the one at the beginning.
Finally, to obtain the atomic percentage of every element it is necessary to consider the atomic mass of each element dividing the weight percentage for

the atomic mass and normalizing it with the following expression for each element:

$$at\ \% = \frac{\frac{element\ weight\ \%_i}{element\ atomic\ mass_i}}{\sum_{i=1}^{n}\frac{element\ weight\ \%}{element\ atomic\ mass}} \cdot 100 \qquad \textbf{(3.2)}$$

The normalization is performed for the three ribbons of pure copper and, exceptionally, we normalize the results of the recycled copper ribbons if there are elements in the measures that we know they are impossible to find in there, in other words, that they are not listed in the chemical analysis performed at MPIE.
The rest of the elements which appear in the chemical analysis are obviously due to the non-purity copper and, therefore, they are not taken into account when we perform the normalization.

Table 3.4. Normalized percentages of the pure copper ribbons.

$Cu_{63,5}Zr_{36,5}$			$Cu_{64,5}Zr_{35,5}$			$Cu_{65,5}Zr_{34,5}$		
Element	Norm. Weight %	Atomic %	Element	Norm. Weight %	Atomic %	Element	Norm. Weight %	Atomic %
Cu	54,687	63,404	Cu	54,112	62,865	Cu	54,505	62,233
Zr	45,313	36,596	Zr	45,888	37,135	Zr	45,495	36,767

Finally we have to compare the normalized atomic percent obtained at the SEM and the theoretical atomic percent of the samples.

Table 3.5. Comparison between the normalized atomic percent obtained and the theoretical atomic percent of the samples

PURE COPPER RIBBONS		
Sample	Element	Relative error
$Cu_{63,5}Zr_{36,5}$	Cu	0,15150817
	Zr	0,2635827
$Cu_{64,5}Zr_{35,5}$	Cu	2,53533843
	Zr	4,60645996
$Cu_{65,5}Zr_{34,5}$	Cu	3,46105784
	Zr	6,57099387

From the table we can observe that $Cu_{63,5}Zr_{36,5}$ sample has a composition quite similar to the theoretical one, while the other samples are very different. There are two possibilities to explain this.

On the one hand, it can be due to non-homogeneity of the elements in the arc melting process.
This possibility is remote since, as it is well-shown in the results of the corresponding chapter, we have not lost mass when we melt the copper and the zirconium, and also two meltings were performed for each sample in order to assure that the two elements are homogeneously melted in the ball obtained.
On the other hand, this difference may be due to the lack of precision in the SEM to detect small variations in the atomic percentage of elements.
We consider this last reason the most consistent and what we should do to obtain more precision is to use another analysis technique as could be fluorescence.

The results of the recycled copper ribbons are listed below:

Table 3.6. Normalized percentages of the recycled copper type 1 ribbons.

$Cu_{63,5}Zr_{36,5}$			$Cu_{64,5}Zr_{35,5}$			$Cu_{65,5}Zr_{34,5}$		
Element	Norm. Weight %	Atomic %	Element	Norm. Weight %	Atomic %	Element	Norm. Weight %	Atomic %
Cu	52,949	61,767	Cu	54,045	62,801	Cu	56,607	65,341
Zr	47,051	38,233	Zr	45,955	37,199	Zr	42,145	33,887
						Sn	1,248	0,771

The model of SEM that we have used to find out the composition of the ribbons does not detect the elements which are present in the copper in less than 1% in percent by weight, this is why we only expect to find copper and zirconium in recycled copper type 1 ribbons and this is what we have found in $Cu_{63,5}Zr_{36,5}$ and $Cu_{64,5}Zr_{35,5}$ribbons. In the $Cu_{65,5}Zr_{34,5}$ ribbon, we have also found tin which is coherent as recycled copper type 1 contains this element and, moreover, this ribbon is the one which has the most amount of copper and, therefore, it is more possible to find in this composition the other elements which are present in the recycled copper.

Table 3.7. Normalized percentages of the recycled copper type 2 ribbons.

$Cu_{63,5}Zr_{36,5}$			$Cu_{64,5}Zr_{35,5}$			$Cu_{65,5}Zr_{34,5}$		
Element	Norm. Weight %	Atomic %	Element	Norm. Weight %	Atomic %	Element	Norm. Weight %	Atomic %
Cu	52,215	61,183	Cu	52,091	61,058	Cu	52,598	61,589
Zr	46,793	38,194	Zr	46,979	38,359	Zr	46,063	37,572
Sn	0,993	0,623	Sn	0,929	0,583	Sn	1,339	0,839

Recycled copper type 2 contains more impurities than recycled copper type 1, this is why we have found tin in the analysis for all the compositions. In addition, tin is present in the recycled copper in more than 1% by weight, so it is normal that we find it in the analysis we have performed in the SEM.

Table 3.8. Normalized percentages of the recycled copper type 3 ribbons.

$Cu_{63,5}Zr_{36,5}$			$Cu_{64,5}Zr_{35,5}$			$Cu_{65,5}Zr_{34,5}$		
Element	Norm. Weight %	Atomic %	Element	Norm. Weight %	Atomic %	Element	Norm. Weight %	Atomic %
Cu	49,1	58,475	Cu	49,686	59,074	Cu	52,697	62,252
Zr	47,248	39,197	Zr	46,434	38,457	Zr	42,445	34,928
Sn	3,652	2,328	Sn	3,88	2,47	Sn	3,822	2,417
						Pb	1,006	0,364
						Ni	0,307	0,039

Recycled copper type 3 is the one which has more impurities of all the types of copper. This can also be observed in the results: all the compositions shows tin in greater proportion and, for the $Cu_{65,5}Zr_{34,5}$ we detect lead and nickel. The reason is the same as when we have detected tin in the $Cu_{65,5}Zr_{34,5}$ for recycled copper type 1: this composition is the one which contains more copper and, therefore, it is the most expected composition to find elements contained in the recycled copper.

CHAPTER 4. MECHANICAL AND THERMAL CHARACTERIZATION

For the mechanical characterization we use micro indentation hardness testing and, for the thermal characterization, we use Differential Scanning Calorimetry (DSC).

4.1. Microindentation hardness testing

Micro indentation hardness testing of metals, ceramics, and composites is useful for a variety of applications for which “macro” hardness measurements are unsuitable: testing very thin materials like foils, measuring individual microstructures within a larger matrix, or measuring the hardness gradients of a part along the cross section [38].

Microhardness testing per ASTM E-384 (Standard Test Method for Microindentation Hardness of Materials) gives an allowable range of loads for testing with a diamond indenter; the resulting indentation is measured and converted to a hardness value. The actual indenters used are Vickers, a square based diamond pyramid with an apical angle of 136° and the most common, or Knoop which is a narrow rhombus shaped indenter.

The result for either Vickers or Knoop microhardness is reported in kg/cm^2 and is proportional to the load divided by the square of the diagonal of the indentation measured from the test.

4.1.1. Vickers hardness test

The Vickers hardness test method consists of indenting the test material with a diamond indenter, in the form of a right pyramid with a square base and an angle of 136 degrees between opposite faces subjected to a load of 1 to 100 kgf (9,81 to 981 N)[1]. The full load is normally applied for 5 to 15 seconds. The two diagonals of the indentation left in the surface of the material after removal of the load are measured using a microscope and their average calculated. The area of the sloping surface of the indentation is calculated [39]
The Vickers test methods are defined in the following standards: ASTM E384 for micro force ranges from 10gf to 1kgf (from 9,81 N to 981 N), ASTM E92 for macro force ranges from 1kgf to 100kgf (from 0,0981 N to 9,81 N) and ISO 6507-1, 2, 3 for micro and macro ranges [40].

[1]The forces on the Vickers test section are expressed in kgf because it is what its corresponding standard provides. Because in academic area it is common to express measurements in SI units, the forces are also expressed in newtons [N].

4.1.1.1. Vickers test method

As we have mentioned above, all Vickers ranges use a 136° pyramidal diamond indenter that forms a square indent (see Fig. 4.1).
The procedure to do the indentation is as follows:
- The indenter is pressed into the sample by an accurately controlled test force.
- The force is maintained for a specific dwell time, normally 5 – 15 seconds.
- After the dwell time is complete, the indenter is removed leaving an indent in the sample that appears square shaped on the surface.
- The size of the indent is determined optically by measuring the two diagonals of the square indent.

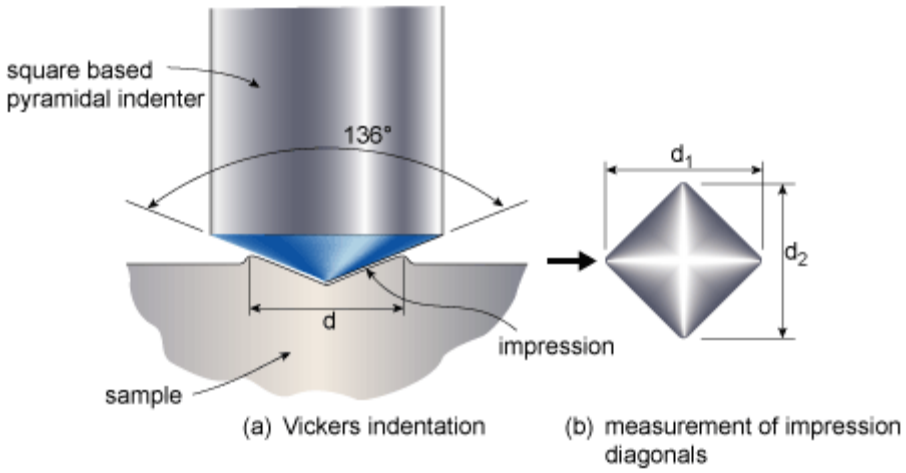

Fig. 4.1 The square based diamond pyramid Vickers hardness indenter and sample indentation [41]

- The Vickers hardness number is a function of the test force divided by the surface area of the indent and it can be calculated with the following formula:

$$HV = \frac{2 \cdot F \cdot \sin\frac{136^{\circ}}{2}}{d^2} \approx 1{,}854 \cdot \frac{F}{d^2} \qquad \textbf{(4.1)}$$

Where:
HV = Vickers hardness
F= Applied load [kgf]
d= Arithmetic mean of the two diagonals, d1 and d2 [mm]

The advantages of the Vickers hardness test are that extremely accurate readings can be taken and that just one type of indenter is used for all types of metals and surface treatments [42].

Knoop hardness test basis and a comparison between both Vickers and Knoop can be seen in annex 7.

4.1.2. Microindentation hardness results

First, in order to do the micro indentation hardness test we choose the ribbons produced with the highest GFA, which means the ribbons with the composition $Cu_{64,5}Zr_{35,5}$.
We use a Vickers indenter to perform the test and we do it with a Duramin 5 microhardner (see Fig. 4.2).

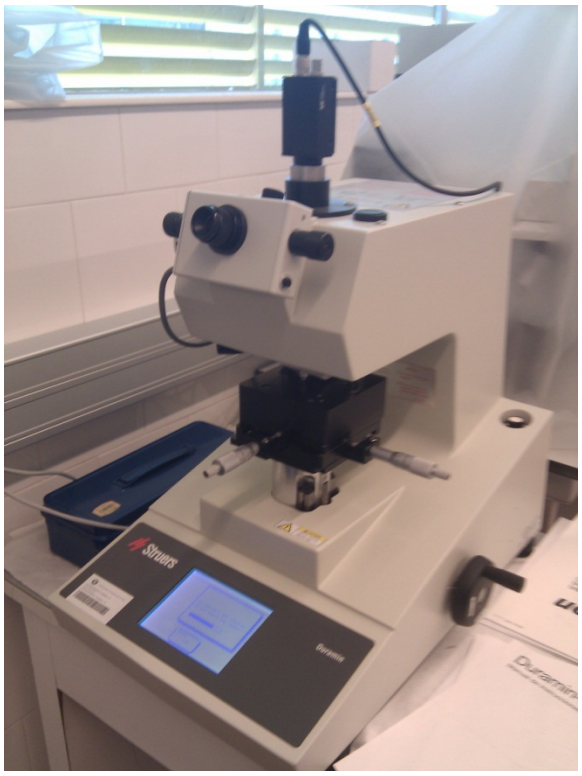

Fig 4.2 Duramin 5 microhardner.

For analysis of the hardness of the ribbons used in the micro hardness test we have used common parameters, in all of them, which are:
Press load: 245,3 mN.
Press time. 5 s.
Objective: x40.

The procedure for making the indentation in the Duramin 5 is very simple:

- Firstly, we measured the thickness of the ribbons to control that the impression made by the indenter does not exceed the thickness of the ribbon used.
- We place the sample, in this case the ribbon, on the base below the objective of the microhardner, we set the objective of x40 and we focus until we obtain a sharp image of the surface of the sample.
- We click on the 'Indent' button and automatically the indenter rotates to where the objective was. Now, the program lowers the indenter on the surface (the selected force and dwell time are the defined ones).

- Once the indentation has been done, we click on the 'Change to objective' button and the objective is automatically placed on the sample, and we will be able to see the impression made by the indenter.
- We click on the lines of screen and we drag one to one of these lines to the vertices of the impression made in the ribbon.

The length of the diagonals of the prints and hardness values are displayed in real time on the lower right corner of the window (see Fig. 4.3)

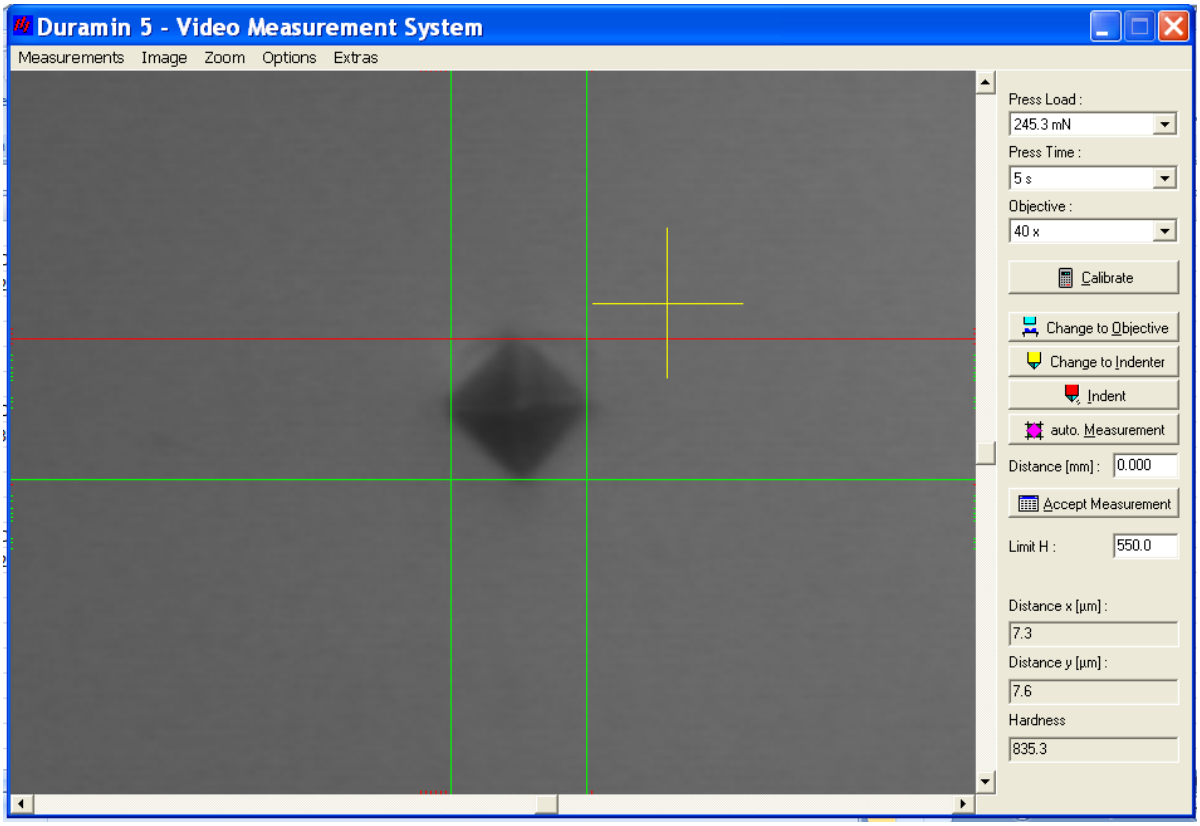

Fig 4.3 Duramin 5 software.

For our results, we perform ten indentations in different parts of the ribbon analysed and, then, we calculate the average harness and the standard deviation of these results, as it is shown in annex 7.

Then we perform the graphical representation of the data in the table as a diagram with error bars in MATLAB.

The code used to plot the diagram is placed in annex 10, and we obtain the following graph (see Fig. 4.4):

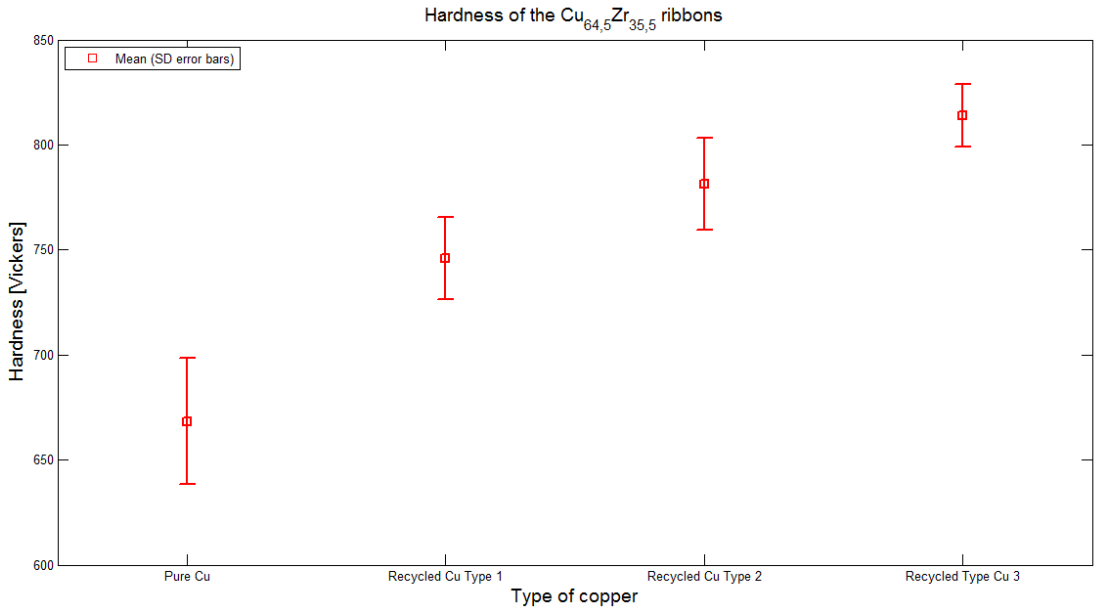

Fig. 4.4 Variation in hardness depending on the type of copper used.

In the diagrams with error bars, for each group which forms the diagram, a dot is plotted which represents the mean of a continuous variable. Around the dot error bars are placed, whose length can be defined by various statistics as, for example, standard deviation, the standard error of the mean or a confidence interval for the mean. In our case we use standard deviation as it gives us information of the error when we perform different measures of the same thing.
The main advantage of this kind of graphs is that allows us to perform a formal approximated statistical comparison of the groups analysed by the graphical representation [43].
The figure above shows the standard deviations and error bars for the variable "Hardness, in Vickers units" for the four types of copper used in our project.
Among other things, we notice that the error bars are shorter for recycled copper types 1 and 3 than for the pure copper and recycled copper type 2, indicating that the accuracy of the estimation is greater in the first ones.

But the most important thing we notice is that the error bars are shorter enough to see that, actually, the hardness of the ribbons has a growing trend or, what is the same, the hardness increases with the type of copper used: the more impurities in the copper, the harder the ribbon.

4.2. Differential Scanning Calorimetry

Differential Scanning Calorimetry (DSC) is one of the most frequently employed Thermal Analysis methods. It allows analysing the thermodynamic evolution of a sample of a certain material according to time or temperature.
The technique was developed by E.S. Watson and M.J. O'Neill in 1962, and introduced commercially at the 1963 Pittsburgh Conference on Analytical Chemistry and Applied Spectroscopy [44].

DSC has several applications and the most important are listed in table 4.1.

Table 4.1. DSC applications [45]

DSC APPLICATIONS
Determination of: - Melting/crystallization behaviour - Solid-solid transitions - Polymorphism - Degree of crystallinity - Glass transitions - Cross-linking reactions - Oxidative stability - Purity determination - Specific heat - Thermokinetics

4.2.1. Calorimeter

DSC analysis is performed with a calorimeter, which requires, besides the sample under analysis, a sample which will be used as a pattern for the analysis called “reference sample”.

The reference sample must meet a number of features in order to not distort the measurements: it should not experience thermal processes in the interval of temperature studied; it should not have to react with the pan or with the thermocouples and its thermal conductivity should be similar to the thermal conductivity of the sample. This is why we generally use an empty pan.

The sample preparation is very important to reduce thermal resistance in the sensor equipment, thus avoiding temperature gradients within the sample and the consequent failure of the recorded signal. For this reason, the samples must fit perfectly at the bottom of the crucible. Therefore, it is often necessary to cut the samples in the smallest possible pieces before putting them in the pan. Then we have to seal the crucible with a lid.

The calorimeter operation is based on measuring the heat flux that is contributed to the sample. This heat flux is variable and is provided by the calorimeter to ensure that the difference of temperature between the sample analysed and reference sample is zero, while the temperature of the cell where the samples are is increased linearly [46].
A basic outline of the calorimeter assembly is presented in Fig. 4.5:

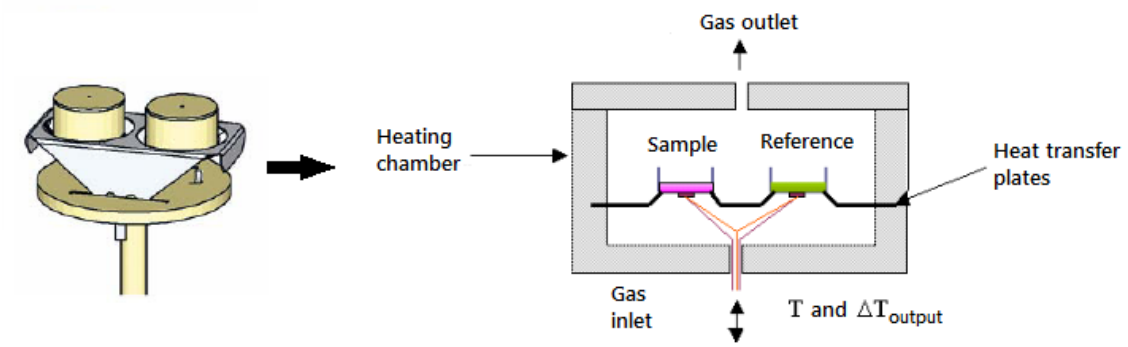

Fig. 4.5 Calorimeter assembly [47]

As it is necessary to increase the temperature of the sample in order to perform the analysis, it is expected that it can experiment an oxidative process that can alter the results. To avoid this phenomenon, it is commonly used an oxygen-free gas such as nitrogen or argon, forming a protective atmosphere around the sample.

As a result of the DSC analysis we obtain a graph of power per unit mass (heat flux delivered to the sample with a known mass) depending on temperature, called "DSC curve"

4.2.2. DSC results

First, in order to perform the DSC analysis, we choose the ribbons produced with the theoretically highest GFA, which means the ribbons with the $Cu_{64,5}Zr_{35,5}$ composition

The equipment used for the analysis is the NETZSCH DSC 404 F3 Pegasus (see Fig. 4.6).

Fig 4.6 DSC equipment NETZSCH DSC 404 F3 Pegasus

Before the DSC performs the analysis of the ribbons, we previously have had to follow all the steps and we have had to enter all the parameters demanded by the equipment as we have specified in annex 9.
Once the analysis of all the ribbons is performed, we have to evaluate the resulting data with the DSC 404 F3 Pegasus software.

In our case, the DSC curves obtained for each type of copper are the following ones:

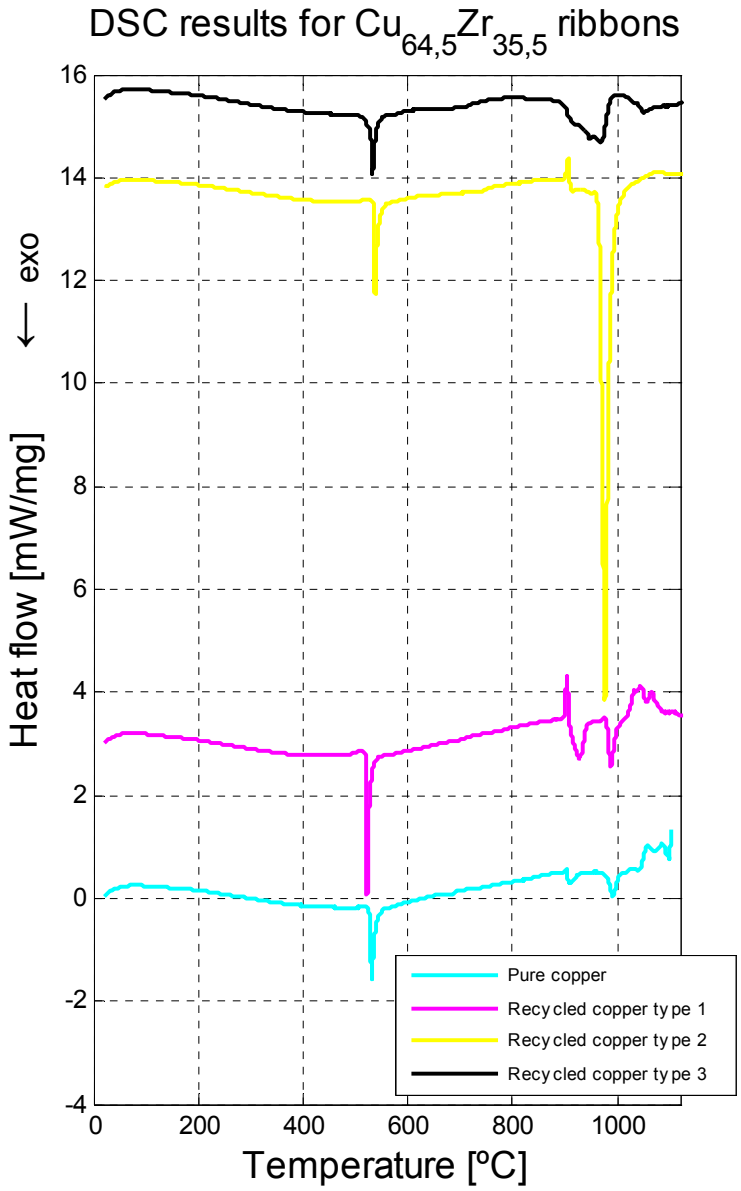

Fig 4.7 DSC curves obtained

And the determination of the temperatures of interest, which are explained in annex 8, are listed in table 4.2.

Table 4.2. Temperatures obtained with DSC software

		Pure Cu	**Recycled Cu Type 1**	**Recycled Cu Type 2**	**Recycled Cu Type 3**
Glass transition	Tg on set [K]	626,1	760,3	699,6	682,2
Crystallization	T_c [K]	800,6	794,8	809,2	803,3
Melting	T_m [K]	1173,4	1172,2	1174,4	1170,6
T_g/T_m	T_{rg}	0,534	0,649	0,596	0,583

As we mentioned in chapter 1, one of the most important factors to take into account to obtain an amorphous material is the GFA and to characterize it we can use the reduced glass transition T_{rg} [48, 49].

In our case, observing table 4.2, we see that we have obtained good values of T_g/T_m close to 0,6 or even higher than this value.
Moreover, the conclusion we can extract is that a small amount of impurities improves the GFA, as T_{rg} for recycled Cu type 1 is greater than for pure Cu. Whereas, too many impurities are counterproductive although still result in a higher GFA than the corresponding for pure Cu. This is consistent with many known experimental results which report that small additions of an element (between 1% and 5 at.%) improve the GFA [50].

CHAPTER 5. PRODUCTION OF RODS

For alloys with very good capacity of vitrification, such as the ones used in our thesis, production techniques with lower cooling rates can be used, thus obtaining pieces with thicknesses of mm or even cm: the so-called bulk metallic glasses (BMG).

For this last part of our project, we proceed to produce BMGs with the $Cu_{64,5}Zr_{35,5}$ composition by copper mold casting.

5.1. Copper mold casting technique

There are several techniques of injection in copper molds, which allow producing rod-shaped pieces of metallic glasses with different diameters (see Fig. 5.1).

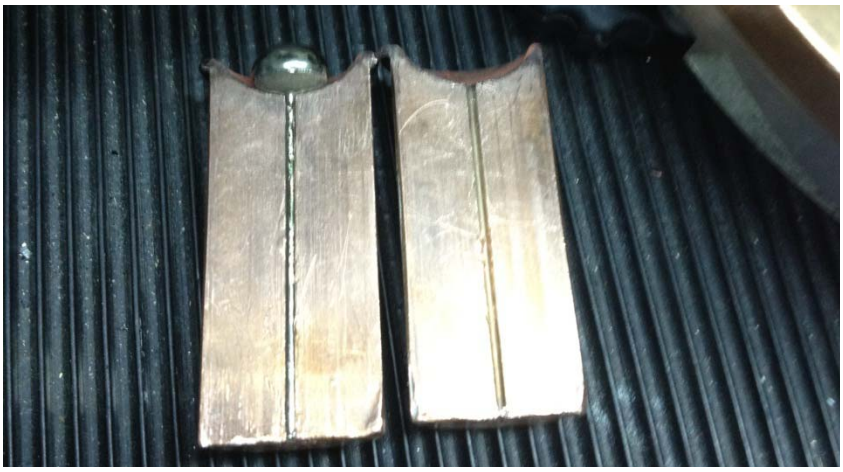

Fig. 5.1 A cylindrical rod of 1 mm of diameter of a metallic glass obtained by suction of the molten metal in an arc furnace.

The melting of the alloy is made in induction furnaces or arc furnaces and the injection is produced by applying pressure or, by the suction of the alloy from below, as it is in our case. In general, a high-purity argon atmosphere is used and copper molds can be cooled with water.

Cu-Zr rods with a composition of $Cu_{64,5}Zr_{35,5}$ were prepared in arc melting in a Ti-gettered high purity Ar atmosphere by the suction casting technique with a copper mold with a cylindrical cavity of 1 mm.
To obtain the $Cu_{64,5}Zr_{35,5}$ rods, we produce Cu-Zr balls with this composition between 1 g and 1,5 g in the arc melter. The procedure for using the arc melter is the same as explained in chapter 3, except for the following:

- The base where we put the alloy is different. In this case we use a base with a hole in the centre, where we introduce a copper mold.
- Below the copper base we couple a suction adaptor.
- Before the three purges we used to do in the arc melter, we make a vacuum in the tank (see Fig. 5.2): we open the vacuum valve of the arc melter until we reach to -1.0 bars and, then, we open the red valve behind the arc melter and wait about five minutes. After this time, we can proceed to make the same three purges we did when we produced the Cu-Zr balls.
- The working pressure is, in this case, 0,3 bar to increase the suction force.
- When we melt the metals, we have to turn up the intensity of the arc melter progressively from 3 to 8. Once at 8, we have to open the suction valve while we rapidly switch off the arc melter.

Fig. 5.2 Tank and red valve of the arc melter

We focus on the production of pure copper rods and recycled copper type 1 rods with the $Cu_{64,5}Zr_{35,5}$ composition. The choice is simple: pure copper because rods may be amorphous as they are produced with Cu and Zr of high purity and will serve us as a reference again and recycled copper type 1 rods because we have obtained the best T_g/T_m ratio for this type of copper.
We will produce rods until we cover the necessary 1 cm^2 of surface of each type needed for the XRD analysis.
The common parameters for the rods production are:

- Mold diameter = 1 mm
- Number of purges = 3
- Duration of the first vacuum (for the suction tank) = 5 min.
- Pressure inside the chamber = 0,3 bar (positive).
- Intensity of the arc = between 7 and 8.

5.2. XRD Results

After taking the rods to XRD, the result can be seen in Fig. 5.3

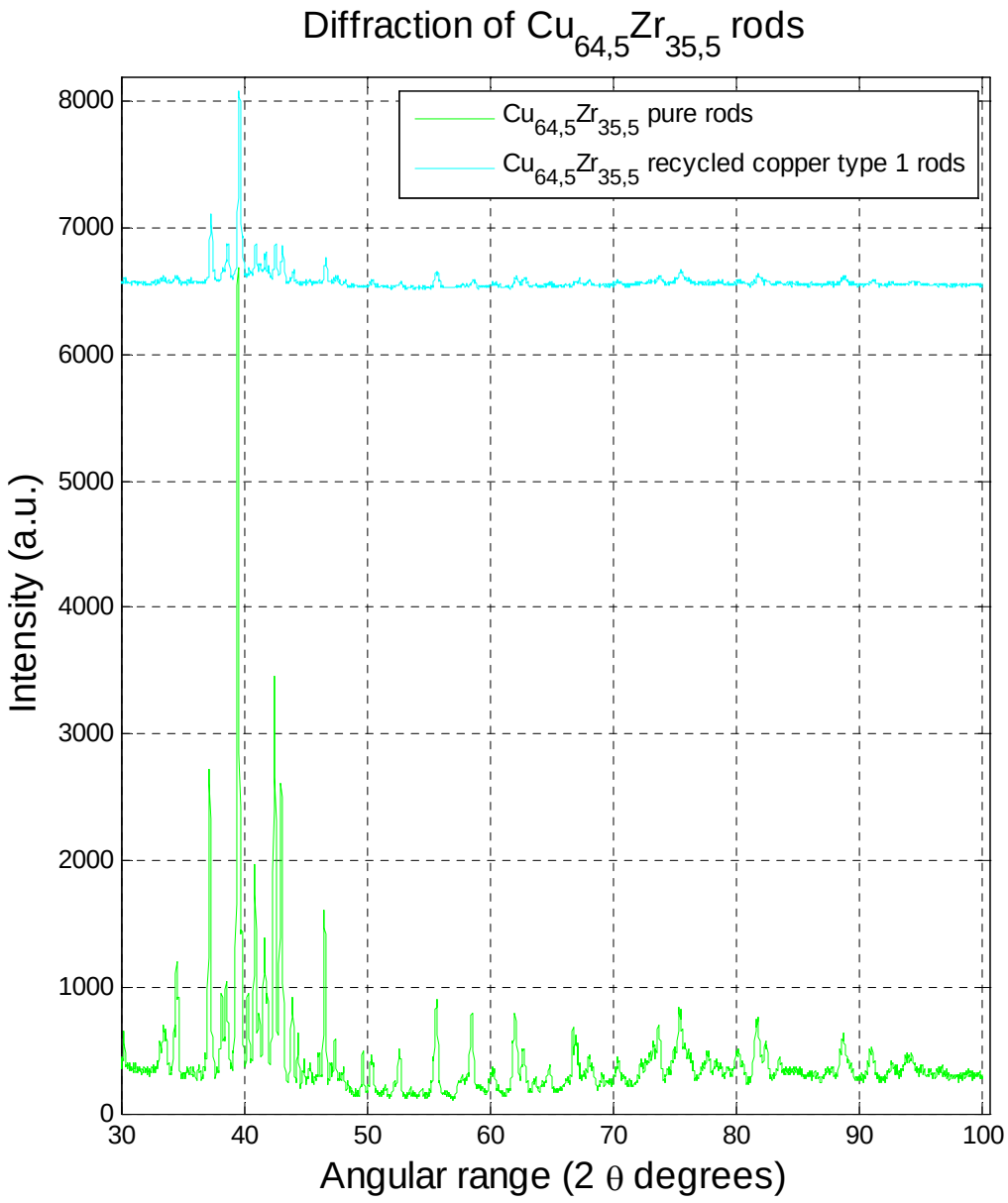

Fig. 5.3 XRD analysis for the pure copper and recycled copper type 1 rods

As we can see in the diffraction pattern, the results show the presence of a lot of sharp peaks, which means that the rods are crystalline.
But there is a noticeable difference between the two graphs: about the diffraction pattern corresponding to the pure Cu rods, we can say that the rods are completely crystalline as we can see lot of sharp peaks and have great intensity, however, if we take a look to recycled copper type 1 rods pattern, the peaks are not that sharp and had less intensity, which suggests that there is some kind of amorphous remnant.

By using Cu and Zr of high purity and producing the rods with the composition with higher GFA, it seemed that the rods produced were going to be

amorphous, but it has not been the case. And, in the case of recycled copper type 1, its high T_{rg} suggested the same.

For obtaining amorphous rods with this composition, we would have to continue studying how to do it and probably we would have to try one of these options to achieve this:
- Using another type of BMGs production technique such as fluxing.
- Improving the cleanliness of the copper mold.
- Maintaining the internal mold surface as clean and polished as possible to avoid crystal nucleation centres.
- Increasing the pressure difference between the chamber pressure and the suction pressure.

Moreover, XRD diffraction pattern results come from the average of the four rods used to cover the 1 cm^2 necessary to perform the analysis, so it is possible that some of the rods were amorphous, which seems the case for recycled copper type 1 results. To find out if this assumption is correct, the XRD analysis of the rods should be done in a non-conventional diffractometer with a capillary adapter or in a synchrotron radiation source where the x-ray spot is small enough to prove only one rod.

CONCLUSIONS

The purpose of this work has been the production of metallic glasses in the Cu-Zr system with Cu of several degrees of impurities. From this fact we can say that we have achieved in part the objectives proposed because we have been capable to obtain metallic glasses as ribbons, but we have failed to obtain BMG.

The first step of this work was to perform the calculations to obtain the necessary amounts of Cu-Zr to perform the samples in the composition $Cu_{64,5+x}Zr_{35,5-x}$ with x = -1, 0, 1 at.%. Once the amounts of Cu and Zr were already prepared, we proceeded to produce the alloys in the arc melter.
In obtaining the alloy, to verify that there was no mass loss during the arc melting, the balls obtained were weighed later. In this process we realized that the more impurities of copper, the more loss of mass. This could be due to the fact that copper impurities difficult the melting. To improve this and prevent the loss of mass, maybe we should have molten copper and zirconium separately and then melt them together.

The next step was to produce the ribbons in the melt spinner. The main factor that controls the production of ribbons in the melt spinner is the difference of pressure between the chamber and the injection pressure. Throughout all the process all the conditions remained the same, and with no doubt, the melt spinning was the process which took more time in the project, as many times the injection did not happen thus we did not obtain the ribbon, so we had to repeat all calculations, the alloy, and we have to return to perform the entire process in the melt spinner, but, in the end, all ribbons were obtained.

XRD analysis confirmed the amorphousness of all the ribbons produced, so we can determine that we can produce metallic glasses without using high purity elements, thus their production cost is lower.
Moreover, as we did not know the composition of the different types of copper with impurities, we performed the analysis of the ribbons in the SEM. In this process we realized that the SEM model in which we analysed our ribbons had little accuracy to detect small variations in the atomic percentage of the elements, hence the notable differences between the chemical analysis of the different types of recycled copper and the results obtained in the SEM analysis. For more accurate results, we should have used other analysis techniques such as X-ray fluorescence (XRF) or cathodoluminescence (CL).

Next, we perform a mechanical and a chemical characterization with the ribbons with higher GFA: those with the $Cu_{64,5}Zr_{35,5}$ composition. First, we characterized the hardness of the ribbons with the Vickers test in a microhardner. The results demonstrate that the more impurities has the copper, the harder the ribbon.
The chemical characterization of the ribbons was made in the DSC. Hence we get the relation Tg / Tm, which is what gives us an idea of the GFA. The conclusion of DSC analysis is that a small amount of impurities (between 1 and 5 at.%) improves the GFA, while too many impurities decrease this value.

As a second part of our project, we try to produce BMG with the $Cu_{64,5}Zr_{35,5}$ composition with pure copper and recycled copper type 1 (which got the highest ratio T_g / T_m).
First, rods were produced in the arc melter with the suction casting technique and, next, we performed the XRD analysis.

The results for the two types of copper showed that the rods were crystalline, although, as for XRD analysis is necessary to cover 1cm^2 of surface and, therefore, several rods were analysed simultaneously, may be some of the rods were amorphous.

As further work, we should study how to produce BMG with this composition with pure copper and with the recycled copper types used in the project. To achieve this, we would have to improve the internal and external cleanliness of the mold where the rods are created, increasing the pressure difference between the chamber and the injection pressure in the arc melter or by using other BMG production techniques.

REFERENCES

[1,3] http://en.wikipedia.org/wiki/Amorphous_metal
[2] http://www.idfuel.com/index.php?blog=2&p=377&more=1&c=1
[4,8] Turnbull, D., "Under what conditions can a glass be formed?, *Contemporary Physics* 10 (5), 473-488 (1969).
[5,6,7] Yang, W.; Liu, F., Liu, H.; Wang, H.F.; Chen, Z.; Yang, G.C., "Glass Forming ability in Cu-Zr Binary alloy: Effect of nucleation mode", *Journal of Alloy And Compounds* 484, 702-707 (2009).
[9] Zhang, W.; Zhang, Q.; Inoue, A., "Mechanical Properties of New Cu-Zr-based Glassy Alloys with high Glass-Forming Ability", *Advanced Engineering Materials* 10 (11), 1034–1038, (2008).
[10,18,19,20] Wang, D.; Li, Y.; Sun, B. B.; Sui, M. L.; Lu, K.; Ma, E., "Bulk metallic glass formation in the binary Cu-Zr system", *Applied Physics Letters* 84 (20), 4029 (2004).
[11] Altounian, Z.; Guo-Hua, T.; Strom-Olsen, J. O., "Crystallization characteristics of Cu-Zr metallic glasses from $Cu_{70}Zr_{30}$ to $Cu_{25}Zr_{75}$", *Journal of Applied Physics* 53 (7), 4755-4760 (1982).
[12]http://glass.ruc.dk/pdf/articles/2007_AEM_09_06.pdf
[13] Inoue, A.; Wang, X.M.; Zhang, W., "Developments and applications of bulk metallic glasses", *Rev. Adv. Mater. Sci.* 18, 1-9 (2008).
[14,16,17] Gierlotka, W.; Zhang, K.C.; Chang, Y.P., "Thermodynamic description of the binary Cu–Zr system", *Journal of Alloys and Compounds* 509 (33), 8313–8318 (2011).
[15] http://www.uca.edu.sv/facultad/clases/ing/m210031/Tema%2006.pdf
[21] García, M.; Bruna, P., "Producció de vidres metal·lics a partir d'escòria", (2012).
[22,23,24,25]
http://chemistry.about.com/od/chemistryglossary/Chemistry_Glossary_and_Dictionary.htm
[26,27] http://www.edmund-buehler.de/english/i-lichtbogen-schmelzgeraete.pml
[28] http://www.chemicool.com/elements/tungsten.html
[29] http://www.edmund-buehler.de/english/i-rascherstarrungstechnologie.pml
[30] http://mie.esab.upc.es/mmn/equips/meltspinner.php?lang=3
[31] Hamed, F.; Razavi, F. S.; Zaleski, H.; Bose, S. K., "Pressure dependence of spin fluctuations in metallic glasses $Ni_{25}Zr_{75}$ and $Fe_{100-x}Zr_x$ (x=75,80)", *Physical Review B (Condensed Matter)* 43 (4), 3649-3651 (1991).
[32]
http://serc.carleton.edu/research_education/geochemsheets/techniques/XRD.html
[33] http://www4.uwm.edu/celtic/ekeltoi/volumes/vol5/5_3/martin_5_3.html
[34] Souza, M.F. de; Batista, P.S.; Regiani, I.; Liborio, J.B.L.; Souza, D.P.F. de, "Rice hull-derived silica: applications in Portland cement and mullite whiskers", Materials Research, 3(2), 25-30 (2000).
[35] http://www.upc.edu/crne/infrastructure/x-ray-diffraction
[36]
http://serc.carleton.edu/research_education/geochemsheets/techniques/SEM.html
[37] http://cabierta.uchile.cl/revista/28/articulos/pdf/edu3.pdf

[38] http://www.gordonengland.co.uk/hardness/microhardness.htm
[39] http://www.matweb.com/reference/vickers-hardness.aspx
[40] http://www.struers.com/default.asp?top_id=5&main_id=156&sub_id=220&doc_id=911
[41] http://www.twi.co.uk/services/technical-information/job-knowledge/job-knowledge-74-hardness-testing-part-1/
[42] http://www.instron.us/wa/applications/test_types/hardness/vickers.aspx
[43] http://biplot.usal.es/DOCTORADO/3CICLO/BIENIO-06-08/SPSS%20Estadistica.pdf
[44] http://www.sccs.swarthmore.edu/users/08/ajb/tmve/wiki100k/docs/Differential_scanning_calorimetry.html
[45]http://www.netzsch-thermal-analysis.com/download/DSC404_F3_Pegasus_E_0411_en_341.pdf
[46,47] Carrasco, W.R; “Cristalización De Aleaciones Amorfas Cu-Zr-Al”, (2009).
[48] Su-Wen, K.; Chi-Chuan, H.; Tsung-Shune, C., "Simulation of reduced glass transition temperature of Cu–Zr alloys by molecular dynamics", *Journal Of Applied Physics*, 105 (6), 064913 - 064913-6 (2009).
[49] Rontó, V.; Nagy, E.; Svéda, M.; Roósz, A.; Tranta, F., "Structural and thermal properties of Cu-Hf-Ti bulk amorphous alloys", *Journal of Physics: Conference Series*, 144 (1), (2009).
[50] Baser, T.A.; Baricco, M., "Glass forming Ability of $(Cu_{50}Zr_{50})_{96}M_4$ (M=None, Al, Nb) Bulk Metallic Glasses, *Reviews on Advanced Materials Science*, 18, 71-76 (2008).

Escola d'Enginyeria de Telecomunicació i Aeroespacial de Castelldefels

UNIVERSITAT POLITÈCNICA DE CATALUNYA

ANNEXS

Title: Production of low cost Cu-based metallic glasses from recycled Cu

Author: Marta García Vera

Director: Pere Bruna Escuer

Date: June, 15th 2012

ÍNDEX

ANNEX 1. METALLIC GLASSES PROPERTIES

Metallic glasses are emerging as useful materials at the materials science research. They combine the advantages and avoid many of the problems of normal metals and glasses, two classes of materials with a very wide range of applications. Some of their mechanical properties are described below:

Brittleness: the tendency of a metal to break being significantly distorted or exposed to a high level of stress, which means, without being deformed.
Density: the mass of a material per unit volume. It gives an idea of the relative compactness of a material.
Ductility: the ability to be molded or shaped into wire or threads before rupture.
Elasticity: the property to return to the original shape when a force is removed.
Elastic limit: the point where the material starts to deform plastically.
Hardness: the resistance to plastic deformation
Plastic deformation: Permanent change in shape or size of a solid body without fracture resulting from the application of sustained stress beyond the elastic limit.
Plasticity: ability to deform permanently without breaking or rupturing.
Poisson's ratio: is the ratio of transverse contraction strain to longitudinal extension strain in the direction of stretching force. Tensile deformation is considered positive and compressive deformation is considered negative.
Resilience: the capacity to absorb energy elastically
Strength: ability to withstand an applied stress without deformation.
Toughness: amount of energy absorbed until rupture.
Yield strength: the stress point at which a material begins to deform plastically
Young's modulus: the division between tensile stress and tensile strain. In a stress vs. strain graph, it is the slope in the elastic region. Out of it, it is no longer available. It is also known as modulus of elasticity.

In general, metallic glasses show good properties. They have high strength, high hardness, high elastic limit, high resilience and high toughness compared to other materials.

However, not all the mechanical properties of metallic glasses are good. Metallic glasses are not ductile, which is a significant barrier to their possible applications. Moreover, ductility is one of the most desirable properties of the materials because this means that metals can be formed in a wide variety of shapes by deformation processes.

In order to summarize, the strengths and weaknesses in terms of properties of the metallic glasses are shown in the following table:

Table 1.1. Strengths and weakness of metallic glasses [1]

Attributes	Attractive	Unattractive
General	- Absence of microstructural features such as grain and phase boundaries and of related composition variations (e.g. segregation). This allows components with features of near-atomic scale	- Present cost of components and processing - Optimization of composition for glass-forming ability prevents easy optimization for other properties, including low density
Mechanical	- High hardness, giving good wear and abrasion resistance - High yield strength - Fracture toughness and toughness can be very high - High specific strength - High resilience per unit volume and mass - Low mechanical damping	- Severe localization of plastic flow (shear-banding), giving zero ductility in tension - Fracture toughness and toughness can be very low - Can be embrittled by annealing - Small process-zone size (d < 1 mm) means that larger components may fail in a brittle manner
Thermal	- $T_g<T_c$ for some metallic glasses, allowing processing as a supercooled liquid (T_g— glass-transition temperature. T_c— temperature of crystallization onset	- Instability above T_c limits high temperature use
Electrical and magnetic	- High magnetic permeability - Resistivity is nearly independent of temperature	- Relatively high magneto-striction gives energy loss in oscillating field
Chemical	- Lack of grain structure and associated microstructural features (e.g. solute segregation) gives corrosion resistance	
Environmental	- Some compositions biocompatible	- Not easily recycled once in a product (non-conventional compositions)

Attributes	Attractive	Unattractive
Processing	- Low solidification shrinkage and lack of grain structure give high precision and finish in castings - The high viscosity and low strain-rate sensitivity of the super cooled liquid permit thermoplastic forming	- Current need for vacuum die-casting gives relatively slow production rate
Aesthetic	-Lack of grain structure allows a very high polish -High hardness and corrosion resistance gives durability	

Finally, graphically, we are going to compare the attractive and unattractive features of metallic glasses with other materials in the following figures and, also, we are going to show where we find the Cu-Zr alloys there.
The orange region shows the values for each one of the properties for the composition range from $Cu_{50}Zr_{50}$ to $Cu_{64}Zr_{36}$, which will give us an idea of what properties have the alloys used in our project.

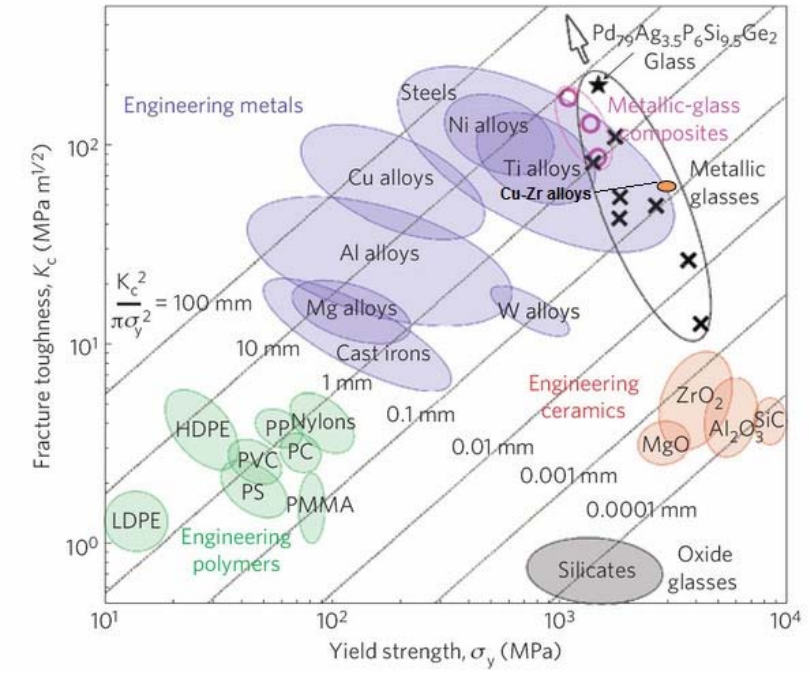

Fig. 1.1 Comparison of metallic glasses with other materials in a Fracture Toughness VS Yield Strength graph [2].

Fig. 1.1 is a chart of fracture toughness against yield strength (or elastic limit). The diagonal contours show the process-zone size, d, where:

$$d = \frac{K_c}{\pi \sigma_y^2} \quad \textbf{(1.1)}$$

If the ultimate size, d, is much smaller than the sample size, fast fracture follows. If d is greater than the sample size, brittle failure is not expected. Shear banding in metallic glasses favours failure which appears macroscopically brittle rather than ductile.
In the case of Cu-Zr alloys, although they have high fracture toughness K_c, they have small zone sizes (d < 1 mm) because σ_y is so large. In terms of d, we can say that Cu-Zr alloys in this range are brittle metallic glasses, not ductile ones.

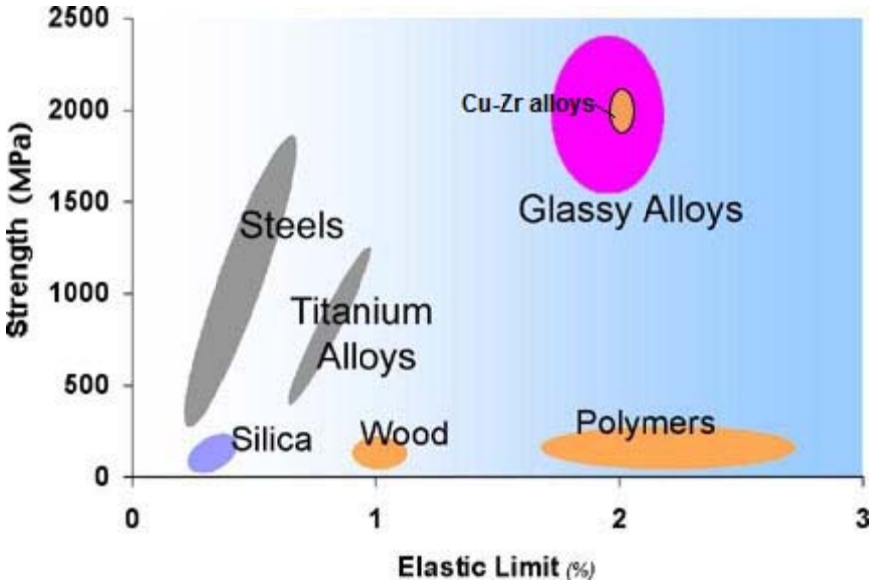

Fig. 1.2 Comparison of metallic glasses with other materials in a Strength VS Elastic Limit graph [3].

Fig. 1.2 is a chart of strength against elastic limit. Metallic glasses have high elastic limit, which means that they have resistance to plastic deformation. In other words: they store higher elastic energy per unit volume than most of the materials on the plot.
Cu-Zr alloys have high elastic limit and high strength, so they don't have the ability to deform permanently without breaking or rupturing which is consistent with the explanation given in Fig.1.1.

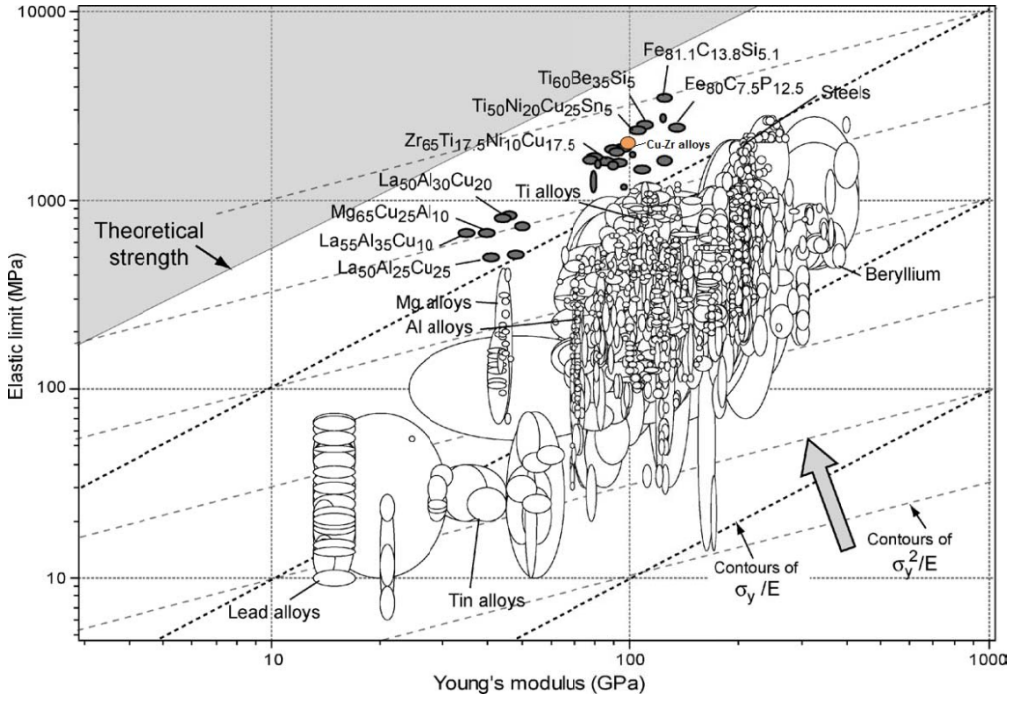

Fig. 1.3 Comparison of metallic glasses with other materials in an Elastic limit VS Young Modulus [4].

The contours on Fig. 1.3 show the property combinations σ_y/E and σ_y^2/E. The first of these is the yield strain; the second we call the resilience, a measure of the ability of the material to store (and return) elastic energy, important for example in springs. By these measures and by what the chart shows, Cu-Zr alloys have a larger yield strain and store more elastic energy per unit volume than more of the other materials on the plot.

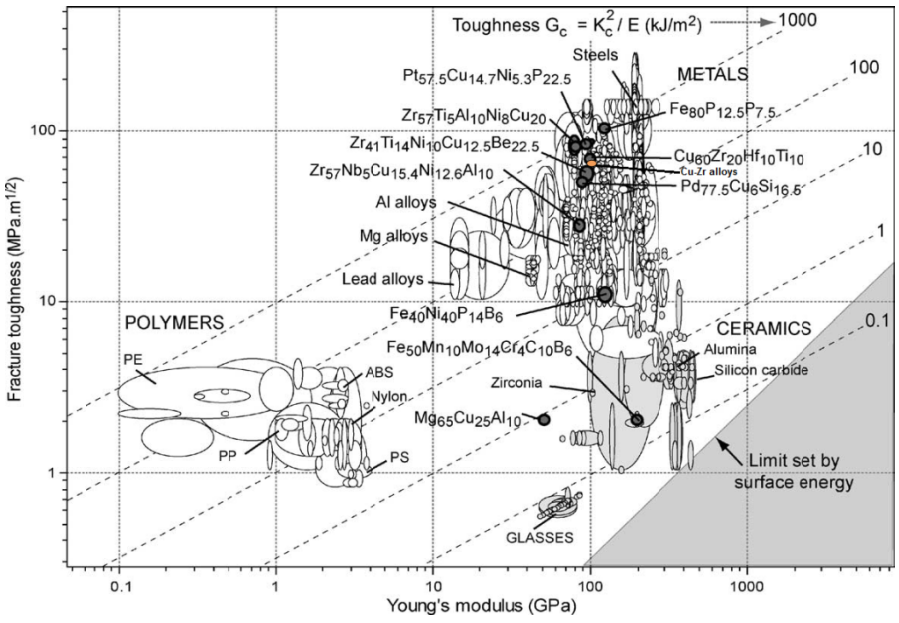

Fig. 1.4 Comparison of metallic glasses with other materials in Fracture toughness VS Young Modulus [5].

Fig. 1.4 shows fracture toughness K_c and modulus E for some materials. For many applications, failure is energy-limited rather than load-limited; the appropriate material index is then not K_c, but rather the toughness
Cu-Zr alloys show high Kc and good G_c, which means that, until their rupture, they absorb a high amount of energy.
Other metallic glasses also remarkably show good G_c, nearly the full known range for all material types.

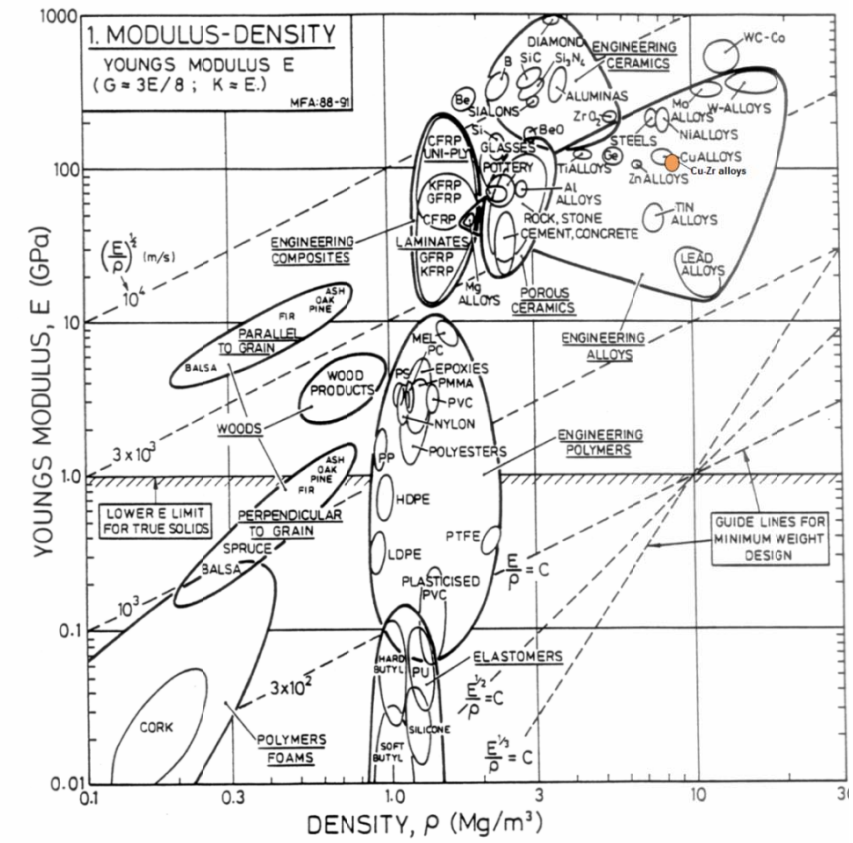

Fig. 1.5 Comparison of metallic glasses with other materials in density VS Young Modulus [6].

Fig. 1.5 is a chart of young modulus against density (or elastic limit). The diagonal contours show the specific Young modulus.
A greater specific young modulus means that the weight design of the material can be reduced. This is a major factor in moving parts where weight reductions result in a higher yield and energy savings.
Cu-Zr alloys show high density and high young modulus, which means that its specific young modulus is high. So, these alloys can be used as moving parts for industrial applications.

As we have seen, metallic glasses have some outstanding properties including: high strength, uniquely high capacity for elastic energy storage per unit volume or mass, high yield strength and very high toughness.
Such properties, combined with an ability to be deposited as thin ribbons, makes metallic glasses attractive for many applications, such as: [7]

- Tooling and information storage and reproduction: The high hardness suggests use in precision tooling and in the production of items for reproducing ultrahigh-density digital data.
- High performance springs: The high elastic energy storage per unit volume and mass, give metallic glasses potential as springs
- MEMS devices: Micro electro-mechanical systems (MEMS) offer outstanding opportunities for the exploitation of metallic glasses. High yield strain is desirable. Crucially for MEMS fabrication, metallic glasses can be deposited as thin films and the glass-forming ability in deposition opens up a much wider range of compositions than is possible for BMGs.

As Cu-Zr metallic glasses are excellent and unique alloys with high electrical conductivity, they are normally used for Electrical Industry and Industry applications.

ANNEX 2. CU-ZR SYSTEM SAMPLES

All the results obtained for each one of the samples from this project have been introduced in the following website: http://mie.esab.upc.es/mediawiki/index.php/ in the Sample Log / Cu-Zr System section.

$Cu_{63,5}Zr_{36,5}$, Cu: 99,9% pureness.

Sample preparation

2.1911 g of Cu + 1.8085 g of Zr
Total mass before Arc-melting: 3.9996 g

Arc melting

800mbar of Ar gas.
Ti-gettered atmosphere.
Total mass after Arc-melting = 3.998 g (loss of 0.040004% during alloying)

Melt Spinning

P chamber = 400 mbar
P injection = 800 mbar
Distance crucible - wheel = 1 mm
Hole diameter = 0.5 mm
Wheel velocity = 40 m/s
T injection = 1610 ºC
Total mass after Melt spinning = 0.8623 g (loss of 78.43171586% during injection)

It has not injected in the first attempt. We have raised the crucible and reaching 1610ºC it has injected (in the second attempt) but not immediately, we have waited for, approximately, 3 seconds. Quality of the ribbon: Very short and very thin. There is quite a lot of mass stuck inside the crucible.

XRD analysis

Cu anode XRD realized at Centre de Recerca en Nanoenginyeria

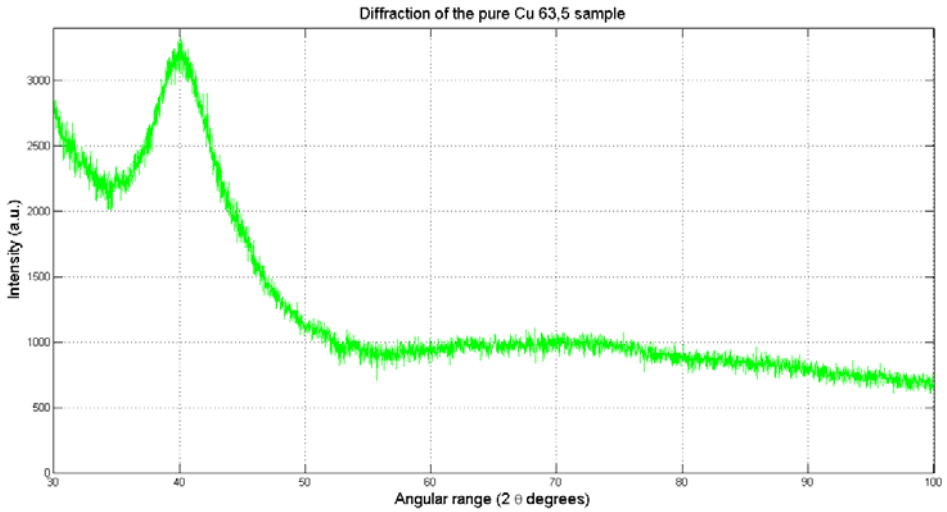

Fig 2.1 Diffraction of the pure Cu $Cu_{63,5}Zr_{36,5}$ sample

There are not narrow peaks that suggest the existence of a crystalline phase. The radiation pattern has a broad peak which means that the ribbon is amorphous.

SEM analysis

The following table shows the average results obtained in the SEM, prior to its normalization.

Table 2.1. SEM results for pure Cu $Cu_{63,5}Zr_{36,5}$ ribbon

Element	Weight %	Atomic %
C K	4,87	22,135
O K	1,645	5,73
Si K	0,56	1,115
Cu K	50,815	45,015
Zr L	42,105	26,01

$Cu_{64,5}Zr_{35,5}$, Cu: 99,9% pureness.

Sample preparation

2.2319 g of Cu + 1.7648 g of Zr
Total mass before Arc-melting: 3.9967 g

Arc melting

800mbar of Ar gas. Ti-gettered atmosphere. Total mass after Arc-melting = 3.9945 g (loss of 0.0550454% during alloying)

Melt Spinning

P chamber = 400 mbar P injection = 800 mbar Distance crucible - wheel = 1 mm Hole diameter = 0.5 mm Wheel velocity = 40 m/s T injection = 1580 ºC Total mass after Melt spinning = 2.098 g (loss of 47.47778195% during injection)

It has not injected in the first attempt. We have raised the crucible and reaching 1580ºC it has injected (in the second attempt). Quality of the ribbon: Very short and very thin. There is quite a lot of mass stuck inside the crucible.

XRD analysis

Cu anode XRD realized at Centre de Recerca en Nanoenginyeria

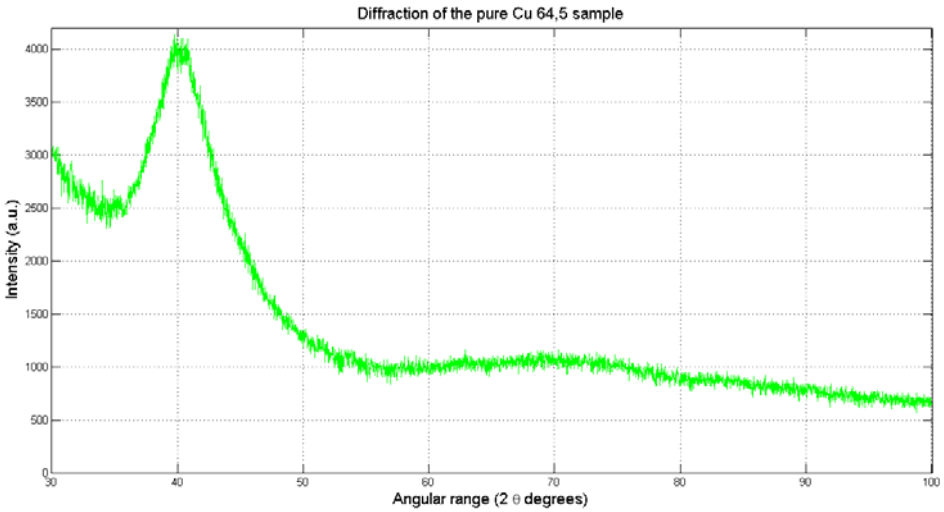

Fig 2.2 Diffraction of the pure Cu $Cu_{64,5}Zr_{35,5}$ sample

There are not narrow peaks that suggest the existence of a crystalline phase. The radiation pattern has a broad peak which means that the ribbon is amorphous.

SEM analysis

The following table shows the average results obtained in the SEM, prior to its normalization.

Table 2.2. SEM results for pure Cu $Cu_{64,5}Zr_{35,5}$ ribbon

Element	Weight %	Atomic %
B K	3,59	14,56
C K	4,67	19,61
Si K	0,375	0,7
Cu K	49,115	39,55
Zr L	41,65	23,415
O K	0,595	2,16

$Cu_{65,5}Zr_{34,5}$, Cu: 99,9% pureness.

Sample preparation

2.2786 g of Cu + 1.7228 g of Zr
Total mass before Arc-melting: 4.0014 g

Arc melting

800mbar of Ar gas.
Ti-gettered atmosphere.
Total mass after Arc-melting = 3.9999 g (loss of 0.0374869% during alloying)

Melt Spinning

P chamber = 400 mbar
P injection = 800 mbar
Distance crucible - wheel = 1 mm
Hole diameter = 0.5 mm
Wheel velocity = 40 m/s
T injection = 1210 ºC
Total mass after Melt spinning = 2.8972 g (loss of 27.5681892% during injection)

We have injected without problems. Quality of the ribbon: good and of a considerable width. No mass without injecting.

XRD analysis

Cu anode XRD realized at Centre de Recerca en Nanoenginyeria

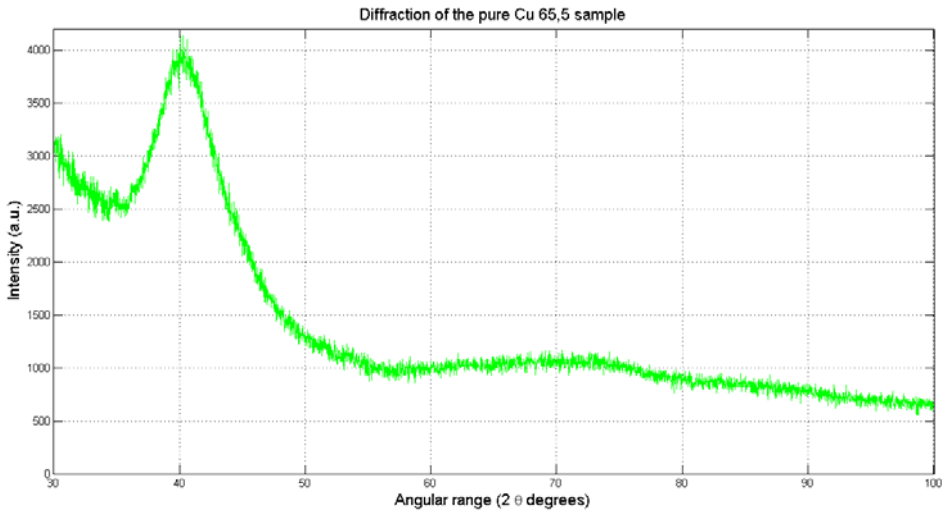

Fig 2.3 Diffraction of the pure Cu $Cu_{65,5}Zr_{34,5}$ sample

There are not narrow peaks that suggest the existence of a crystalline phase. The radiation pattern has a broad peak which means that the ribbon is amorphous.

SEM analysis

The following table shows the average results obtained in the SEM, prior to its normalization.

Table 2.3. SEM results for pure Cu $Cu_{65,5}Zr_{34,5}$ ribbon

Element	Weight %	Atomic %
C K	4,265	20,7
O K	1,275	4,64
Cu K	51,485	47,215
Zr L	42,975	27,45

$Cu_{63,5}Zr_{36,5}$, Cu: Recycled. Type 1.

Sample preparation

2.6529 g of Cu + 2.1915 g of Zr
Total mass before Arc-melting: 4.8444 g

Arc melting

800mbar of Ar gas. Ti-gettered atmosphere. Total mass after Arc-melting = 4.8402 g (loss of 0.086698% during alloying)

Melt Spinning

P chamber = 400 mbar P injection = 800 mbar Distance crucible - wheel = 1 mm Hole diameter = 0.5 mm Wheel velocity = 40 m/s T injection = 1260 ºC Total mass after Melt spinning = 3.379 g (loss of 30.18889517% during injection)

We have injected without problems. Quality of the ribbon: very good and of a considerable width. No mass without injecting

XRD analysis

Cu anode XRD realized at Centre de Recerca en Nanoenginyeria

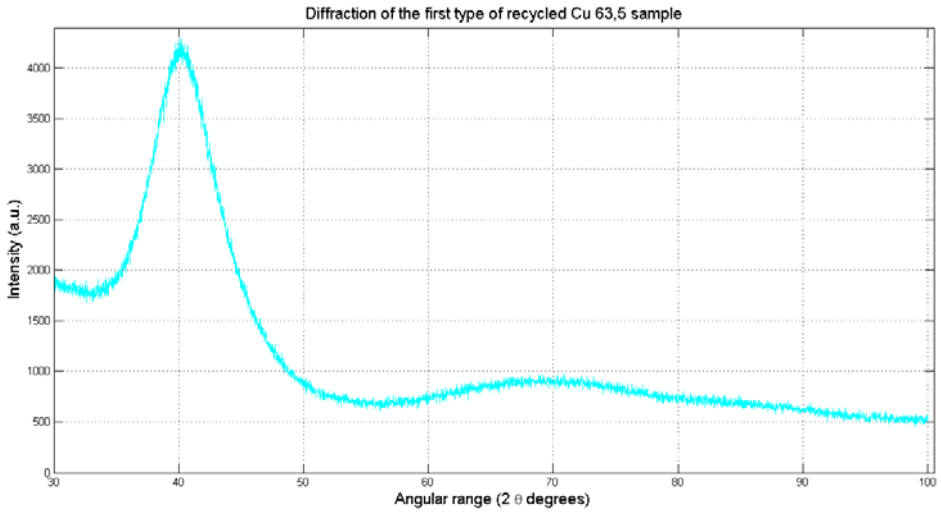

Fig 2.4 Diffraction of the recycled Cu type 1 $Cu_{63,5}Zr_{36,5}$ sample

There are not narrow peaks that suggest the existence of a crystalline phase. The radiation pattern has a broad peak which means that the ribbon is amorphous.

SEM analysis

The following table shows the average results obtained in the SEM, prior to its normalization.

Table 2.4. SEM results for recycled Cu type 1 $Cu_{63,5}Zr_{36,5}$ ribbon

Element	Weight %	Atomic %
C K	14,106	49,055
O K	1,245	3,25
Cu K	44,82	29,46
Zr L	39,827	18,235

$Cu_{64,5}Zr_{35,5}$,Cu: Recycled. Type 1.

Sample preparation

2.3341 g of Cu + 1.8414 g of Zr
Total mass before Arc-melting: 4.1755 g

Arc melting

800mbar of Ar gas.
Ti-gettered atmosphere.
Total mass after Arc-melting = 4.1692 g (loss of 0.15088% during alloying)

Melt Spinning

P chamber = 400 mbar
P injection = 800 mbar
Distance crucible - wheel = 1 mm
Hole diameter = 0.5 mm
Wheel velocity = 40 m/s
T injection = 1571 ºC
Total mass after Melt spinning = 3.5941 g (loss of 13.79401324% during injection)

We have injected without problems. Quality of the ribbon: good and of a considerable width. No mass without injecting.

XRD analysis

Cu anode XRD realized at Centre de Recerca en Nanoenginyeria

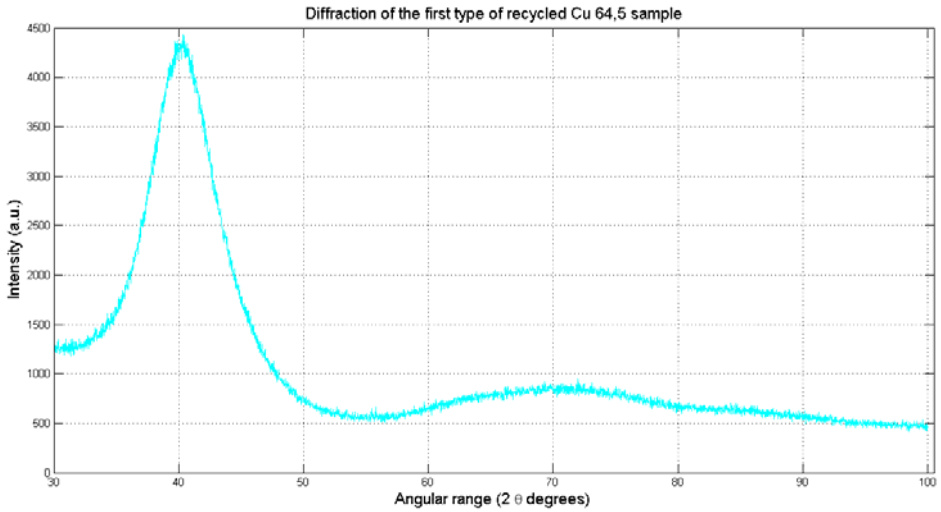

Fig 2.5 Diffraction of the recycled Cu type 1 $Cu_{64,5}Zr_{35,5}$ sample

There are not narrow peaks that suggest the existence of a crystalline phase. The radiation pattern has a broad peak which means that the ribbon is amorphous.

SEM analysis

The following table shows the average results obtained in the SEM, prior to its normalization.

Table 2.5. SEM results for recycled Cu type 1 $Cu_{64,5}Zr_{35,5}$ ribbon

Element	Weight %	Atomic %
C K	6,758	30,354
O K	0,578	1,949
Cu K	50,08	42,515
Zr L	42,584	25,183

$Cu_{65,5}Zr_{34,5}$, Cu: Recycled. Type 1.

Sample preparation

2.4936 g of Cu + 1.8879 g of Zr
Total mass before Arc-melting: 4.3815 g

Arc melting

800mbar of Ar gas.
Ti-gettered atmosphere.
Total mass after Arc-melting = 4.3807 g (loss of 0.018259% during alloying)

Melt Spinning

P chamber = 400 mbar
P injection = 800 mbar
Distance crucible - wheel = 1 mm
Hole diameter = 0.5 mm
Wheel velocity = 40 m/s
T injection = 1502 ºC
Total mass after Melt spinning = 0.2202 g (loss of 94.97340608% during injection)

We haven't injected until the third attempt. Quality of the ribbon: good although we have obtained a very few pieces. There is quite a lot of mass stuck inside the crucible.

XRD analysis

Cu anode XRD realized at Centre de Recerca en Nanoenginyeria

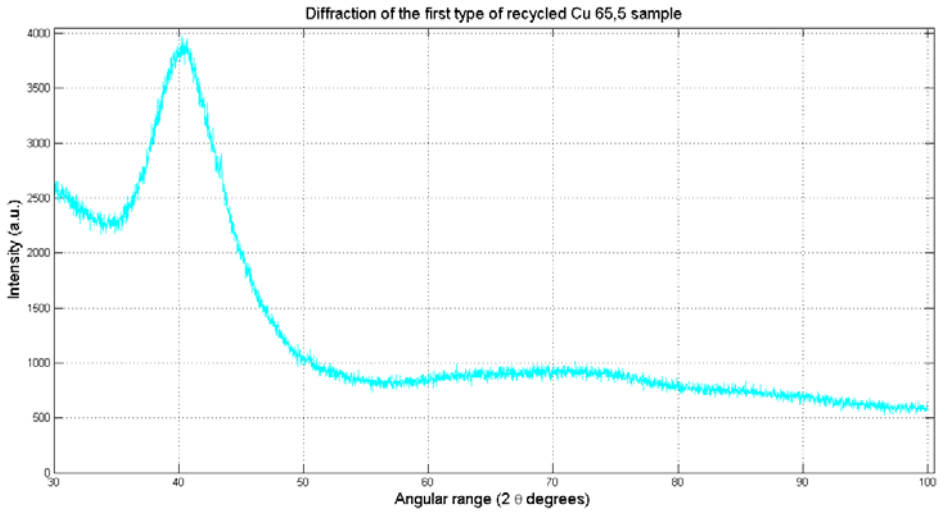

Fig 2.6 Diffraction of the recycled Cu type 1 $Cu_{65,5}Zr_{34,5}$ sample

There are not narrow peaks that suggest the existence of a crystalline phase. The radiation pattern has a broad peak which means that the ribbon is amorphous.

SEM analysis

The following table shows the average results obtained in the SEM, prior to its normalization.

Table 2.6. SEM results for recycled Cu type 1 $Cu_{65,5}Zr_{34,5}$ ribbon

Element	Weight %	Atomic %
C K	2,625	10,025
B K	2,86	12,125
Sn L	1,18	0,595
Cu K	53,505	50,855
Zr L	39,835	26,4

$Cu_{63,5}Zr_{36,5}$, Cu: Recycled. Type 2.

Sample preparation

2.3407 g of Cu + 1.9329 g of Zr
Total mass before Arc-melting: 4.2736 g

Arc melting

800mbar of Ar gas. Ti-gettered atmosphere. Total mass after Arc-melting = 4.258 g (loss of 0.360503% during alloying)

Melt Spinning

P chamber = 400 mbar P injection = 800 mbar Distance crucible - wheel = 1 mm Hole diameter = 0.5 mm Wheel velocity = 40 m/s T injection = 1300 ºC Total mass after Melt spinning = 2.8788 g (loss of 32.3907938% during injection)

We have injected without problems. Quality of the ribbon: good but some pieces of the ribbon are very thin. No mass without injecting.

XRD analysis

Cu anode XRD realized at Centre de Recerca en Nanoenginyeria

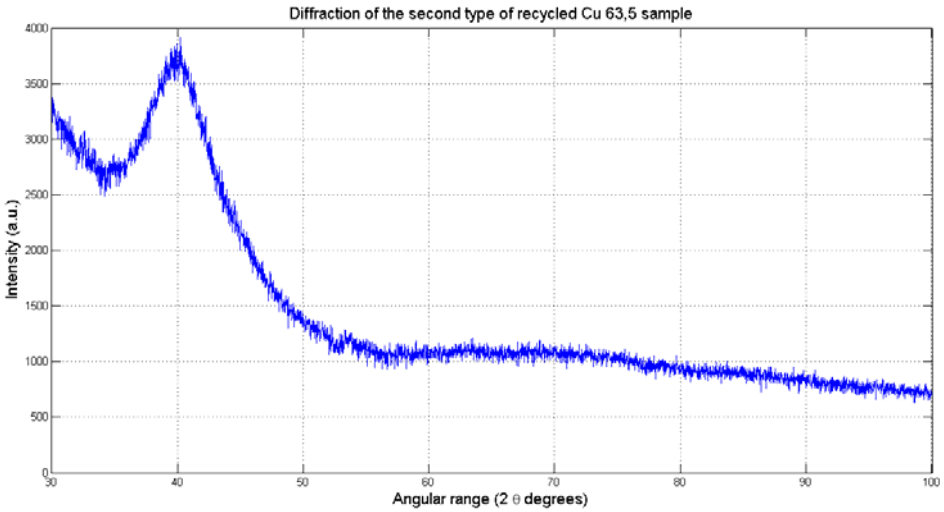

Fig 2.7 Diffraction of the recycled Cu type 2 $Cu_{63,5}Zr_{36,5}$ sample

There are not narrow peaks that suggest the existence of a crystalline phase. The radiation pattern has a broad peak which means that the ribbon is amorphous.

SEM analysis

The following table shows the average results obtained in the SEM, prior to its normalization.

Table 2.7. SEM results for recycled Cu type 2 $Cu_{63,5}Zr_{36,5}$ ribbon

Element	Weight %	Atomic %
C K	6,2	28,155
O K	1,13	3,855
Sn L	0,92	0,42
Cu K	48,39	41,585
Zr L	43,365	25,98

$Cu_{64,5}Zr_{35,5}$ Cu: Recycled. Type 2.

Sample preparation

2.7227 g of Cu + 2.1518 g of Zr
Total mass before Arc-melting: 4.8745 g

Arc melting

800mbar of Ar gas.
Ti-gettered atmosphere.
Total mass after Arc-melting = 4.8561 g (loss of 0.37747% during alloying)

Melt Spinning

P chamber = 400 mbar
P injection = 800 mbar
Distance crucible - wheel = 1 mm
Hole diameter = 0.5 mm
Wheel velocity = 40 m/s
T injection = 1350 ºC
Total mass after Melt spinning = 3.7103 g (loss of 23.595066% during injection)

We have injected without problems. Quality of the ribbon: very good and of a considerable width. There is quite a lot of mass stuck inside the crucible.

XRD analysis

Cu anode XRD realized at Centre de Recerca en Nanoenginyeria

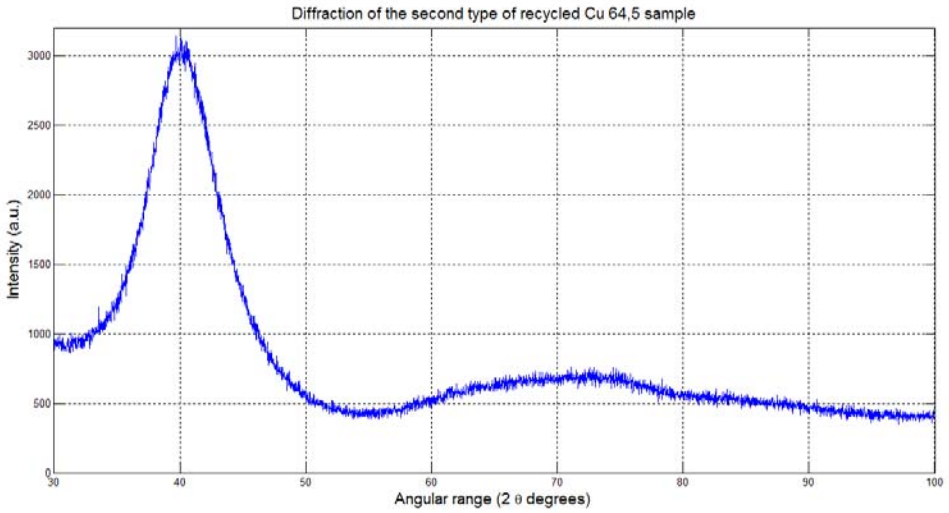

Fig 2.8 Diffraction of the recycled Cu type 2 $Cu_{64,5}Zr_{35,5}$ sample

There are not narrow peaks that suggest the existence of a crystalline phase. The radiation pattern has a broad peak which means that the ribbon is amorphous.

SEM analysis

The following table shows the average results obtained in the SEM, prior to its normalization.

Table 2.8. SEM results for recycled Cu type 2 $Cu_{64,5}Zr_{35,5}$ ribbon

Element	Weight %	Atomic %
C K	8,899	37,311
O K	0,443	1,394
Sn L	0,84285714	0,358
Cu K	47,2257143	37,428
Zr L	42,5914286	23,512

$Cu_{65,5}Zr_{34,5}$ Cu: Recycled. Type 2.

Sample preparation

2.6135 g of Cu + 1.9774 g of Zr
Total mass before Arc-melting: 4.5909 g

Arc melting

800mbar of Ar gas. Ti-gettered atmosphere. Total mass after Arc-melting = 4.5731 g (loss of 0.387724% during alloying)

Melt Spinning

P chamber = 400 mbar P injection = 800 mbar Distance crucible - wheel = 1 mm Hole diameter = 0.5 mm Wheel velocity = 40 m/s T injection = 1280 ºC Total mass after Melt spinning =3.1487 g (loss of 31.14736175% during injection)

We have injected without problems. Quality of the ribbon: good and of a considerable width. No mass without injecting.

XRD analysis

Cu anode XRD realized at Centre de Recerca en Nanoenginyeria

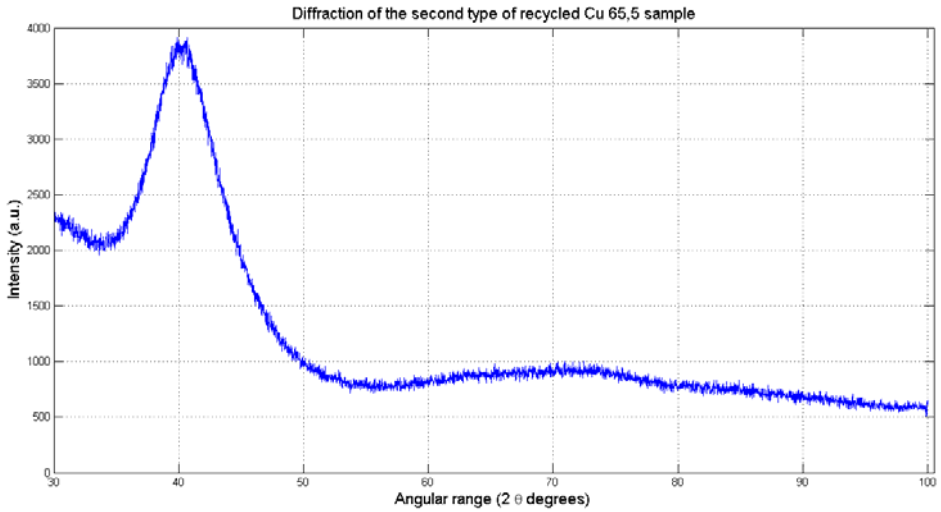

Fig 2.9 Diffraction of the recycled Cu type 2 $Cu_{65,5}Zr_{34,5}$ sample

There are not narrow peaks that suggest the existence of a crystalline phase. The radiation pattern has a broad peak which means that the ribbon is amorphous.

SEM analysis

The following table shows the average results obtained in the SEM, prior to its normalization.

Table 2.9. SEM results for recycled Cu type 2 $Cu_{65,5}Zr_{34,5}$ ribbon

Element	Weight %	Atomic %
C K	5,515	26,56
Sn L	1,265	0,615
Cu K	49,695	45,23
Zr L	43,52	27,59

$Cu_{63,5}Zr_{36,5}$, Cu: Recycled. Type 3.

Sample preparation

2.3946 g of Cu + 1.9757 g of Zr
Total mass before Arc-melting: 4.3703 g

Arc melting

800mbar of Ar gas. Ti-gettered atmosphere. Total mass after Arc-melting = 4.3524 g (loss of 0.409583% during alloying)

Melt Spinning

P chamber = 400 mbar P injection = 800 mbar Distance crucible - wheel = 1 mm Hole diameter = 0.5 mm Wheel velocity = 40 m/s T injection = 1300 ºC Total mass after Melt spinning = 4.341 g (loss of 0.261924455% during injection)

We have injected without problems. Quality of the ribbon: good, of a considerable width and in a huge quantity. No mass without injecting. Note: the pyrometer has stopped working for a few seconds.

XRD analysis

Cu anode XRD realized at Centre de Recerca en Nanoenginyeria

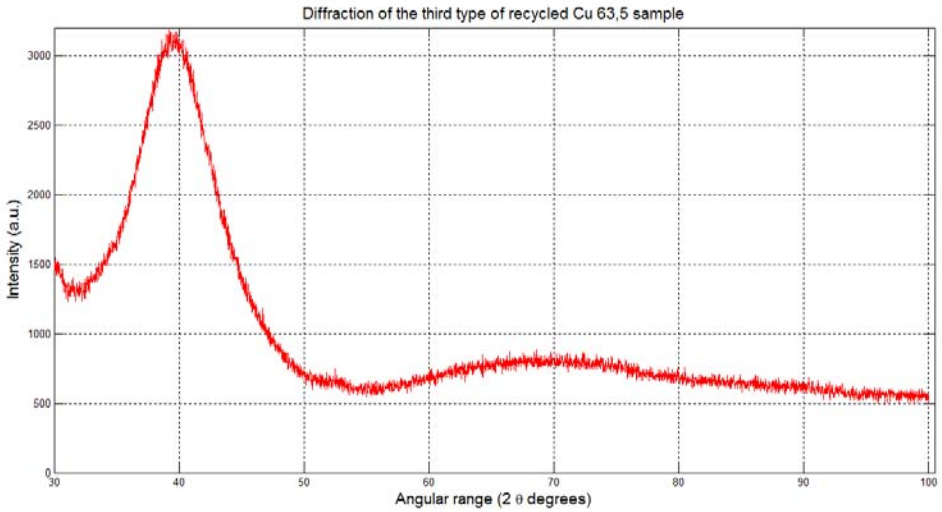

Fig 2.10 Diffraction of the recycled Cu type 3 $Cu_{63,5}Zr_{36,5}$ sample

There are not narrow peaks that suggest the existence of a crystalline phase. The radiation pattern has a broad peak which means that the ribbon is amorphous.

SEM analysis

The following table shows the average results obtained in the SEM, prior to its normalization.

Table 2.10. SEM results for recycled Cu type 3 $Cu_{63,5}Zr_{36,5}$ ribbon

Element	Weight %	Atomic %
C K	12,42	45,67
O K	1,215	3,37
Si K	0,515	0,805
Sn L	3,135	1,17
Cu K	42,155	29,33
Zr L	40,565	19,66

$Cu_{64,5}Zr_{35,5}$, Cu: Recycled. Type 3.

Sample preparation

2.4019 g of Cu + 1.8963 g of Zr
Total mass before Arc-melting: 4.2982 g

Arc melting

800mbar of Ar gas. Ti-gettered atmosphere. Total mass after Arc-melting = 4.2805 g (loss of 0.4118% during alloying)

Melt Spinning

P chamber = 400 mbar P injection = 800 mbar Distance crucible - wheel = 1 mm Hole diameter = 0.5 mm Wheel velocity = 40 m/s T injection = 1280 ºC Total mass after Melt spinning = 2.8282 g (loss of 33.92827941% during injection)

We have injected without problems. Quality of the ribbon: very good and of a considerable width. There is quite a lot of mass stuck inside the crucible.

XRD analysis

Cu anode XRD realized at Centre de Recerca en Nanoenginyeria

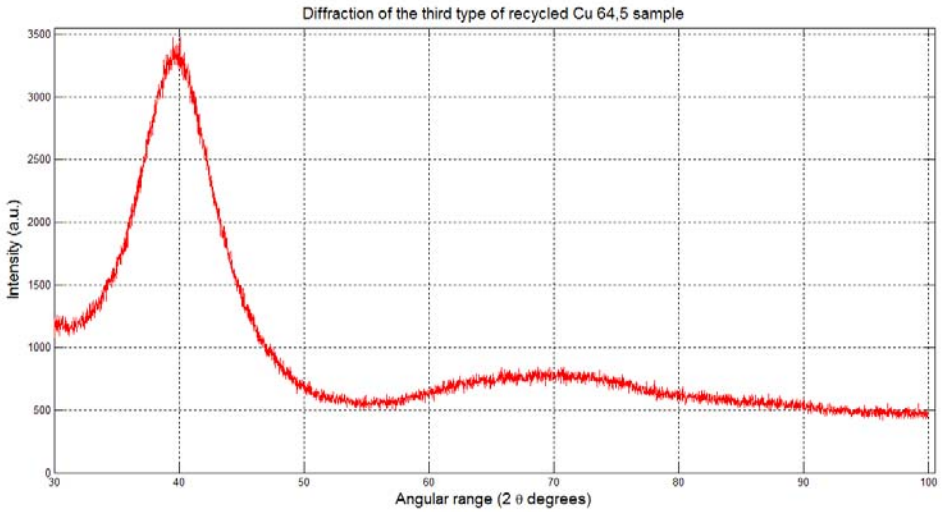

Fig 2.11 Diffraction of the recycled Cu type 3 $Cu_{64,5}Zr_{35,5}$ sample

There are not narrow peaks that suggest the existence of a crystalline phase. The radiation pattern has a broad peak which means that the ribbon is amorphous.

SEM analysis

The following table shows the average results obtained in the SEM, prior to its normalization.

Table 2.11. SEM results for recycled Cu type 3 $Cu_{64,5}Zr_{35,5}$ ribbon

Element	Weight %	Atomic %
C K	9,848	40,422
O K	0,310	0,955
Sn L	3,486	1,448
Cu K	44,638	34,63
Zr L	41,716	22,544

$Cu_{65,5}Zr_{34,5}$, Cu: Recycled. Type 3.

Sample preparation

2.8232 g of Cu + 2.1344 g of Zr
Total mass before Arc-melting: 4.9576 g

Arc melting

800mbar of Ar gas. Ti-gettered atmosphere. Total mass after Arc-melting = 4.9329 g (loss of 0.498225% during alloying)

Melt Spinning

P chamber = 400 mbar P injection = 800 mbar Distance crucible - wheel = 1 mm Hole diameter = 0.5 mm Wheel velocity = 40 m/s T injection = 1270 ºC Total mass after Melt spinning = 4.0823 g (loss of 17.24340652% during injection)

We have injected without problems. Quality of the ribbon: good , but some pieces are very thin. No mass without injecting.

XRD analysis

Cu anode XRD realized at Centre de Recerca en Nanoenginyeria

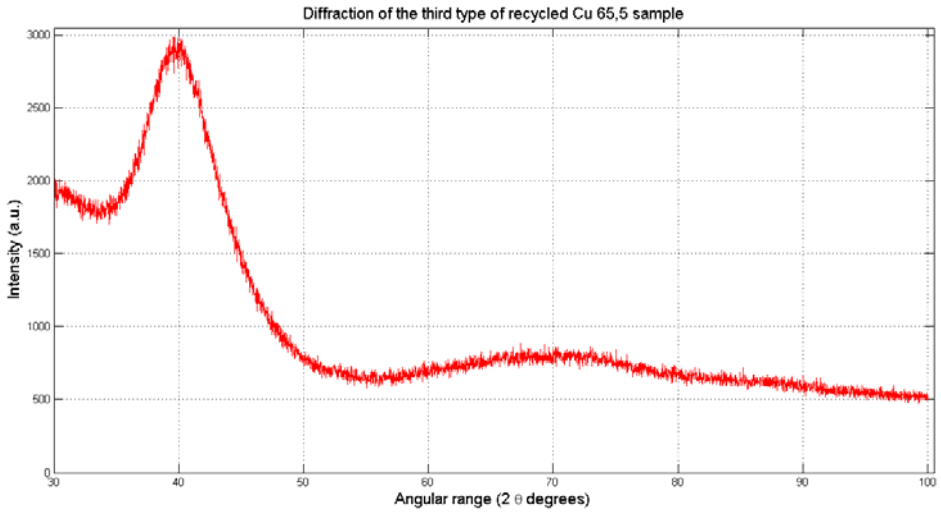

Fig 2.12 Diffraction of the recycled Cu type 3 $Cu_{65,5}Zr_{34,5}$ sample

There are not narrow peaks that suggest the existence of a crystalline phase. The radiation pattern has a broad peak which means that the ribbon is amorphous.

SEM analysis

The following table shows the average results obtained in the SEM, prior to its normalization.

Table 2.12. SEM results for recycled Cu type 3 $Cu_{65,5}Zr_{34,5}$ ribbon

Element	Weight %	Atomic %
C K	3,876	19,3
O K	1,403	5,243
Sn L	3,62	1,824
Ni K	0,029	0,03
Pb K	0,953	0,275
Cu K	49,915	46,973
Zr L	40,205	26,355

ANNEX 3. SAMPLES OBTAINED

The calculations for the masses of Cu and Zr necessary to produce the alloys with the desired compositions have been collected in the following tables:

Table 3.1. $Cu_{63,5}Zr_{36,5}$ sample of pure copper.

PURE COPPER			
Element	Cu	Zr	Sum
Atomic weight	63,546	91,224	
Atomic per cent	**63,5**	**36,5**	
Molecular weight	4035,171	3329,676	7364,847
Mass percentage	54,7896	45,2104	
Pure Cu sample			
Actual Cu mass	2,1911		
Total mass	3,9991		
Ideal corresponding mass of Zr		1,808	
Actual corresponding mass of Zr		1,8085	
Relative error Zr sample		0,0268	
Ideal mass of the alloy			3,9991
Actual mass of the alloy			3,9996
Relative error of the alloy			0,0121

Table 3.2. $Cu_{64,5}Zr_{35,5}$ sample of pure copper.

PURE COPPER			
Element	Cu	Zr	Sum
Atomic weight	63,546	91,224	
Atomic per cent	**64,5**	**35,5**	
Molecular weight	4098,717	3238,452	7337,169
Mass percentage	55,8624	44,1376	
Pure Cu sample			
Actual Cu mass	2,2319		
Total mass	3,9954		
Ideal corresponding mass of Zr		1,7635	
Actual corresponding mass of Zr		1,7648	
Relative error Zr sample		0,0763	
Ideal mass of the alloy			3,9954
Actual mass of the alloy			3,9967
Relative error of the alloy			0,0337

Table 3.3. $Cu_{65,5}Zr_{34,5}$ sample of pure copper.

PURE COPPER			
Element	Cu	Zr	Sum
Atomic weight	63,546	91,224	
Atomic per cent	**65,5**	**34,5**	
Molecular weight	4162,263	3147,228	7309,491
Mass percentage	56,9433	43,0567	
Pure Cu sample			
Actual Cu mass	2,2786		
Total mass	4,0015		
Ideal corresponding mass of Zr		1,7229	
Actual corresponding mass of Zr		1,7228	
Relative error Zr sample		0,0073	
Ideal mass of the alloy			4,0015
Actual mass of the alloy			4,0014
Relative error of the alloy			0,0032

Table 3.4. $Cu_{63,5}Zr_{36,5}$ sample of type 1 of recycled copper.

RECYCLED COPPER. TYPE 1			
Element	Cu	Zr	
Atomic weight	63,546	91,224	
Atomic per cent	**63,5**	**36,5**	
Molecular weight	4035,171	3329,676	7364,847
Per cent by mass	54,7896	45,2104	
Recycled Cu sample			
Actual mass	2,6529		
Total mass	4,842		
Ideal corresponding mass of Zr		2,1891	
Actual corresponding mass of Zr		2,1915	
Relative error Zr sample		0,1107	
Ideal mass of the alloy			4,842
Actual mass of the alloy			4,8444
Relative error of the alloy			0,0501

Table 3.5. $Cu_{64,5}Zr_{35,5}$ sample of type 1 of recycled copper.

RECYCLED COPPER. TYPE 1			
Element	Cu	Zr	
Atomic weight	63,546	91,224	
Atomic per cent	**64,5**	**35,5**	
Molecular weight	4098,717	3238,452	7337,169
Per cent by mass	55,8624	44,1376	
Recycled Cu sample			
Actual mass	2,3341		
Total mass	4,1783		
Ideal corresponding mass of Zr		1,8442	
Actual corresponding mass of Zr		1,8414	
Relative error Zr sample		0,1521	
Ideal mass of the alloy			4,1783
Actual mass of the alloy			4,1755
Relative error of the alloy			0,0671

Table 3.6. $Cu_{65,5}Zr_{34,5}$ sample of type 1 of recycled copper.

RECYCLED COPPER. TYPE 1			
Element	Cu	Zr	
Atomic weight	63,546	91,224	
Atomic per cent	**65,5**	**34,5**	
Molecular weight	4162,263	3147,228	7309,491
Per cent by mass	56,9433	43,0567	
Recycled Cu sample			
Actual mass	2,4936		
Total mass	4,3791		
Ideal corresponding mass of Zr		1,8855	
Actual corresponding mass of Zr		1,8879	
Relative error Zr sample		0,1275	
Ideal mass of the alloy			4,3791
Actual mass of the alloy			4,3815
Relative error of the alloy			0,0549

Table 3.7. $Cu_{63,5}Zr_{36,5}$ sample of type 2 of recycled copper.

RECYCLED COPPER. TYPE 2			
Element	Cu	Zr	Sum
Atomic weight	63,546	91,224	
Atomic per cent	**63,5**	**36,5**	
Molecular weight	4035,171	3329,676	7364,847
Mass percentage	54,7896	45,2104	
Recycled Cu sample			
Actual Cu mass	2,3407		
Total mass	4,2722		
Ideal corresponding mass of Zr		1,9315	
Actual corresponding mass of Zr		1,9329	
Relative error Zr sample		0,0745	
Ideal mass of the alloy			4,2722
Actual mass of the alloy			4,2736
Relative error of the alloy			0,0337

Table 3.8. $Cu_{64,5}Zr_{35,5}$ sample of type 2 of recycled copper.

RECYCLED COPPER. TYPE 2			
Element	Cu	Zr	
Atomic weight	63,546	91,224	
Atomic per cent	**64,5**	**35,5**	
Molecular weight	4098,717	3238,452	7337,169
Mass percentage	55,8624	44,1376	
Recycled Cu sample			
Actual Cu mass	2,727		
Total mass	4,8739		
Ideal corresponding mass of Zr		2,1512	
Actual corresponding mass of Zr		2,1518	
Relative error Zr sample		0,0259	
Ideal mass of the alloy			4,8739
Actual mass of the alloy			4,8745
Relative error of the alloy			0,0114

Table 3.9. $Cu_{65,5}Zr_{34,5}$ sample of type 2 of recycled copper.

RECYCLED COPPER. TYPE 2			
Element	Cu	Zr	
Atomic weight	63,546	91,224	
Atomic per cent	**65,5**	**34,5**	
Molecular weight	4162,263	3147,228	7309,491
Mass percentage	56,9433	43,0567	
Recycled Cu sample			
Actual Cu mass	2,6135		
Total mass	4,5897		
Ideal corresponding mass of Zr		1,9762	
Actual corresponding mass of Zr		1,9774	
Relative error Zr sample		0,063	
Ideal mass of the alloy			4,5897
Actual mass of the alloy			4,5909
Relative error of the alloy			0,0271

Table 3.10. $Cu_{63,5}Zr_{36,5}$ sample of type 3 of recycled copper.

RECYCLED COPPER. TYPE 3			
Element	Cu	Zr	Sum
Atomic weight	63,546	91,224	
Atomic per cent	**63,5**	**36,5**	
Molecular weight	4035,171	3329,676	7364,847
Mass percentage	54,7896	45,2104	
Recycled Cu sample			
Actual Cu mass	2,3946		
Total mass	4,3705		
Ideal corresponding mass of Zr		1,9759	
Actual corresponding mass of Zr		1,9757	
Relative error Zr sample		0,012	
Ideal mass of the alloy			4,3705
Actual mass of the alloy			4,3703
Relative error of the alloy			0,0054

Table 3.11. $Cu_{64,5}Zr_{35,5}$ sample of type 3 of recycled copper.

RECYCLED COPPER. TYPE 3			
Element	Cu	Zr	Sum
Atomic weight	63,546	91,224	
Atomic per cent	**64,5**	**35,5**	
Molecular weight	4098,717	3238,452	7337,169
Mass percentage	55,8624	44,1376	
Recycled Cu sample			
Actual Cu mass	2,4019		
Total mass	4,2997		
Ideal corresponding mass of Zr		1,8978	
Actual corresponding mass of Zr		1,8963	
Relative error Zr sample		0,0777	
Ideal mass of the alloy			4,2997
Actual mass of the alloy			4,2982
Relative error of the alloy			0,0343

Table 3.12. $Cu_{65,5}Zr_{34,5}$ sample of type 3 of recycled copper.

RECYCLED COPPER. TYPE 3			
Element	Cu	Zr	Sum
Atomic weight	63,546	91,224	
Atomic per cent	**65,5**	**34,5**	
Molecular weight	4162,263	3147,228	7309,491
Mass percentage	56,9433	43,0567	
Recycled Cu sample			
Actual Cu mass	2,8232		
Total mass	4,9579		
Ideal corresponding mass of Zr		2,1347	
Actual corresponding mass of Zr		2,1344	
Relative error Zr sample		0,0149	
Ideal mass of the alloy			4,9579
Actual mass of the alloy			4,9576
Relative error of the alloy			0,0064

ANNEX 4. PROCEDURES

4.1. Arc melter procedure

1- Open the gas
2- Let the gas flow across the tube to purge it.
3- Clean the Cu base with alcohol.
4- Put the sample on the Cu base.
5- Put the Ti ball on the Cu base.
6- Check that V-1 and V-2 from the melt spinner are closed.
7- Switch on the pump (at the front panel of the melt spinner).
8- Guarantee that the arm of the arc melter is jammed by the hose clamp.
9- With the gas and air connections closed, proceed to create the vacuum.
10- Close the vacuum and introduce the Ar (gas). Repeat this procedure three times.
11- Set the desired pressure on the inside.
12- Switch on the main switch.
13- Close the door and push the button.
14- Plug the water pump.
15- Check that the front valve of the melt spinner is opened.
16- Take out the hose clamp.
17- Point the tip of the arc melter outwards.
18- Set the power indicator to 3 and switch on the arc melter.
19- Melt the Ti ball.
20- Move the beam towards the sample.
21- If it is needed, join the pieces of the sample with the tip.
22- Turn the alloy ball upside down.
23- When the procedure is finished, wait a few minutes until the ball cools down
24- Switch off the vacuum pump and the water pump.
25- Take out the sample and put the hose clamp again.
26- Clean the Cu base and the crystal accurately.
27- Close the gas.

4.2. Melt Spinner procedure

1- Preparing the chamber
   a. Check the melt spinner state.
   b. Check the exhausting pipe (orange) is placed correctly (with its end out of the lab window.
   c. If the chamber is in vacuum, fill the chamber with air opening the venting valve V-7.
   d. Put on the gloves before touching anything.
   e. Put the crucible with the sample inside the induction coil.
   f. Adjust the crucible-wheel distance.
   g. Close chamber doors.

2- Primary vacuum
   a. Switch on S-1 and check pressure gauges and pyrometer are connected.
   b. Open inert gas bottle, let inert gas fill the pipes opening and closing valves V-4 and V-6.
   c. Open red valve V-1 and guillotine valve V-2.
   d. Close venting valve V-7.
   e. Open V-3 and V-5 valves to ensure vacuum in chamber, crucible and injection containers.
   f. Switch on rotatory pump.
   g. Wait until P < 1 mbar.

3- High vacuum
   a. Close red valve V-1.
   b. Switch on water pump.
   c. Open valve V-8 (high vacuum pump cooling).
   d. Switch on high vacuum pump.
   e. Wait until P < 10^{-3} mbar.
   f. Close guillotine valve V-2.
   g. Close valve V-8 (high vacuum pump cooling).
   h. Switch off high vacuum pump.

4- Start copper wheel rotation
   a. Check the wheel in not in polishing position.
   b. Switch on S-2 and S-3.

5- Filling chamber and injection containers
   a. Fill chamber opening V-4 up to the desired pressure.
   b. Close V-4.
   c. Close V-3 and V-5.
   d. Fill injection containers opening V-6 up to the desired pressure.
   e. Close V-6.

6- Melting and injecting
   a. Open V-9 (induction coil cooling).
   b. Switch on S-4.
   c. Adjust to the desired intensity.
   d. Start on the induction furnace pressing the black pedal.
   e. Wait until the sample is melted.
   f. Open V-5 to inject the melt.

7- Stopping the system
   a. Switch off S-3 and S-4.
   b. Switch off water pump.
   c. Open red valve V-1.
   d. Wait until pressure drops enough to ensure exhaustion of chamber gases.
   e. Switch off rotatory pump.

f. Open venting valve V-7.
g. Close V-8 and V-9.
h. Open chamber doors and collect ribbons.
i. Clean the chamber and the wheel (use mask while polishing the copper wheel).
j. Close the gas.

ANNEX 5. XRD INSTRUMENTATION AND PHYSICAL BASIS

The photograph below shows a typical X-ray diffractometer with its parts:

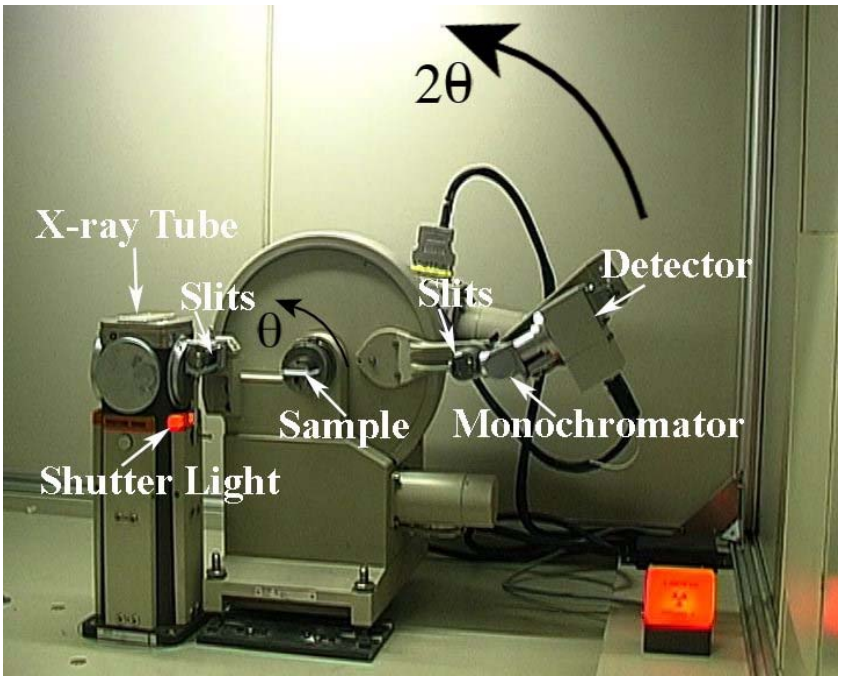

Fig. 5.1 Parts of a diffractometer [8

In order to understand how a diffractometer works, we can assume that it, basically, consists of:
- X-ray tube
- X-ray detector
- Goniometer
- Secondary monochromator

One type of photon beam generator is an X-ray tube. In this, in which vacuum has been made, electrons are emitted as a result of a filament warming, then, these electrons are accelerated by an electric potential of an order of magnitude of tens of keV. This high potential, maintained over the electrodes, leads the photons to the target metal sample. The X-rays are produced in the moment of the impact between the electron beam and the metal objective, and they are radiated in all directions.
The most used X-ray radiation is the one which is emitted by copper, which has a characteristic wavelength for the K radiation of 1.5418 Å [9].
When an X-ray beam founds a crystal lattice, rays are scattered in all directions. However, a lot of scattering interfere destructively with others from other atoms and, because of this, they are eliminated. Thus, diffraction occurs when the direction and the phase dispersion of an X-ray coincide with those of another ray (or rays) scattered by another atom (or atoms) to another level atomic (or

atomic planes), i.e., when the interference is constructive. With this interference, the reflections are combined to form new wave fronts (figure 5.2)

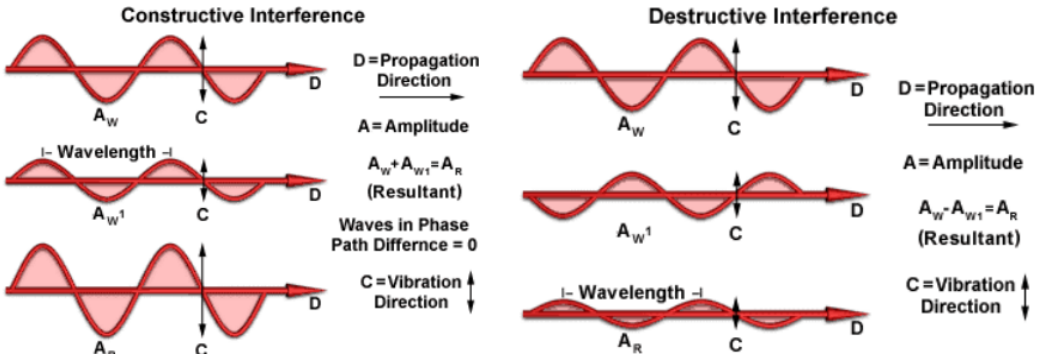

Fig. 5.2 Scheme of the basis of a constructive and a destructive interference [10]

The simple geometric interpretation that relates the angle of diffraction with the interplanar distance is known as Bragg's law.

$$n\lambda = 2 \cdot d \cdot \sin\theta \qquad \textbf{(5.1)}$$

Where *n* is an integer
λ is the wavelength of the X-rays
d is the interplanar spacing generating the diffraction and
θ is the diffraction angle
λ and *d* are measured in the same units, usually angstroms [11].

The rays reflected in different atomic planes interfere positively if the difference of their ways is a multiple of $\frac{2\cdot\pi}{\lambda}$ (figure 5.3).

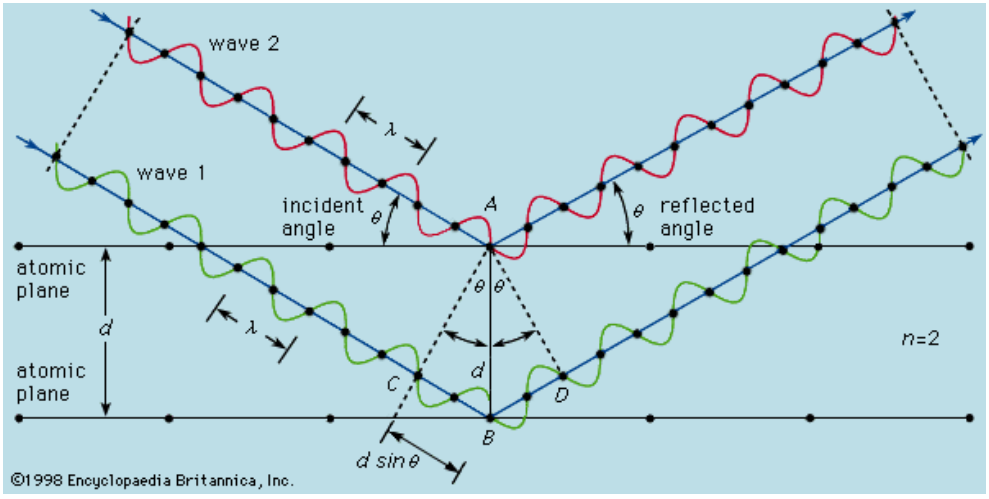

Fig. 5.3 Constructive interference (Bragg's law) [12]

The X-ray detector is placed on the circumference of a graduated circle, in which centre is placed the sample to analyse. In addition, the detector and the sample stand are connected mechanically to a goniometer, so the turnover ratio is 2:1. This means that when the detector rotates an angle of 2θ, the sample only makes an angle θ. The diagram that follows this type of goniometer is shown in figure 5.4.

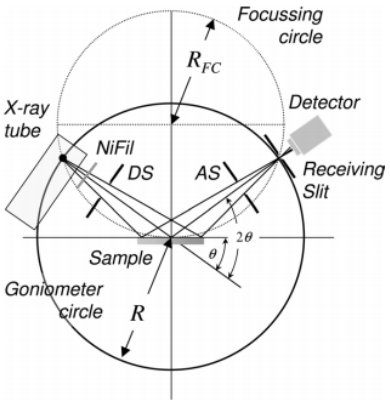

Fig. 5.4 Schematic representation of θ/2θ diffraction in Bragg–Brentano geometry [13].

The secondary monochromator is used in order to ensure that the radiation detected is monochromatic. When it is placed in the corresponding position in front of the detector, only the K_α radiation is directed to the detector. However, the K_β and the fluorescence background radiation (noise caused by electrons directed to other regions within the X-ray source) are diffracted in another angle and they are not detected.

ANNEX 6. SEM INSTRUMENTATION AND PHYSICAL BASIS

The photograph below shows a typical SEM with its parts:

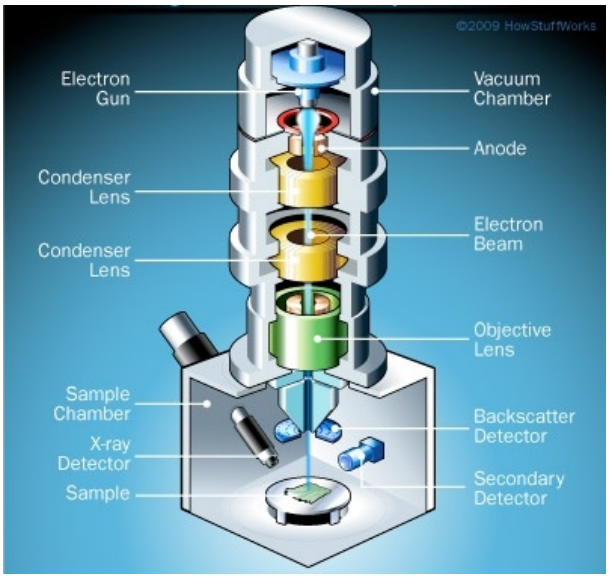

Fig. 6.1 Parts of the SEM [14]

The main part of SEM is called the electron column, which basically has housed within the following elements: [15]

- Electron gun
- Lenses
- Samples chamber
- Detectors
- Vacuum chamber

The electron gun produces the steady stream of electrons necessary for SEMs to operate. Electron guns are typically of two types:
On the one hand, thermionic guns, which are the most common type, apply thermal energy to a filament (usually made of tungsten, which has a high melting point) to coax electrons away from the gun and towards the sample under examination.
Field emission guns, on the other hand, create a strong electrical field to pull electrons away from the atoms they are associated with. Electron guns are located either at the very top or at the very bottom of a SEM and fire a beam of electrons at the object under examination. These electrons do not naturally go where they need to, which gets us to the next component of SEM.

A system of electromagnetic lenses is the responsible to produce clear and detailed images.
The lenses of a SEM are made of magnets capable of bending the path of electrons. By doing so, the lenses focus and control the electron beam, ensuring that the electrons end up precisely where they need to go.

The sample chamber of a SEM is where the sample to analyse is put in order to be examined. Because the specimen must be kept extremely still for the microscope to produce clear images, the sample chamber must be very sturdy and insulated from vibration.

The detectors find the various ways that the electron beam interacts with the sample object and convert this beam in an electric signal.
For instance, Everhart-Thornley detectors register secondary electrons, which are electrons dislodged from the outer surface of a sample. These detectors are capable of producing the most detailed images of a sample surface, due to the large depth of field of this signal.
Other detectors, such as backscattered electron detectors and X-ray detectors, can inform about the composition of a sample and, thus, an elemental chemical analysis of the sample can be obtained.

The vacuum chamber is required for the correct operation of the SEM because, without a vacuum, the electron beam generated by the electron gun would encounter constant interference from air particles in the atmosphere.

Furthermore, the microscope has various systems which monitor the electrical signals from the detectors as images on a TV monitor, as elements spectrum, etc.

The SEM technique essentially consists in the incision of an electron beam in the sample. The electron bombardment results in the appearance of different signals that, captured with suitable detectors, can provide information about the nature of the sample.

Secondary electron signal, as we mentioned above, provides an image of the sample surface morphology. The backscattered electron signal provides a qualitative image of zones with different average atomic number, and the X-ray signal, spectrum and images about chemical elements founded in the sample.

6.1 Detection of secondary electrons

Secondary electrons (SE) are generated by an inelastic collision between an electron of the primary beam and the sample, transferring part of its energy to an electron in an atom of the sample. As a result of this energy loss, a deviation of the trajectory of the incident electron occurs, as well as the ionization of the electron in the atom. Thus, the ionized electron leaves the atom with a very low kinetic energy (around 5 eV and usually less than 50 eV).
The name of the secondary electron, therefore, arises from the low kinetic energy of the electron in comparison of the kinetic energy of incident electrons, which can reach keV as we can see in the figure below.

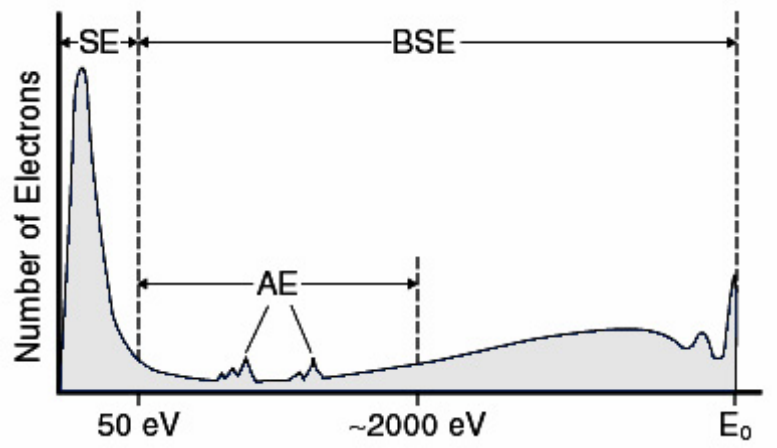

Fig. 6.2 Electron Energy Spectrum [16]

Every incident electron can generate multiple secondary electrons because they have undergone multiple scattering events on their way.
The image formed by such electrons gives mainly a real image of the surface under study, since the low kinetic energy of the electron cannot get far from the sample so the geometric shape can be determined with accuracy. Thus, images are obtained with large increases (from 100.000x or more) and high resolutions (up to about 40Å).

6.2. Detection of backscattered electrons

Backscattered electrons (BSE) are produced, unlike the SE, as a result of elastic collisions between the sample and the incident electron beam. In this kind of collisions, the energy exchange is negligible and, therefore, the detected electrons have high kinetic energy. However, these electrons show a change in the momentum with respect the incident electrons, more specifically, in the direction of the vector speed. The scattering angle can vary between 0º and 180º, being typically value close to 5º

In this case, the images obtained by BSE provide information on the chemical composition of the sample, because in these images we can observe a contrast between different chemical compositions.

The production efficiency of BSE is proportional to the atomic number of the sample, so that the contrast of the image is a function of composition (the higher the atomic number, the brighter the sample) [17].

ANNEX 7. MICROHARDNESS TESTS

7.1. Knoop hardness test

The Knoop hardness test method consists of indenting the test material with a rhombic-based pyramidal diamond indenter that forms an elongated diamond shaped indentation having approximate ratio between long and short diagonals of 7:1. The depth of indentation is about 1/30 of its length. When measuring the Knoop hardness, only the longest diagonal of the indentation is measured, unlike the Vickers test.
The Knoop test method is defined in ASTM E-384 [18].

7.2. Vickers VS Knoop

In summary, we present a table comparing the strengths and weaknesses of each of the tests.

Table 7.1. Strengths and weakness of both testing methods

	Vickers	**Knoop**
Strengths	One scale covers the entire hardness range.	The elongated diamond indenter and low test forces allows testing very small parts or material features not capable of being tested in any other way.
	A wide range of test forces to suit every application.	One scale covers the entire hardness range.
	Non-destructive, sample can normally be used.	A wide range of test forces to suit every application.
Weaknesses	The weaknesses are common for both tests and consist of the need to optically measure the indent size and the slowness to perform the test (it can take 30 seconds not counting the sample preparation time).	

And comparing the indentations made with Knoop and Vickers Diamond Pyramid indenters for a given load and test material: [19]

- Vickers indenter penetrates about twice as deep as Knoop indenter
- Vickers indentation diagonal is about 1/3 of the length of Knoop major diagonal
- Vickers test is less sensitive to surface conditions than Knoop test

- Vickers test is more sensitive to measurement errors than Knoop test
- Vickers test is best for small rounded areas
- Knoop test is best for small elongated areas
- Knoop test is good for very hard brittle materials and very thin sections

7.3. Microindentation hardness results

The results obtained performing the Vickers test for each of the ribbons are shown in the following table:

Table 7.2. Micro indentation hardness results

Ribbon	y [µm]	#	Load [mN]	Time [s]	Hardness [Vickers]	Average Hardness [Vickers]	Standard Deviation
Pure copper	25	1	245.3	5	674	668,29	30,07
		2			674,1		
		3			674,2		
		4			674		
		5			591,2		
		6			697,7		
		7			697,6		
		8			651,9		
		9			674		
		10			674,2		
Recycled copper type 1	25	1	245.3	5	748,1	745,9	19,64
		2			722,2		
		3			748,2		
		4			748,2		
		5			722,3		
		6			748,4		
		7			722,2		
		8			775,6		
		9			748,2		
		10			775,6		
Recycled copper type 2	36	1	245.3	5	804,7	796,64	21,95
		2			748,2		
		3			775,8		
		4			804,7		
		5			748,2		
		6			804,7		
		7			804,7		
		8			835,3		
		9			835,3		
		10			804,8		
Recycled	28	1	245.3	5	804,7	813,9	14,79

copper type 3		2			804,7		
		3			835,3		
		4			835,3		
		5			804,8		
		6			804,7		
		7			804,7		
		8			804,8		
		9			804,6		
		10			835,4		

ANNEX 8. DSC CURVE MEASURES

As discussed in the corresponding chapter, the DSC analysis measures the amount of heat absorbed or emitted by a sample as a function of temperature and / or time, due to physical and / or chemicals changes in the material.
The temperatures that interest us here are the glass transition temperature (T_g), the crystallization temperature (T_c) and the melting temperature (T_m).

8.1. Glass transition temperature (T_g)

The glass transition temperature (T_g) (see Fig. 8.1) of a non-crystalline material is the critical temperature at which the material changes its behaviour from being 'glassy' to being 'rubbery'. 'Glassy' in this context means hard and brittle (and therefore relatively easy to break), while 'rubbery' means elastic and flexible.

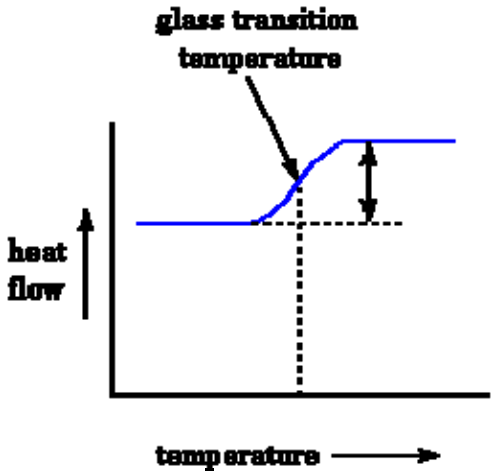

Fig 8.1 Glass transition temperature [20]

The glass transition is a property which manifests itself in the amorphous materials, i.e. materials whose atoms are not arranged in a crystalline structure, but randomly distributed.

8.1.1 Point of Tg Determination

In the literature, researchers report glass transition temperature data as either the midpoint or the onset Tg. As shown below in Fig 8.2, the point chosen for the determination of Tg can affect the value of the glass transition temperature. The onset Tg is generally considered the most appropriate temperature to report. However, many researchers report midpoint Tg values since a plot of the first derivative of the glass transition curve shows a peak at the midpoint glass transition temperature making this point easy to identify. [21]

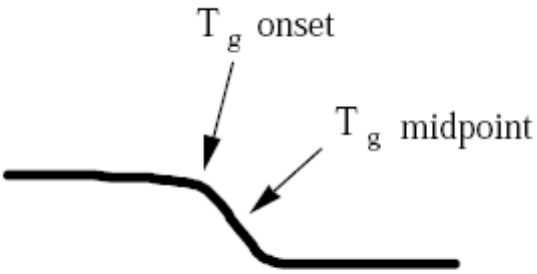

Fig. 8.2 Determination of Tg from DSC curve [22]

8.2. Crystallization temperature (T_c)

In increasing the temperature, the material becomes less viscous and there comes a time when the atoms have enough energy to rearrange and acquire a crystalline structure. At this point, we have crystallization temperature (T_c). The crystallization process is exothermic thus the sample releases heat, manifesting itself in the DSC curve as a peak.

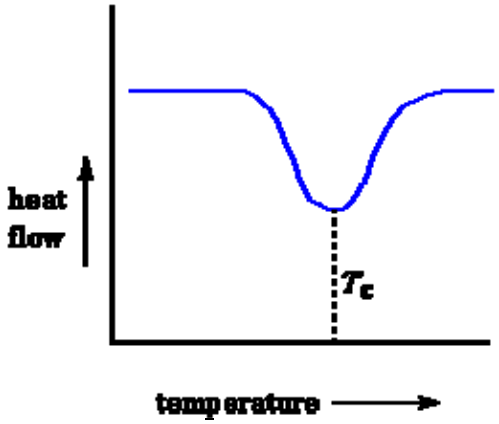

Fig 8.3 Crystallization temperature [23]

8.3. Melting temperature (T_m)

Finally, as the temperature further increases, the sample eventually reaches another thermal transition: the melting temperature (T_m). The melting process leads to an endothermic peak in the DSC curve, therefore, the calorimeter

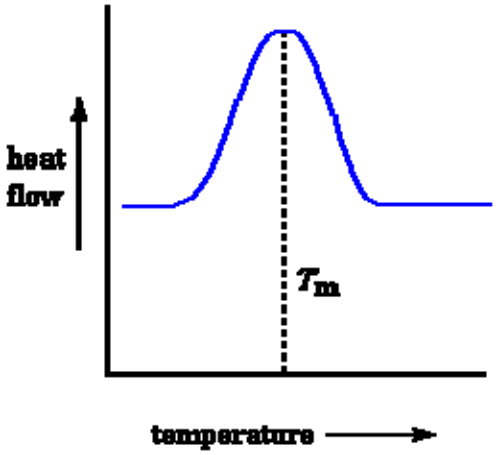

Fig 8.4 Melting temperature [24]

Finally, if we put all the temperatures of interest together, we obtain a standard DSC curve (Fig 8.5)

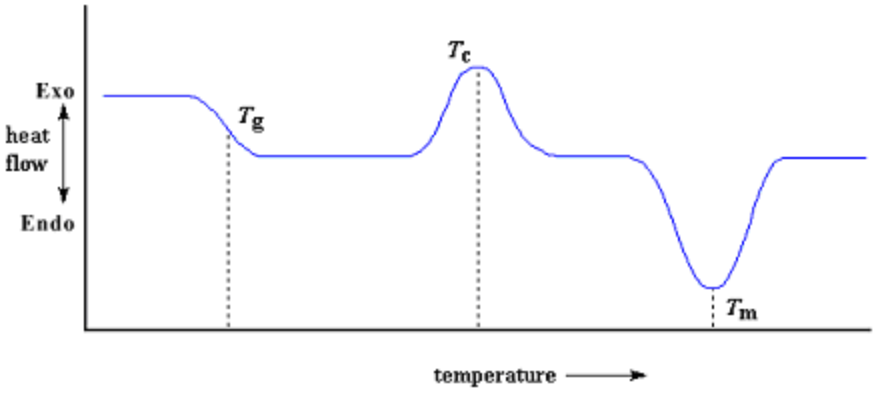

Fig 8.5 A standard output for a polymer from a DSC machine [25]

From the diagram, it can be seen that a sudden upward jump in the curve signifies an exothermic process. A sudden drop in heat flux indicates an endothermic process.

Apart from these temperatures, a temperature of great interest that can be drawn from the DSC curve is the reduced glass transition temperature (T_{rg}), which can be obtained by simply dividing the T_g over the T_m.
The value of reduced glass transition temperature, $T_{rg} = T_g/T_m$, serves as a useful indication of GFA: Experimentally, it has been observed that a good GFA implies values of T_{rg} equal or higher than 0,6 and, of course, the higher this value, the better.

ANNEX 9. HOW TO RUN DSC404F3 SOFTWARE

After entering the reference crucible and the crucible with the desired sample to measure in the calorimeter, we have to run the DSC404F3 software to start the analysis.
In this section we will explain what parameters we have to enter or to select in each of the screens to leave the program ready for analysis.

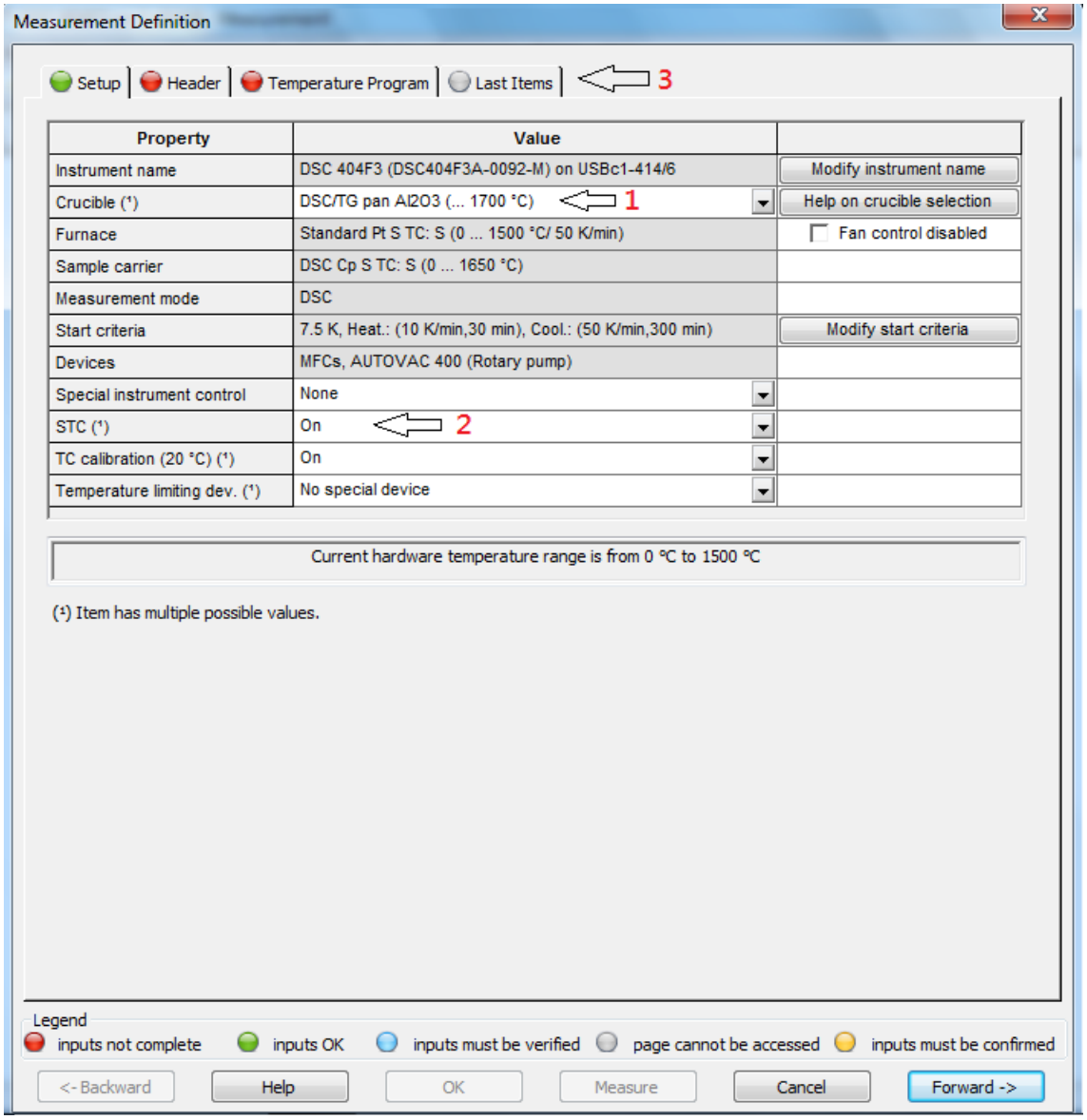

Fig 9.1 Screen 1

1: In this screen, what we have to do first is to select the crucible we are going to use. In our case, we use alumina crucibles (Al_2O_3), so, in this this drop-down menu we have to select "DSC / TG pan Al2O3 (... 1700 ° C)".
2: In the STC drop-down menu we have to check that it is always set “ON”.

3: Once these two steps are done, the ball "Setup" which was in red colour, it has turned down to green now and we can proceed to the next step "Header" by selecting the appropriate tab.

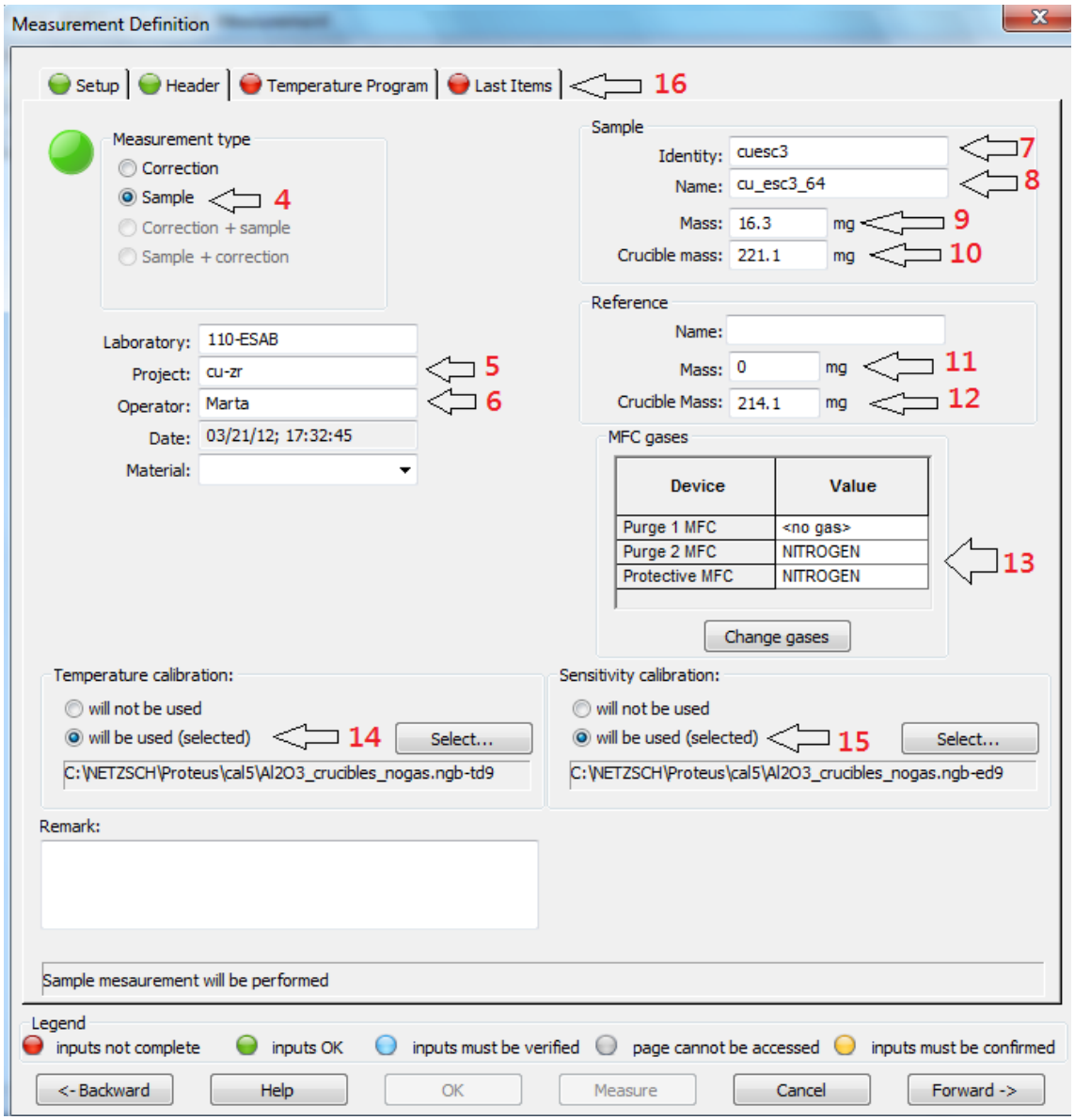

Fig 9.2 Screen 2

4: In "Measurement type" we have to select "Sample".
5: In "Project" we must give a name to the project we are doing. In our case, we work with copper and zirconium, so we decided to call it "cu-zr".
6: In "Operator" we put the name of the person who will perform the analysis. In our case, "Marta".
7: In "Sample - Identity" we have to put a name to identify the sample that we are going to analyse. In this case, we would make the analysis of recycled copper type 3, so we call it "cuesc3".

8: In "Sample - Name", we give a name to the sample, in our case "cu_esc3_64".
9: In "Sample - Mass", we put the value of the sample mass in mg, having weighed it before in a precision scale. In this case "16.3 mg".
10: In "Sample - Mass Crucible" we put the value of the mass of the alumina crucible where we have to introduce the sample in mg, having weighed it before in a precision scale. In this case "221.1 mg".
11: In "Reference - Mass" we have to put “0 mg” as the reference crucible is empty.
12: In "Reference - Mass Crucible" we put the value of the mass of the reference crucible in mg, having weighed it before a precision scale. In this case "214.1 mg".
13: In "MFC gases" we must verify that the gas for "Purge 2 MFC" and "Protective MFC" is the nitrogen.
14: In "Temperature calibration" we must mark "will be used (selected)" and we have to select the file for the alumina, which is "Al2O3_crucibles_nogas.ngb-TD9."
15: In "Sensitivity calibration" we must mark "will be used (selected)" and we have to select the file for the alumina, which is "Al2O3_crucibles_nogas.ngb-DE9".
16: When all these steps are done, the ball of "Header" will turn green and we can move to "Temperature Program" by selecting the corresponding tab.

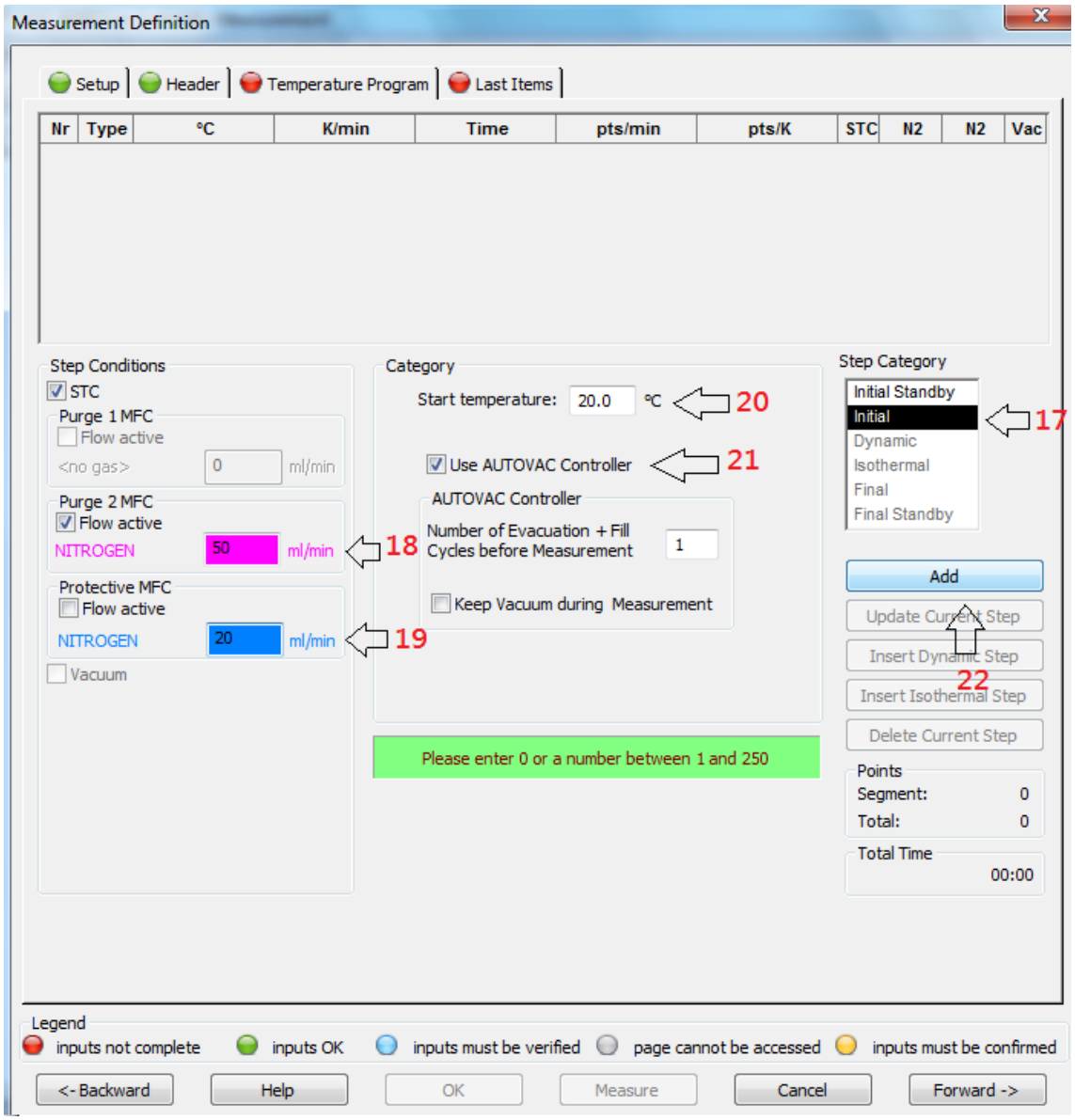

Fig 9.3 Screen 3.1

17: First of all, we must define an initial step, so in "Step Category" we check "Initial".
18: According to the manual of this model of DSC in "Purge 2 MFC" the amount of nitrogen must be "50 ml / min", so we put "50" in the pink blank space.
19: According to the manual of this model of DSC, in "Protective MFC" the amount of nitrogen must be "20 ml / min", so we put "20" in the blue blank space.
20: In "Start temperature" we have to put the temperature of the furnace in that moment, in this case "20.0 ° C".
21: We have to check the option "Use AUTOVAC Controller" and, in "Number of Evacuation + Fill Cycles before Measurement" we set "1". The option "Keep Vacuum During Measurement" must be unchecked.
22: When all the above steps are done, we can click the "Add" button.

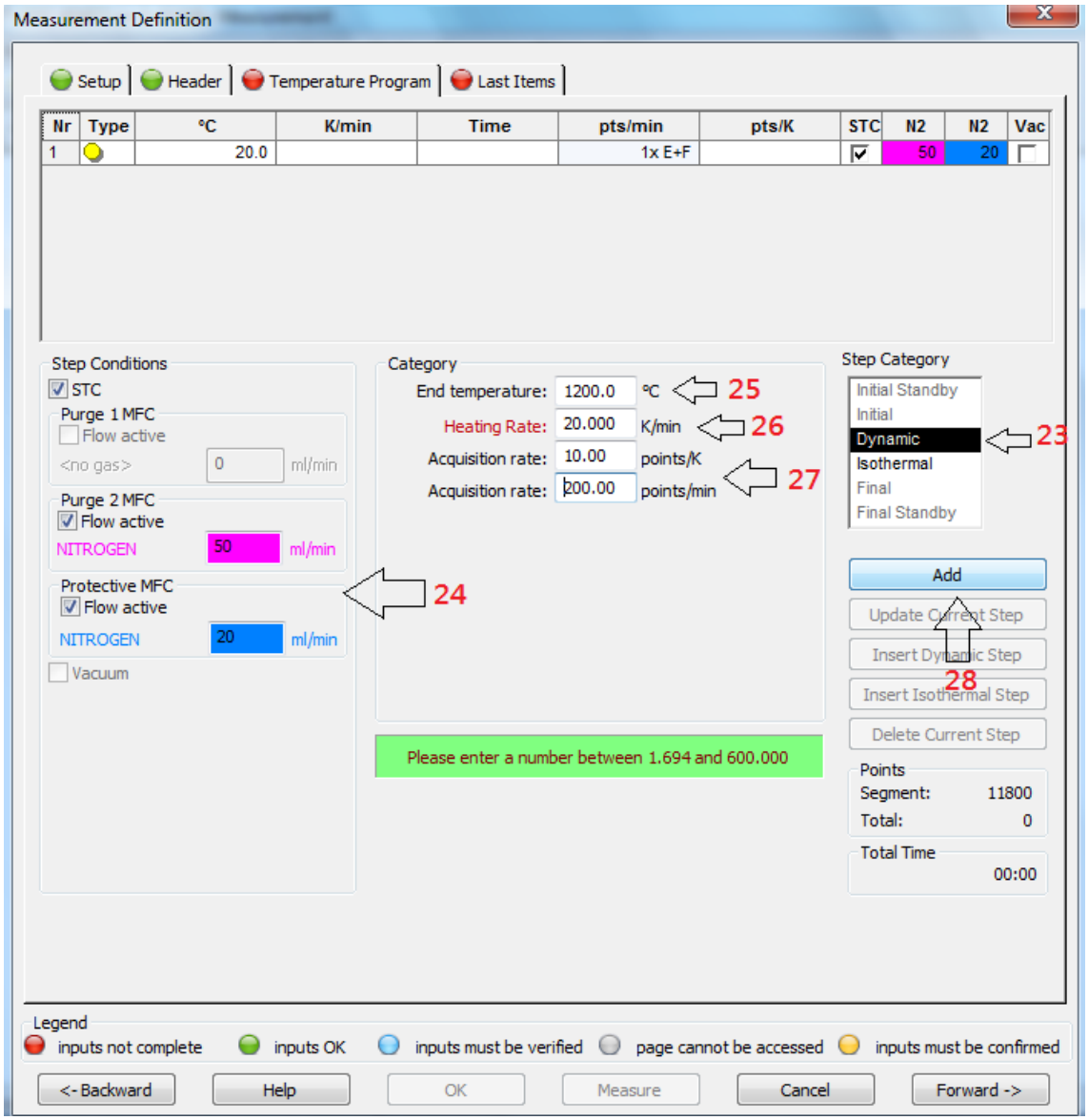

Fig 9.4 Screen 3.2

23: Now we define an increasing dynamic step, so in "Step Category" we have to check "Dynamic".
24: The amounts of nitrogen of "Purge 2 MFC" and "Protective MFC" must remain "50 ml / min" and "20 ml / min" respectively, so we put “50” and “20” in pink and blue blank spaces.
25: In "End temperature" we agreed to set it in "1200 ° C" looking at the phase diagram of Cu-Zr in order to view the melting in the DSC curve.
26: In "Heating Rate" we have to put "20 K / min"
27: The values of "Acquisition rate" appear by default when we enter the two previous fields.
28: When all the steps are done, we can click the "Add" button.

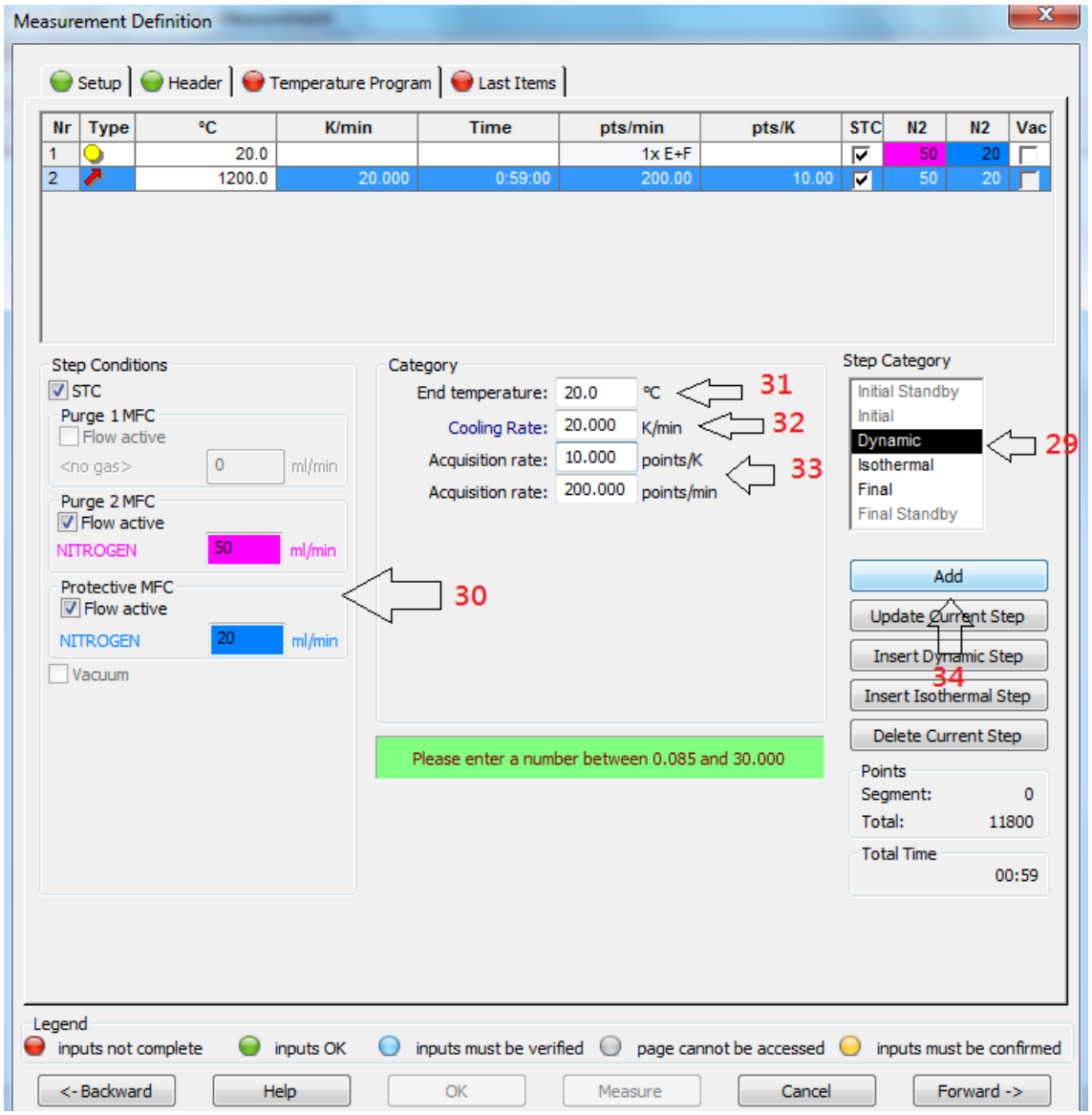

Fig 9.5 Screen 3.3

29: Now we define a decreasing dynamic step, so in "Step Category" check "Dynamic".
30: The amounts of nitrogen of "Purge 2 MFC" and "Protective MFC" must remain "50 ml / min" and "20 ml / min" respectively, so we put “50” and “20” in pink and blue blank spaces.
31: In "End temperature" we have to put the same temperature as "Start temperature", which is "20 ºC".
32: In "Cooling Rate" we have to put "20 K / min".
33: The values of "Acquisition rate" appear by default when we enter the two previous fields.
34: When all the steps are done, we can click the "Add" button.

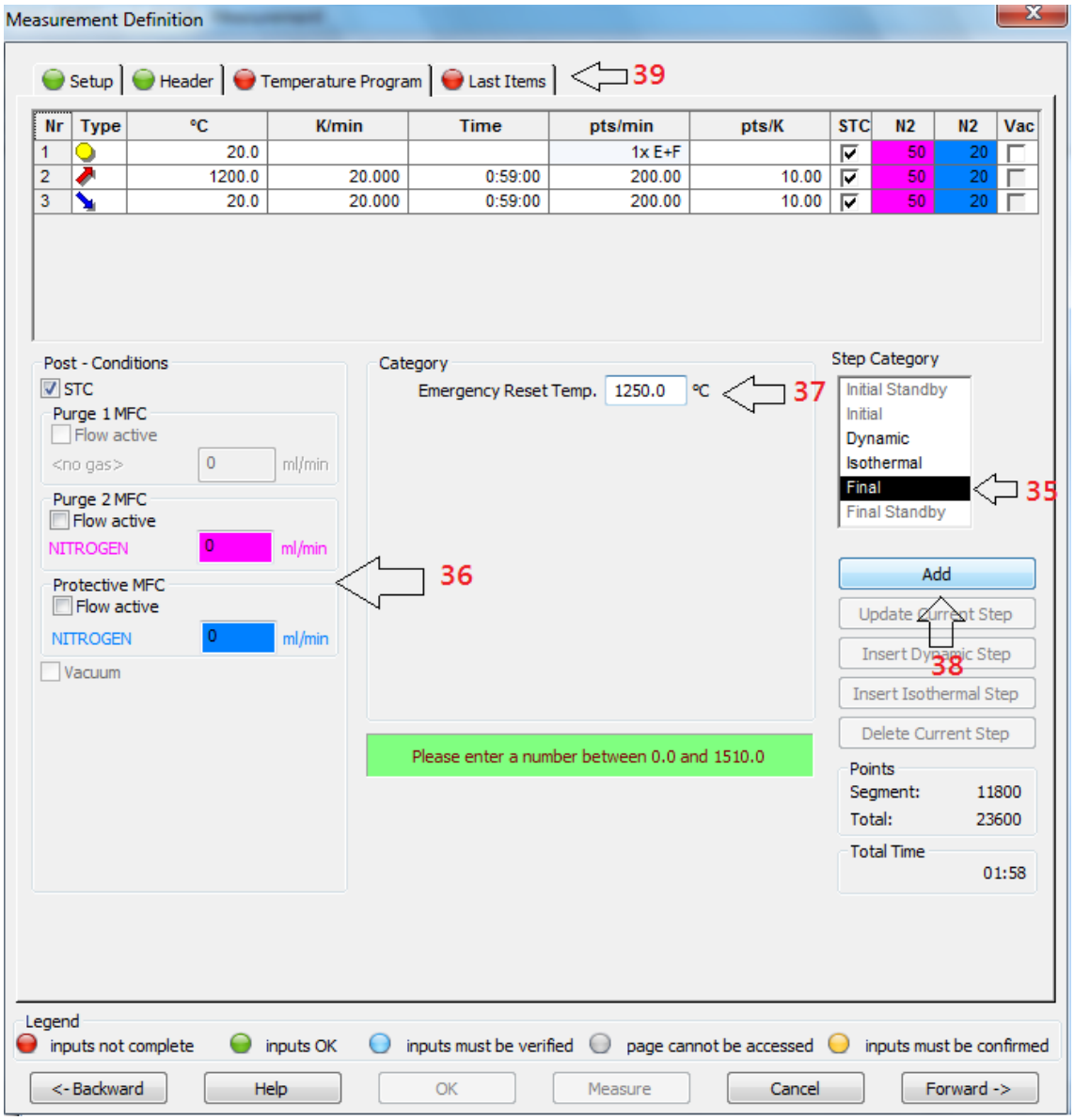

Fig 9.6 Screen 3.4

35: Now, we have to define a final step, so in "Step Category" we have to mark "Final".
36: In this step, the amounts of nitrogen to "Purge 2 MFC" and "Protective MFC" should be "0 ml / min", so we have to enter "0" in the pink and blue blank spaces.
37: In "Emergency Reset Temp." we put the same temperature we put in "End Temperature" plus adding “50 ºC”, which in our case is "1250.0 ºC".
38: When all the steps are done, we can click the "Add" button.

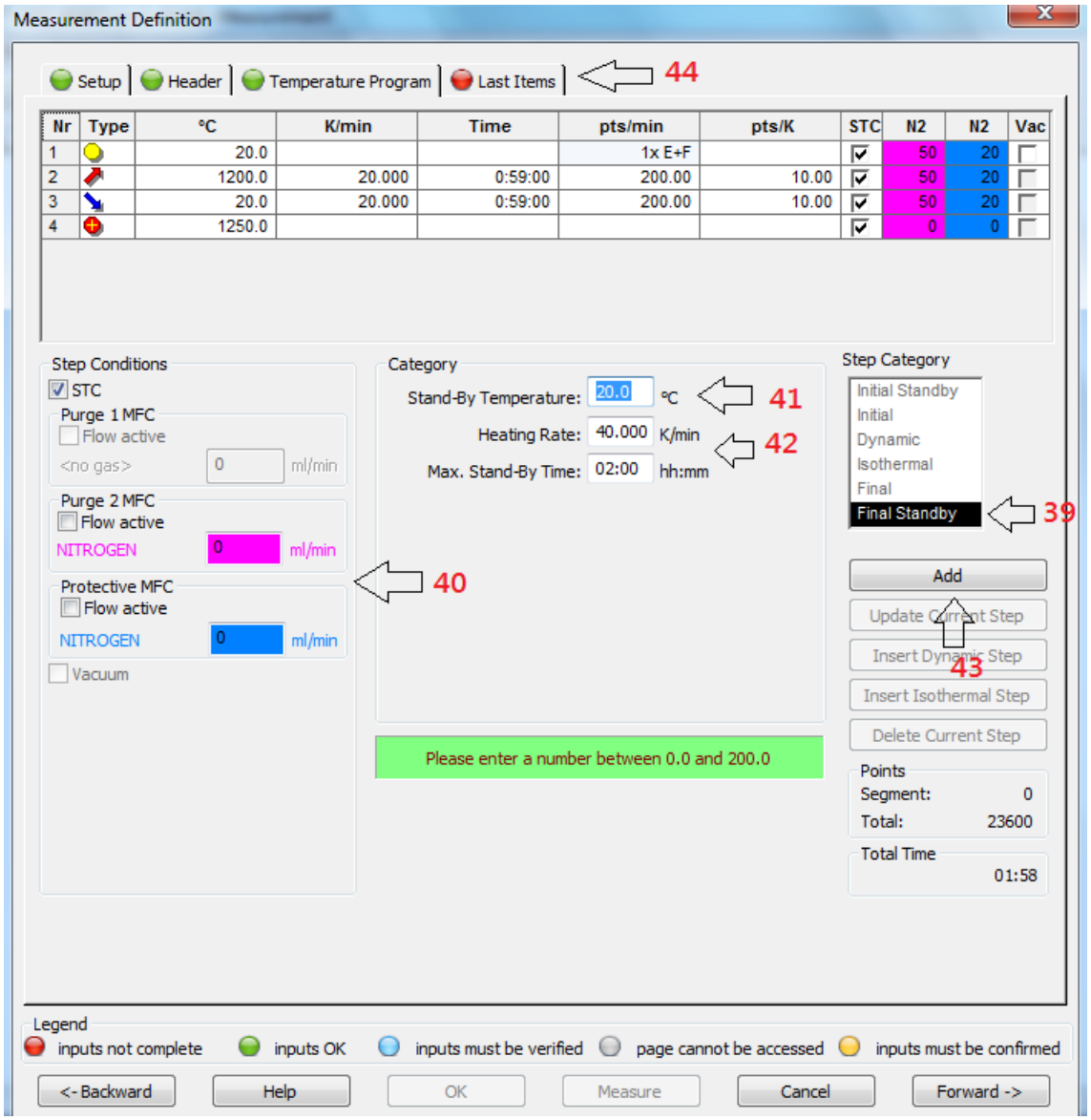

Fig 9.7 Screen 3.5

39: Now, we add the last step. For that in "Step Category" we have to select "Final Standby".
40: In this step, the amounts of nitrogen to "Purge 2 MFC" and "Protective MFC" should be "0 ml / min" too, so we have to enter "0" in the pink and blue blank spaces.
41: In "Stand-by Temperature" we have to put "20 ºC".
42: The "Heating Rate" and the "Max. Stand-By Time" fields appear by default when we fill the "Stand-by Temperature" field.
43: When all the steps are done, we can click the "Add" button.
44: When we click the “Add” button, the ball of "Temperature Program" will turn green and we can move to "Last Items" by selecting the corresponding tab.

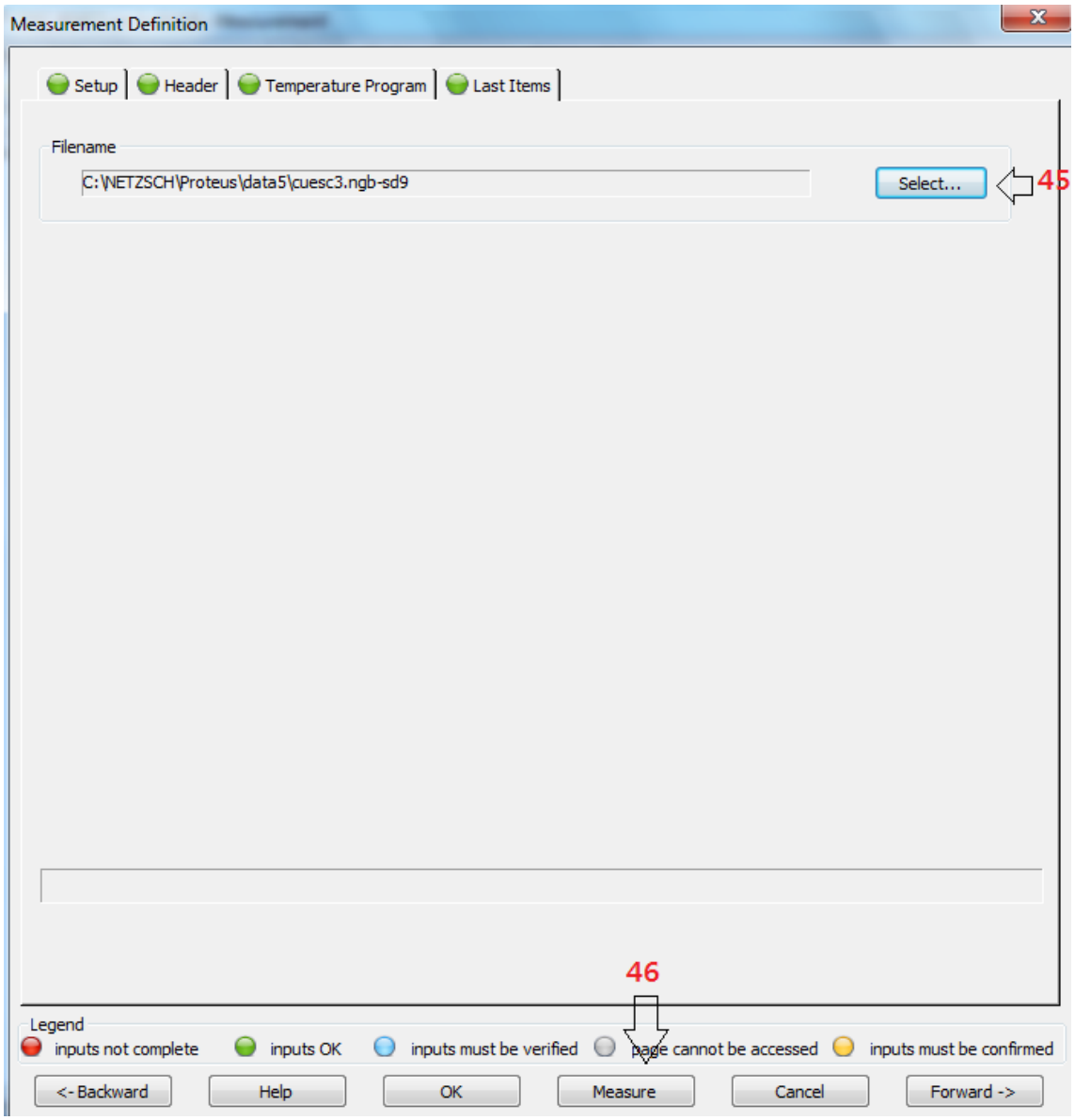

Fig 9.8 Screen 4

45: We must save the DSC generated when we will finish the analysis, for doing this we have to click on "Select" and select the directory where we want to save the file.
46: Once we have completed the step 45, we have click on the “Measure” button and a window will appear. Then, we will have to click "Start Evacuation." From here we have to wait until the purge and the analysis are done to analyse the DSC curve obtained.

ANNEX 10. MATLAB CODES

Generation of XRD patterns

```
format long
a=     load     ('C:\Users\MARTA\Desktop\TFC\XRD\Diffraction
patterns\recycled1_cu_63.txt'); %we load the data files
b=     load     ('C:\Users\MARTA\Desktop\TFC\XRD\Diffraction
patterns\recycled1_cu_64.txt');
c=     load     ('C:\Users\MARTA\Desktop\TFC\XRD\Diffraction
patterns\recycled1_cu_65.txt');
x1=a(:,1); %assignment of column 1 of the txt file to the x
axis
y1=a(:,2); %assignment of column2 of the txt file to the y
axis
x2=b(:,1);
y2=b(:,2);
x3=c(:,1);
y3=c(:,2);
figure(1)
plot (x1,y1,'b')
hold on
plot (x2,y2,'g')
plot (x3,y3,'r')
axis ([30 100.05 0 4500]); %definition of the appropriate
range of the graph looking at the values that we have
obtained
title ('Diffraction patterns of the first type of recycled
Cu samples', 'FontName', 'Arial', 'Fontsize', 14);
xlabel ('Angular range (2 \theta degrees)','FontName',
'Arial', 'Fontsize', 14);
ylabel ('Intensity (a.u.)','FontName', 'Arial', 'Fontsize',
14);%a.u.=arbitrary unit
legend
('Cu_6_3_,_5Zr_3_6_,_5','Cu_6_4_,_5Zr_3_5_,_5','Cu_6_5_,_5Z
r_3_4_,_5');
hold off;
grid on;
```

Plot of error bars

```
format long
load
('C:\Users\MARTA\Desktop\TFC\Microdurometer\results.txt');
%we load the data files
cuLens = reshape(results(:, 2), 10, 4);  % Make column 2
into a 10 x 4 array
cuMeans = mean(cuLens);  % Calculate the means for the 4
types of copper
```

```
cuSDs = std(cuLens);          % Calculate the standard
deviations for the 4 types of copper
cuTypes = {'Pure Cu', 'Recycled Cu Type 1', 'Recycled Cu
Type 2', 'Recycled Type Cu 3'}; % Used for legend
figure
errorbar(cuMeans, cuSDs, 'rs', 'LineWidth',2); % Error bars
as red squares
set(gca, 'XTick', 1:4, 'XTickLabel', cuTypes) % Set ticks
and tick labels
xlabel('Type of copper','FontName', 'Arial', 'Fontsize',
14);
ylabel ('Hardness [Vickers]','FontName', 'Arial',
'Fontsize', 14);
title ('Hardness of the Cu_6_4_,_5Zr_3_5_,_5
ribbons','FontName', 'Arial', 'Fontsize', 14);
legend('Mean (SD error bars)', 'Location', 'Northwest') %
Put in upper left corner
grid on;
```

REFERENCES

[1,4,5,7] Ashby, M.F; Greer, A.L, “Metallic glasses as structural materials”, *Scripta Materalia* 54 (3), 321-326 (2005).
[2] Demetriou, M.D; Launey, M.E; Garrett, G.;Schramm, J.P; Hofmann, D.C; Johnson, W.L; Ritchie, R.O, "A damage-tolerant glass", *Nature Materials* 10, 123–128 (2011)
[3] http://www.its.caltech.edu/~vitreloy/development.htm
[6] http://www.ccm.udel.edu/Personnel/homepage/class_web/Lecture%20Notes/Materials_Selection/unit1pres.pdf
[8] http://www.doitpoms.ac.uk/tlplib/xray-diffraction/powder.php
[9] http://www.javeedakhtar.com/comsats/XRD-SEM-TEM-AFM.pdf
[10] http://web.pdx.edu/~pmoeck/phy381/Topic5a-XRD.pdf
[11] http://www.ibt.unam.mx/computo/pdfs/met/Cristalografia.pdf
[12] http://www.britannica.com/EBchecked/media/17859/Bragg-diffraction
[13] Birkholz, M., “Principles of X-ray Diffraction”, Ch. 1 at *Thin Film Analysis by X-Ray Scattering* WILEY-VCH Verlag GmbH & Co. (2006).
[14,15] http://science.howstuffworks.com/scanning-electron-microscope2.htm
[16] http://www4.nau.edu/microanalysis/Microprobe-SEM/Signals.html
[17] http://www.mty.itesm.mx/dia/deptos/im/m00-862/Lecturas/SEM_ICP.pdf
[18] http://www.instron.us/wa/applications/test_types/hardness/knoop.aspx
[19] http://www.gordonengland.co.uk/hardness/microhardness.htm
[20,23,24,25] http://pslc.ws/macrog/dsc.htm
[21,22] http://www.ejpau.media.pl/volume8/issue4/art-69.html